NASA TECHNICAL MEMORANDUM

NASA TM X-2416

NASA TM X-2416

PERFORMANCE OF A BICONE INLET DESIGNED FOR MACH 2.5 WITH INTERNAL DISTRIBUTED COMPRESSION AND 40-PERCENT INTERNAL CONTRACTION

by Joseph F. Wasserbauer and David A. Choby

Lewis Research Center

Cleveland, Ohio 44135

NATIONAL AERONAUTICS AND SPACE ADMINISTRATION • WASHINGTON, D. C. • FEBRUARY 1972

1. Report No. NASA TM X-2416	2. Government Accession No.	3. Recipient's Catalog No.
4. Title and Subtitle PERFORMANCE OF A BICONE INLET DESIGNED FOR MACH 2.5 WITH INTERNAL DISTRIBUTED COMPRESSION AND 40-PERCENT INTERNAL CONTRACTION		5. Report Date February 1972 6. Performing Organization Code
7. Author(s) Joseph F. Wasserbauer and David A. Choby		8. Performing Organization Report No. E-6579
9. Performing Organization Name and Address Lewis Research Center National Aeronautics and Space Administration Cleveland, Ohio 44135		10. Work Unit No. 764-74 11. Contract or Grant No.
12. Sponsoring Agency Name and Address National Aeronautics and Space Administration Washington, D.C. 20546		13. Type of Report and Period Covered Technical Memorandum 14. Sponsoring Agency Code
15. Supplementary Notes		

16. Abstract

The inlet was designed to have the minimum internal contraction consistent with high total-pressure recovery and low cowl drag. Without a bypass system, the peak pressure recoveries increased from 0.890 to 0.936 when the supercritical bleed mass flow ratio was varied from 0.035 to 0.060. With an operating bypass system and installed centerbody vortex generators, a slight increase in peak pressure recovery was obtained. The values of steady-state distortion $((P_{max} - P_{min})/P_{av})_5$ and dynamic distortion $(\Delta P_{rms}/P_{av})_6$ were below 0.10 and 0.02, respectively, near critical operation. Simulation of a turbofan engine with concentric pipes showed no effect on compressor face flow profiles with varying bypass flow ratio.

17. Key Words (Suggested by Author(s))	18. Distribution Statement
Supersonic cruise inlets Inlets Propulsion systems	Unclassified - unlimited

19. Security Classif. (of this report)	20. Security Classif. (of this page)	21. No. of Pages	22. Price*
Unclassified	Unclassified	68	$3.00

* For sale by the National Technical Information Service, Springfield, Virginia 22151

PERFORMANCE OF A BICONE INLET DESIGNED FOR MACH 2.5 WITH INTERNAL DISTRIBUTED COMPRESSION AND 40-PERCENT INTERNAL CONTRACTION

by Joseph F. Wasserbauer and David A. Choby

Lewis Research Center

SUMMARY

An investigation was conducted to determine the performance characteristics of an axisymmetric, bicone, mixed-compression inlet system designed for Mach 2.5 operation. Forty percent of the supersonic area contraction occurred internally. The internal compression was accomplished by the cowl-lip oblique shock and isentropic compression from the cowl surface. The isentropic compression from the cowl was distributed over a length of centerbody equal to four-tenths of the cowl-lip radius.

Without a bypass system, increasing the supercritical bleed mass flow ratio from 0.035 to 0.060 increased the peak total-pressure recovery from 0.890 to 0.936. Inlet operation with vortex generators on the cowl and centerbody substantially reduced the steady-state distortion with only about 1-percent loss in the total-pressure recovery. At the critical operation, the steady-state distortion levels were about 0.10 for all bleed configurations when vortex generators were used.

With an operating bypass system and only centerbody vortex generators installed, the peak pressure recoveries for all configurations remained the same or increased slightly when compared with the no-bypass, no-vortex-generator configurations. Also, the steady-state distortion levels were reduced to values below 0.10 for a large part of the inlet's operating range. The dynamic distortion levels varied from about 0.01 at peak and match operating conditions to about 0.05 for the far supercritical operating conditions. This variation was the same for all inlet configurations tested.

To simulate a bypass engine, a concentric cold-pipe configuration was installed and the annular- to core-flow ratio was varied. The results showed that there was no effect on compressor face total-pressure profiles or dynamic distortion when the annular- to core-flow ratio was varied.

INTRODUCTION

For design flight speeds above Mach 2.0, supersonic mixed-compression inlets offer the capability of efficient operation with low drag over most of the flight range of the airplane. The inlets reported in references 1 to 4 are typical axisymmetric and two-dimensional mixed-compression inlets designed for operation above Mach 2.0. These inlets require some change in inlet geometry to vary the contraction ratio when operating at off-design Mach numbers.

The design philosophy of the inlet reported in reference 5 was to use a two-cone spike to provide the maximum external compression compatible with high total-pressure recovery and low cowl drag. To vary the contraction ratio, the second cone would be collapsed, and at its lowest position it would blend into the first-cone contours so as to provide a single-cone centerbody. This approach avoids the sharp curves that normally result when a single-cone surface is collapsed. This philosophy provided 40 percent of the supersonic area contraction internally for a design Mach number of 2.5. The present investigation evaluates a bicone inlet similar to the inlet of reference 5 except that the internal supersonic diffuser length has been increased. The inlet of reference 5 was designed such that the isentropic compression fan from the cowl and the cowl-lip oblique shock were focused on the centerbody at one point. This compression was canceled at the centerbody with an abrupt turn. For the inlet of this investigation the resulting cowl shock was canceled at the centerbody shoulder, while subsequent isentropic compression from the cowl was distributed over a length of centerbody equal to four-tenths of the cowl-lip radius. The manner in which this supersonic compression is accomplished is described in reference 6.

The test was conducted in the Lewis 10- by 10-Foot Supersonic Wind Tunnel at Mach numbers of 2.02 to 2.58 and at a Reynolds number of 8.2×10^6 per meter. The test inlet did not have a collapsing centerbody; therefore, the off-design Mach number performance was obtained with centerbody translation. The investigation evaluates inlet performance at several bleed locations and bleed flow rates. Local flow conditions were evaluated by flow surveys made ahead of and just downstream of the throat region, midway in the subsonic diffuser, and at the diffuser exit. Dynamic instrumentation was also used to evaluate the dynamic behavior of the flow at the diffuser exit. In addition to the flow surveys, measurements were made of the inlet and bleed flow rates, the total-pressure recovery, and the engine face distortion. The effect of vortex generators on the performance of the various bleed configurations was also determined. The maximum angle of attack before an inlet unstart was determined for critical and supercritical inlet operation. The effect of an overboard bypass system was also evaluated.

An additional investigation was conducted to determine if variations in the bypass ratio of a turbofan engine could influence the inlet flow distortion measurements. In this test the turbofan engine was simulated by two concentric cold pipes. The effect of

various bypass flow ratios of the concentric ducts on pressure recovery, steady-state distortion, and dynamic distortion at the simulated compressor face was determined.

APPARATUS AND PROCEDURE

The inlet of this investigation was designed for operation at a Mach number of 2.5. At the design condition, 60 percent of the supersonic flow area contraction was external and 40 percent was internal. The inlet was attached to a cylindrical nacelle 0.635 meter in diameter in which a J85-13 engine or a cold-pipe, choked-exit plug assembly could be installed. For this study, only the cold-pipe assembly was used. Figure 1(a) shows the inlet nacelle combination mounted from a vertical strut in the wind tunnel test section. Figure 1(b) is a schematic view of the inlet - cold-pipe combination with the choked-exit plug. Figure 1(c) is an isometric view of the inlet.

At the design Mach number of 2.5 and a free-stream temperature of 390 K, the inlet was sized to match the J85-13 engine-corrected airflow requirements of 15.83 kilograms per second (military operation) with 88.6 percent of the capture mass flow at a total-pressure recovery of 0.90. This required an inlet capture area of 0.1757 square meter. Of the remaining flow, 6 to 7 percent was allotted for performance bleed; 4 percent for engine cooling air; and the rest for overboard bypass flow, which was varied for terminal shock position control. Total-pressure distortion at the engine face of 0.10 or less was desired at the design conditions.

The essential features of the inlet were a bicone centerbody of 10° and 18.5° half-angle cones and an initial internal cowl angle of 5° (fig. 1(d)). The internal oblique shock emanating from the cowl lip was canceled at the centerbody impingement point. The remaining compression of the flow to a throat Mach number of 1.3 was isentropic. The isentropic compression fan from the cowl was distributed over a length of centerbody equal to four-tenths of the cowl-lip radius. This distributed compression on the centerbody started after the cowl shock impingement point and ended at the inlet throat.

The supersonic portion of the inlet was designed with the aid of a method-of-characteristics computer program which had an error that has since been corrected. The same program was used to design the inlet of reference 5. As in reference 5, the predicted second-cone shock position was too far upstream and resulted in a slightly imperfect inlet. Because of this error the oblique shock from the cowl lip impinges on the centerbody slightly downstream of its theoretical impingement point. The resulting flow mismatch at this point on the centerbody prevents the shock cancellation criterion from being met. However, since the cowl compression fan is distributed over a short portion of the centerbody, the inlet is less sensitive to an error of this type than when the cowl compression fan is focused on the centerbody, as in reference 5. The solution for the desired diffuser contours and flow properties using the subsequently available program

of reference 6 is shown in figure 2. The coordinates of the actual centerbody and cowl for the inlet of this investigation are listed in table I.

The subsonic diffuser consisted of an initial throat region four hydraulic radii in length with a 1° equivalent conical expansion followed by the main diffuser. The diffuser just downstream of the throat was mated to an existing subsonic diffuser described in references 2 and 3. Since the throat of the present inlet had a larger radius than the throat of the reference 2 inlet, a relatively sharp curve in the cowl contour occurred at the diffuser mating location. The overall design length from cone tip to compressor face was 7.86 cowl-lip radii. Figure 3 shows the internal area distribution through the inlet for various cowl-lip-position parameters. Provisions were included for installing vortex generators on the cowl and the centerbody aft of the throat region at an x/R_c of 3.97. (All symbols are defined in the appendix.) Details of the vortex generator design are shown in figure 4. Inlet configurations using vortex generators are identified herein as shown in the figure.

The aft portion of the subsonic diffuser contained three hollow centerbody support struts which divided the duct into three compartments back to the engine face. The inlet diffuser also included two bypass systems: a high-response overboard system for shock position control, and a low-speed valve to control secondary flow through the nacelle for engine cooling. Both systems were sealed for the bleed study and opened for the overall performance study presented in this report. The duct entrance into the bypass plenum was modified to minimize resonance by the installation of louvered segments, as discussed in reference 7.

To minimize the shock boundary-layer interaction, the inlet design included four porous bleed regions shown schematically in figure 5. The porous bleed regions were composed of holes 0.3175 centimeter in diameter and drilled normal to the surfaces in circumferential rows. The rows were alternately staggered to obtain maximum coverage. The porous bleed pattern could be varied in each region by filling selected holes. The five bleed pattern configurations considered in this study are shown in figures 5(a) to (c). For each configuration, the specific bleed patterns on the cowl are presented in figure 5(b) and those on the centerbody in figure 5(c). Configuration 1 was designed to give distributed bleed at all bleed locations. Configuration 2 had concentrated bleed at all bleed locations with increased bleed in the inlet throat, on the centerbody, and on the cowl. Configuration 3 eliminated all bleed downstream of the geometric throat but increased the forward cowl bleed slightly near the throat. The forward centerbody bleed remained the same as in configuration 1. For configuration 4, all bleed holes were opened on the forward and aft cowl bleed locations. However, the bleed in each cowl section was backpressured to give a supercritical bleed mass flow ratio of 0.02 for the forward cowl and 0.01 for the aft cowl. The centerbody bleed for configuration 4 was the same as that for configuration 1. The bleed patterns for configuration 5 are the same as

those for configuration 1 except that the forward centerbody bleed was replaced with a flush slot. The flush slot details and location are shown on figure 5(c). The flush slot on the centerbody was located ahead of the cowl shock, as in references 5 and 8.

The cowl bleed flow forward and aft of the throat is discharged overboard through exits shown in figure 6(a). Each exit has a 20° discharge angle relative to the external surface. The centerbody bleed flows into one plenum and is then ducted through the hollow centerbody support struts to 30° louvered exits. All exits were sized large enough to ensure choking of the bleed holes. However, the cowl bleed exit area for configuration 4 was reduced so that choking occurred at the bleed exit rather than at the bleed holes.

Boundary-layer properties were investigated on the centerbody and cowl by total-pressure-tube rakes ahead of the throat (stations 2a and 2b, fig. 6(a)). Rakes in the subsonic diffuser aft of the throat region (station 3), at the subsonic diffuser midpoint (station 4), and at the diffuser exit (station 5) were used to determine local flow profiles. The rakes were circumferentially indexed to avoid mutual interference effects. Details of the total-pressure rakes are shown in figure 6(b).

Figure 6(c) shows the compressor face, steady-state pressure instrumentation (station 5). The overall diffuser exit, total-pressure recovery was determined from rakes 1 to 6. Each 10-tube rake consisted of six equal-area-weighted tubes with additional tubes added at each side of the extreme equal-area-weighted tubes in positions corresponding to an 18-tube area-weighted rake. The additional measurement by rake 7 was included in the distortion calculations and in the duct local flow profile. Static-pressure distributions along the top centerline of both the cowl and centerbody were also measured. The static-pressure-tap locations along the cowl and centerbody are presented in table II.

In order to measure the fluctuating component of total pressure, subminiature absolute pressure transducers were mounted in rotating rakes (fig. 6(d)). These rakes were cantilevered from the centerbody in both the top and lower left duct segments (looking downstream). An assumption was made that the pressures in the lower left segment were similar to the pressures in the lower right segment. The total-pressure transducer was mounted tangential to the tube to protect the transducer diaphragm from particle damage. The 1.905-centimeter tube length was necessary to obtain an accurate total pressure but still was short enough to yield a flat response to at least 1000 hertz. The output signals of the rotating rake transducers were filtered by first-order, low-pass filters with a 1000-hertz corner frequency and measured with true rms meters. Further details of the response characteristics of the transducer-tube apparatus are given in reference 9.

At each steady-state operating condition, dynamic data were recorded at the four rotating rake positions shown in figure 6(d). The average value of the 16 rms measurements of the fluctuating component of total pressure in each segment was obtained. The face average rms value was obtained by adding one-third of the top segment value to

two-thirds of the lower left segment value. The dynamic distortion level for that particular operating condition was obtained by ratioing this face average rms value to the face average steady-state recovery pressure.

An additional investigation was conducted to define problems and to provide experimental data for a flow field ahead of two concentric cylinders. This particular flow field could be related to a duct feeding a bypass engine. The inlet model with the concentric cold pipes is shown in figure 7(a). Details of the duct entrance into the concentric cold pipes are shown in figure 7(b). The duct flow areas at the entrance are 405.59 square centimeters for the core duct and 556.92 square centimeters for the annulus duct. The flow in the core duct was controlled by the variable-exit plug shown in figure 7(a). The annulus exit area was varied by a series of fixed-exit-area plug configurations that were attached to the center duct cold pipe. The steady-state instrumentation used to survey the duct flows is shown in figure 7(c). The plane of this survey station is located in figure 7(b). The existing steady-state and dynamic instrumentation ahead of the concentric cold pipes (figs. 6(c) and (d)) were used to determine what the varying amounts of annular- to core-flow ratio would have on the compressor face flow.

All measurements and calculations were made in English units and then converted to SI units.

RESULTS AND DISCUSSION

Performance Bleed

All the data presented in this section are for inlet operation at the design Mach number of 2.5. The data are compared at three inlet operating conditions; peak, critical, and supercritical operation. Peak operation is defined as the minimum stable condition with the terminal shock at its most forward position in the inlet. Critical operation is defined as the terminal shock positioned at the inlet's geometric throat. The supercritical operation condition selected was that with the terminal shock positioned slightly ahead of the throat exit station ($x/R_c = 3.72$).

The effect of the various bleed configurations on peak inlet performance with variation of the cowl-lip-position parameter θ_l is shown in figure 8 for 0^o angle of attack. No vortex generators were used in the inlet for this portion of the investigation. Configurations 1 and 5 show identical performance over the range of cowl-lip-position parameters. The difference in performance for all the configurations can be attributed largely to the variation of throat bleed. Configuration 3 (no throat bleed) shows the poorest performance, while configuration 2 shows the best performance, for values of θ_l less than 25.3^o. A slight degradation in pressure recovery for configuration 2 is noted for higher values of θ_l. The most noticeable improvement is in the distortion level for

configuration 2. With the increased throat bleed, configuration 2 shows almost a 50-percent decrease in distortion over configuration 3. The high distortions of configuration 3 most probably result from the uncontrolled interaction of the terminal shock with the boundary layer when no throat bleed is used. The penalty for the good performance of configuration 2 is the large amount of performance bleed required. The moderate bleed configurations 1 and 5 show slightly less performance than configuration 2.

The effect of bleed on overall inlet performance at design θ_l of 25.28° and 0° angle of attack with no vortex generators is shown in figure 9. In general, the peak pressure recovery increased from 0.890 (configuration 3) to 0.937 (configuration 2) when the supercritical bleed mass flow ratio increased from 0.035 to 0.06. Configurations 1 and 5 show comparable performance over the inlet's operating range. The bleed mass flow ratio at critical operation (defined as the terminal shock at the geometric throat) for both configuration 1 and configuration 5 was about 0.064, while the pressure recovery was 0.924 for configuration 1 and 0.917 for configuration 5. At critical operation, configuration 2 required a bleed mass flow ratio of about 0.09 to obtain the high pressure recovery of 0.937. Configuration 3, showing the poorest performance, had a pressure recovery of 0.883 at critical operation with about 0.039 in bleed mass flow ratio. Since most of the performance bleed variation was in the throat region, its effect on distortion is evident. The most acceptable distortion levels were exhibited by configuration 2 over the inlet's operating range. However, even for this configuration, distortions are still higher than desired and the need for vortex generators is evident.

All four configurations show little or no subcritical stable range. The peak and critical conditions coincide for configuration 2. This was probably caused by very little bleed capability immediately upstream of the throat on either the cowl or centerbody. Providing bleed capability upstream of the throat on both the centerbody and cowl would probably increase the inlet's subcritical operating range.

The variation of cowl and centerbody bleed flows at design θ_l and at 0° angle of attack with overall pressure recovery is shown in figure 10. The bleed pattern on the forward centerbody was nearly the same for configurations 1, 2, and 3. Since configuration 3 had no throat bleed, the only centerbody bleed was on the forward centerbody. This pattern provided about 0.004 in bleed mass flow ratio. It is reasonable to assume that for configurations 1 and 2 approximately the same amount of bleed flow was provided at this location. The static pressures in the common centerbody plenum were low enough to maintain choked conditions at the bleed holes. Configuration 5 had a flush slot ahead of the cowl shock impingement point. The amount of bleed provided by the slot is masked by the total centerbody bleed for this configuration. As shown in figure 10(c) the greater portion of the centerbody bleed is taken in the throat region for configurations 1, 2, and 5.

Shown in figure 11 is the effect of various bleed configurations on peak inlet performance ($\alpha = 0^{\circ}$) with variation of the cowl-lip-position parameter θ_l when vortex generators were installed on both the cowl and the centerbody. Configuration 4CCB was tested only with vortex generators. Configurations 1CCB, 3CCB, and 5CCB show little change in peak pressure recovery when θ_l is varied from 24.8° to 25.5°. Configurations 1CCB, 4CCB, and 5CCB have about the same level of pressure recovery for values of θ_l up to 25.4°. Configurations 2CCB and 4CCB experience a sharp degradation in pressure recovery when θ_l is greater than 25.3°. All configurations show about 1- to 1.5-percent loss in pressure recovery with vortex generators installed. However, significant improvement is noted in the distortion level. All configurations experienced distortions less than 0.10 for cowl-lip-position parameters θ_l less than 25.5°. This represents a reduction in distortion levels of about 50 percent for most of the bleed configurations. At a θ_l of 25.4° a slight variation from the expected curves of mass flow ratio and distortion is noted for configuration 4CCB. Examination of the static-pressure distribution throughout the inlet indicated that the terminal shock did not travel to or beyond the inlet's geometric throat at this value of θ_l for the peak condition. As a result, the cowl and centerbody bleed flow was reduced slightly, which increased the distortion level for this condition. In general, installing vortex generators on the cowl and centerbody reduces the peak pressure recovery about 1 to 1.5 percent but with about 50-percent improvement in the distortion levels.

The overall inlet performance at design θ_l and 0° angle of attack with vortex generators installed on the cowl and centerbody is shown in figure 12. The total-pressure recovery levels were reduced at all the inlet operating conditions. However, the distortion levels over the inlet's operating range show significant reductions. The distortion level at critical operation was equal to or better than the desired value of 0.10 for all configurations except configuration 3CCB. The distortion levels ranged from about 0.085 at the peak conditions to about 0.15 at the far supercritical operating conditions for all configurations. The performance of configuration 4CCB is about the same as that of configurations 1CCB and 5CCB. However, configuration 4CCB has slightly higher bleed flows and no subcritical operating range.

The variation of bleed flows at the various locations with total-pressure recovery is shown in figure 13 for the configurations with vortex generators installed and at design θ_l and $\alpha = 0^{\circ}$. The bleed flows are the same as those in figure 10 but reflect the loss in total-pressure recovery due to the vortex generators. The bleed flows for configuration 4CCB are also presented in this figure.

The pitot pressure profiles at the various stations in the inlet are shown in figure 14 for critical operation, in figure 15 for peak operation, and in figure 16 for supercritical operation (all at design θ_l and $\alpha = 0^{\circ}$). Since the vortex generators affected only the flow downstream of the inlet throat, one curve is shown for each of the boundary-layer and throat exit rakes on configurations 1, 2, 3, and 5.

All the configurations tested showed little or no terminal shock travel ahead of the geometric throat at peak recovery. Therefore, the centerbody boundary-layer rake (station 2a) should not be affected and the cowl boundary-layer rake (station 2b) should be affected only slightly at the peak conditions. The centerbody profile for configuration 2 shows a slight thickening over configurations 1, 3, and 5 at critical and peak operation (figs. 14(a) and 15(a)). Examination of the common bleed plenum static pressure showed that the forward centerbody bleed holes of configuration 2 and the forward bleed slot of configuration 5 were not choked at these conditions. However, the static pressure in the common centerbody bleed plenum was still lower than the cone surface values and therefore only reduced the bleed flow at the forward centerbody bleed location. Compartmentation of the centerbody bleed would result in profiles as shown for supercritical operation in figure 16(a).

The pitot pressure profiles after the cowl shock impingement point (centerbody rake station 2a) show less distortion than the profiles of reference 5. The theoretical normal shock total-pressure recovery at this station is 0.852. Configurations 1 and 3 compare favorably at all the operating conditions. Configuration 2 agrees with theory only at the supercritical condition (fig. 16(a)). For the peak and critical operating conditions, configuration 2 shows the largest distortion profiles. Because of the reduced bleed flow at the forward centerbody bleed location of configuration 2 for these conditions, adequate control of the boundary layer at the cowl shock impingement point was not maintained. Configuration 5, which had a flush slot ahead of the cowl impingement point, shows consistently higher normal shock recoveries at this location than do the other configurations. The local flow expansion into the slot may result in a slightly stronger shock on the centerbody surface. Examination of the centerbody static-pressure distributions of configuration 5 showed a slightly larger static-pressure rise at the cowl shock impingement point than for the other configurations. Since the flush slot was located ahead on the cowl shock impingement point and not behind it as for the porous bleed, the manner in which the incident shock reflected could have influenced the normal shock recovery at rake station 2a. However, little or no effect of this local flow difference is seen at the throat exit (station 3). Distributing the cowl compression fan over a short portion of the centerbody in the supersonic diffuser appears to minimize the design error of this inlet.

The boundary-layer profiles at the end of the forward cowl bleed (rake station 2b) are well behaved. These profiles show little or no change at the various operating conditions and match the theoretical normal shock pressure recovery of 0.965 at this station (figs. 14(a), 15(a), and 16(a)). It is interesting to note that despite the change in the forward cowl bleed patterns (localized for configuration 2 to distributed for configurations 1, and 3, and 5) the flow profiles show little change. Since configurations 1 and 5 had less cowl bleed flow than configuration 2, the distributed bleed porosity pattern would be more desirable in this instance.

At the throat exit (station 3), configurations 1, 4, and 5 have about the same centerbody boundary-layer control at critical and peak operation (figs. 14(b) and 15(b)). As expected, configuration 3, with no throat bleed, shows the largest boundary-layer growth, while configuration 2 shows the most effective boundary-layer control on the centerbody (figs. 14(b) and 15(b)). At peak inlet operating conditions, all configurations appear to have the same cowl boundary-layer profiles (fig. 15(b)). For supercritical operation, figure 16(b) illustrates the flow profiles of all configurations for the terminal shock just upstream of the throat exit rakes.

The effect of vortex generators on the diffuser flow is observed at the mid-diffuser rake and the compressor face rakes (parts (c), (d), and (e) of figs. 14, 15, and 16). Inlet operation with no vortex generators shows the effect of bleed amount, especially on the centerbody. The use of vortex generators on the cowl and centerbody effectively flattens the flow profiles for all bleed configurations.

Figure 17 shows the static-pressure distributions on the cowl and centerbody for all configurations tested with vortex generators. The critical, peak, and supercritical inlet operating conditions for each configuration are presented. These conditions represent the range of shock movement through the throat region. In general, configurations 2CCB and 4CCB show the sharpest rise in pressure ratio in the throat at the peak operating condition. This would indicate that the terminal shock train has almost condensed into a plane wave for these larger throat bleed configurations.

The inlet performance through an angle-of-attack range is presented in figure 18. The performance is presented for each bleed configuration with and without vortex generators. The following procedure was used to obtain the angle-of-attack data. For maximum angle of attack at critical inlet operation, (1) the inlet was set at critical for 0° angle of attack; and (2) the model angle of attack was increased until an unstart occurred. Data were recorded for an angle slightly less than the unstart angle of attack. For maximum angle of attack at supercritical inlet operation, (1) the inlet mass flow plug was fully retracted; (2) the model angle of attack was increased until an unstart occurred; (3) the inlet was restarted and the model angle of attack was set slightly less than the unstart angle; (4) the mass flow plug was then closed until the inlet unstarted; (5) after the inlet restarted, the plug was relocated near the position causing unstart. This data point is defined as the peak recovery at that condition. At the angles of attack less than maximum, just the peak pressure recovery condition was determined. All data presented in figure 18 are for these peak pressure recovery conditions.

In general the angle-of-attack range for each bleed configuration was about the same with and without vortex generators. However, the large reduction in distortion at the compressor face over the angle-of-attack range is evident in figure 18 when vortex generators are used. Also, about 1- to 1.5-percent reduction in pressure recovery was observed over the angle-of-attack range with vortex generators. The maximum angle of attack of 3.9° was obtained with configurations 5 and 5CCB. The maximum angle of

attack of the other configurations was about 3.5°. The major difference of these configurations was the flush slot bleed of configurations 5 and 5CCB, which may have been more effective at the angle-of-attack operation.

The maximum angle of attack for critical operation of about 2.5° was exhibited by configurations 3 and 3CCB. These configurations had no throat bleed but had a larger porous bleed pattern on the cowl just upstream of the throat than the other configurations, except configuration 4CCB. As shown in reference 10 and as will be shown in later figures, when the angle of attack was increased, the local internal static pressure on top of the cowl (leeward side of the inlet) ahead of the throat increased to values that are even higher than sonic values. The ability of the forward cowl bleed to support this high pressure affects the angle-of-attack operation. An angle-of-attack limit is reached when the forward cowl bleed plenum pressure reaches the cowl surface pressure at the upstream end of the bleed region ($x/R_c = 2.76$). Examination of the forward cowl bleed plenum pressures of configurations 3CCB and 4CCB indicated that at the maximum angle of attack for critical operation the limit of these parameters was reached. Improvements in angle of attack may be possible if the forward bleed plenum were compartmented and if bleed capability were provided on the centerbody just upstream of the throat.

The high angle-of-attack operation obtained with the focused-compression inlet of reference 5 was not realized with the distributed-compression inlet of this investigation. As shown in reference 12, when the distance from the cowl lip to the inlet's throat was increased, the angle of attack was reduced. However, data presented in reference 10 showed that, for this inlet, angles of attack as high as 7.5° were obtained when centerbody bleed was provided just upstream of the inlet throat.

Inlet Operation with Bypass Flow

All data presented in this section were taken with the overboard and ejector bypass systems operating. The bypass system is the same as in reference 3 and 5. In reference 3 it was shown that at the compressor face the total-pressure profiles on the cowl were improved when the inlet bypass systems were operating. Therefore, the cowl side vortex generators were removed and only the vortex generators on the centerbody were used for this portion of the investigation. Data are presented for configurations 1CB, 3CB, and 4CB. These were selected as possible configurations for later investigations which included testing with the J85-13 turbojet engine. The data presented include (1) performance for constant corrected airflow (bypass door area increase), (2) performance for increasing corrected engine airflow (fixed bypass exit area), (3) steady-state distortion data, (4) dynamic distortion data, and (5) data at maximum unstart angle of attack and at an intermediate angle-of-attack condition. Also, the total-pressure profiles

and static-pressure distributions on the cowl and centerbody are presented for each configuration.

Figure 19(a) presents the overall performance of configuration 4CB with bypass flow at a Mach number of 2.5 and at design θ_l. The peak pressure recovery obtained was 0.932 at a bleed mass flow ratio of 0.081. At the match condition selected, the pressure recovery was 0.916 with a bleed mass flow ratio of 0.063. The apparent stability range is due to positioning the terminal shock between the inlet's geometric throat ($x/R_c = 3.26$) and the throat exit ($x/R_c = 3.72$). The steady-state distortion varied between values of 0.05 and 0.10 for supercritical pressure recoveries within 10 percent of the match-point pressure recovery. For supercritical pressure recoveries lower than this value, a rapid increase in distortion is exhibited. This is associated with flow separation from the sharp turn of the cowl wall where the subsonic diffuser was mated to the existing hardware. The dynamic distortion levels vary from about 0.011 to about 0.05 and are at an acceptable level for most of the operating range of the inlet.

Figures 19(b) and (c) present the off-design performance for configuration 4CB. The off-design Mach number data are presented to show the inlet's performance when the spike is not collapsed but is translated. The design philosophy is to collapse the spike for off-design performance; however, some translation may be desirable in some cases. At Mach 2.30 the peak pressure recovery was 0.944, and at Mach 2.02 the peak recovery was 0.931. The steady-state distortion for both Mach 2.02 and 2.30 was less than 0.10 at the match conditions.

Compressor face total-pressure profiles for the various operating conditions at Mach 2.50 are shown in figure 20. The various data points were selected as representative of the overall inlet operation. Only the total-pressure profiles in the top third of the duct are presented (figs. 20(a) to (f)) since at 0° angle of attack the flow is assumed to be symmetrical. The combination of vortex generators on the centerbody and the operating bypass results in relatively flat profiles, even at the supercritical conditions. The complete compressor face total-pressure profiles are shown in figure 20(g) for the angle-of-attack operation. At rakes 2 and 3 the flow profiles indicate incipient separation near the cowl surface.

The cowl and centerbody static-pressure distributions for each data point of figure 20 at 0° angle of attack are shown in figure 21(a). Shown in figure 21(b) are the static-pressure distributions for the angle-of-attack data presented in figure 20(g). As stated earlier and shown here, at the maximum angle of attack the overcompression on the cowl surface at an x/R_c of about 3.1 approaches sonic conditions. The ability of the bleed system to support this overcompression may determine the angle-of-attack capability of the inlet. For configuration 4CB the maximum angle of attack was 3.33°.

The overall performance of configuration 3CB at Mach 2.50 and design θ_l is presented in figure 22. Configuration 3CB had no throat bleed; however, the peak pressure recovery attained was 0.908. In order to obtain the required match condition of 0.90

pressure recovery, more mass flow was bypassed overboard than for the other configurations. The steady-state distortion exhibited lower values than expected and remained below a value of 0.075 to about 93 percent of the match pressure recovery. The larger bypass flow on the cowl side may have contributed to these low distortions. The dynamic distortion over the inlet's operating range varied from a value of 0.015 to about 0.042.

The compressor face total-pressure profiles for configuration 3CB at the various bypass door settings and engine mass flow ratios are shown in figure 23. The pressure profiles near the match condition appear to be fairly flat (fig. 23(b)). As the inlet operates further supercritical, the flow migrates toward the centerbody, where the higher pressure recoveries are observed (figs. 23(c) to (f)). The total-pressure profiles at a maximum angle of attack of 3.42° and at an intermediate angle of attack of 1.74° are shown in figure 23(g). At an angle of attack of 1.74°, the total-pressure profiles indicate good flow for this condition. At the maximum angle of attack of 3.42°, the flow tends to separate on the cowl at rakes 2 and 3.

The cowl and centerbody static-pressure distributions for the data points of figure 23 are shown in figure 24. The static-pressure distribution at 0° angle of attack is shown in figure 24(a) and that for angle-of-attack operation in figure 24(b). A localized sonic condition is again observed on the cowl at $x/R_c = 2.95$ for operation at an angle of attack of 3.42°.

The overall performance of inlet configuration 1CB at Mach 2.50 at design θ_l with bypass flow is shown in figure 25. The pressure recovery at the match condition (corrected airflow of 15.76 kg/sec) is 0.914 with a bleed mass flow ratio of 0.056 and corresponding steady-state distortion of 0.102. Bypass air always accounted for the remainder of the capture mass flow. At the minimum stable or peak inlet operating condition, the pressure recovery was 0.928 with a bleed mass flow ratio of 0.072. The steady-state distortion at this condition was 0.071. Increasing supercritical operation from the match condition showed the steady-state distortion remaining below 0.10 to about a pressure recovery of 0.830. Further increases resulted in a rapid rise in the distortion level. At the match condition the dynamic distortion was 0.012 and only increased to 0.042 at the far supercritical operating condition.

The compressor face total-pressure profiles of configuration 1CB for the various operating conditions of figure 25 are shown in figure 26. For operation near the match condition, both supercritical and subcritical, the flow profiles appear to be well behaved. At a supercritical pressure recovery of about 0.82, the distortion increases rapidly (see fig. 25). At this point the terminal shock passes downstream of the vortex generators. The total-pressure profiles at angle-of-attack operation are shown in figure 26(i).

The static-pressure distributions on the cowl and centerbody at the various operating conditions of figure 25 are shown in figure 27. As the terminal shock moves downstream and passes over the vortex generators ($x/R_c = 4.0$), the distortion increases, as

indicated in the table in figure 27(a). The static-pressure distributions at angle-of-attack operation are shown in figure 27(b).

The overall performance of configuration 1CB at off-design Mach numbers is presented in figure 28. The peak pressure recovery at Mach 2.58 was 0.878 with a distortion value of 0.081. At Mach 2.30 the peak recovery was 0.944, while at Mach 2.02 the peak recovery was 0.932. The steady-state distortion at the match condition for Mach 2.58 was about 0.11, while at Mach 2.30 and 2.02 the steady-state distortion remained below 0.10.

The total-pressure profiles at the compressor face are presented in figure 29 for various operating conditions at a Mach number of 2.58. For the high distortion values presented (figs. 29(c) and (g)), the profiles indicate the possibility of high circumferential as well as radial distortion. Figure 30 presents the static-pressure distributions on the cowl and centerbody for the various operating conditions at a Mach number of 2.58.

Performance During Restart Cycle

Overall inlet pressure recovery and distortion during the restart cycle at a Mach number of 2.5 are shown in figure 31. Since the centerbody could not be collapsed to restart the inlet, the centerbody was translated during the restart cycle. The data of figure 31 are plotted against the combined engine and overboard bypass mass flow. These data (other than started conditions at design θ_l) were obtained by varying the bypass with the exit plug set for engine match airflow. The inlet was unstarted at the design spike setting by closing the overboard bypass doors. Immediately after unstart the external shock structure was unstable but could be stabilized by opening the overboard bypass doors. The minimum stable condition occurred at a larger bypass door opening than used for critical operation. The minimum stable unstarted pressure recovery at design spike setting was 0.76 and remained within 1 percent of this value as the spike was extended to the restart position. Total-pressure distortions at these conditions varied between values of about 0.07 and 0.11. Minimum stable started total-pressure recovery increased from about 0.79 immediately after restart to 0.914 at the design spike position. Total-pressure distortions for these conditions also varied between values of 0.11 and 0.07.

Cowl and centerbody static-pressure distributions corresponding to the data of figure 31 are presented in figure 32. These data, along with spike position, can provide representative pressure signals for bypass door position control during a restart cycle. With such a control, it should be possible to minimize the distortion and to maximize the pressure recovery during a restart cycle. In actual application to an aircraft, some combination of collapsing and translating the centerbody may be desirable to restart the inlet. The diffuser pressures then would differ from those shown.

Experimental and Predicted Restart Area Ratios

In a variable-geometry, mixed-compression inlet, the initial start or any restart of supersonic flow in the inlet is usually accomplished by increasing the ratio of the throat area to the entering flow area. Mixed-compression inlets have been found to restart with less throat area than would be predicted from a one-dimensional flow analysis assuming uniform flow in front of a normal shock at the cowl lip. Reference 11 suggests a prediction technique based on measurements of flow separation within the unstart flow field just before restart to determine the necessary contraction ratio to restart the inlet. Data for a Mach 3.0 inlet from reference 11, which were used to develop the prediction technique, are presented in figure 33. As shown, the inlet restarts well below normal shock values. Data are also presented for the actual and predicted restart contraction ratios for the present inlet and also for the inlets of references 3 and 5. The inlet of reference 5 used the same design philosophy as the present inlet except that the isentropic compression from the cowl was focused on the centerbody rather than distributed over some centerbody length. As shown in figure 33, the contraction ratios for the present inlet and the inlet of reference 5 were similar. However, slightly more spike translation was required to obtain the contraction ratio needed for restart with the present inlet (6.6 cm compared to 5 cm for the inlet of ref. 5).

Effect of Turbofan Simulation

In this portion of the investigation the flow field ahead of two concentric cylinders was examined experimentally. This particular flow field may be related to duct flow feeding a bypass engine. Data were obtained to determine the effect of bypass ratio change on the duct flow field by simulation of different radial flow splits.

The effect on the flow at the compressor face of various radial flow splits through the two concentric cold pipes shown in figure 7 is discussed on this section. All the data presented in this section were obtained with bleed configuration 4CB. The flow split downstream of the compressor face is defined as the ratio of the mass flow through the annular cold pipe to the mass flow through the core cold pipe and is called the annular- to core-flow ratio. Shown in figure 34 are compressor face total-pressure distortion and dynamic distortion as a function of total-pressure recovery for varying overboard bypass area. In figures 34(a) to (d) data are presented for Mach numbers of 2.5 and 2.58 for 0° and positive angles of attack. As can be seen from figure 34 the distortion parameters were not affected by different annular- to core-flow ratios over the range of Mach numbers and angles of attack tested.

Compressor face total-pressure profiles for various annular- to core-flow ratios are presented in figure 35. All the data of figure 35 were obtained at 0° angle of attack.

For similar inlet operating conditions (same total-pressure recovery and overboard bypass setting), the annular- to core-flow ratio had no effect on the dynamic or steady-state profiles. The data of figure 36 are similar to those of figure 35 but were obtained at various angles of attack. The results again show that the annular- to core-flow ratio did not affect the distribution of total pressure or dynamic distortion.

Shown in figure 37 are the total-pressure profiles at the compressor face and in the concentric cold pipes for the data of figure 35(c). While the profiles in the concentric cold pipes varied drastically the compressor face pressures were unaffected.

SUMMARY OF RESULTS

An investigation was conducted to determine the performance characteristics of an axisymmetric, bicone, mixed-compression inlet system designed for Mach 2.5 operation. Forty percent of the supersonic area contraction occurred internally. The internal compression was accomplished by the cowl-lip oblique shock and by isentropic compression from the cowl surface, which was distributed over a length of centerbody equal to four-tenths of the cowl-lip radius.

Data were obtained at free-stream Mach numbers of 2.02 to 2.58 and at a Reynolds number of 8.2×10^6 per meter. Performance characteristics were obtained for various bleed configurations (1) at 0° angle of attack, (2) at angle of attack, (3) with and without vortex generators, and (4) with and without the inlet's bypass system operating.

Four bleed regions were provided to control the inlet boundary layer. These regions were located forward and aft of the throat on the cowl and the centerbody. The forward centerbody bleed was located just aft of the cowl shock impingement on the centerbody. Without the inlet's bypass system operating, the total supercritical bleed mass flow ratio was varied from a value of 0.035 to 0.06 at the design Mach number of 2.5. The following results were obtained:

1. The peak total-pressure recovery increased from a value of 0.89 to 0.925 when the supercritical bleed mass flow ratio was increased from 0.035 to 0.045. A further increase in pressure recovery to 0.936 was obtained when the supercritical bleed mass flow ratio was increased to 0.06.

2. All throat bleed configurations were located at or downstream of the geometric throat and showed little or no subcritical stability range.

3. The maximum angle of attack obtained before an inlet unstart was about 3.5° for all configurations except configuration 5, which showed a maximum angle of attack of 3.9°.

4. Inlet distortion was substantially reduced when vortex generators were installed on the centerbody and the cowl. A little more than 1-percent loss in total-pressure recovery was observed when vortex generators were used.

5. With an operating bypass system and only centerbody vortex generators installed, the peak pressure recoveries for all configurations remained the same or increased slightly when compared with the no-bypass, no-vortex-generator configuration. Also the steady-state distortion levels were reduced to values below 0.10 for a large part of the inlet's operating range.

6. The dynamic distortion levels varied from about 0.01 at peak and match operating conditions to about 0.05 for the far supercritical operating conditions. This variation was the same for all inlet configurations tested.

7. During the inlet restart cycle, with inlet operation in the unstarted mode, the peak pressure recovery was about 0.76 over the range of cowl-lip-position parameters, and the distortion level varied between 0.065 and 0.125.

8. With the concentric cold pipe installed the annular- to core-flow ratio was varied. The results showed that there was no effect on compressor face total-pressure profile or on dynamic distortion when the annular- to core-flow ratio was varied.

Lewis Research Center,
National Aeronautics and Space Administration,
Cleveland, Ohio, October 21, 1971,
764-74.

APPENDIX - SYMBOLS

A	flow area, m^2
A_c	capture area, 0.1757 m^2
b	fig. 4
H	annulus height at local diffuser station, m
h	distance from centerbody surface, m
M	Mach number
m/m_0	mass flow ratio
P	total pressure, N/m^2
ΔP	fluctuating component of total pressure, N/m^2
p	static pressure, N/m^2
R_c	inlet capture radius, 0.2365 m
r	radius, m
T	total temperature, K
W	weight flow rate, kg/sec
$W\sqrt{\theta/\delta}$	engine-corrected airflow, kg/sec
x	axial location, m
α	angle of attack, deg
δ	$P/(10.13\times10^4\ N/m^2)$
θ	T/288.2 K
θ_l	cowl-lip-position parameter, $\tan^{-1}[1/(x/R)]$
φ	rake circumferential position, deg

Subscripts:

a	annular
av	average
bl	bleed
by	bypass
cr	core

max	maximum
min	minimum
rms	root-mean-square value
t	throat
x	local
0	free stream
5	diffuser exit station
6	dynamic rake station

REFERENCES

1. Sorensen, Norman E.; and Smeltzer, Donald B.: Investigation of a Large-Scale Mixed-Compression Axisymmetric Inlet System Capable of High Performance at Mach Numbers 0.6 to 3.0. NASA TM X-1507, 1968.

2. Cubbison, Robert W.; Meleason, Edward T.; and Johnson, David F.: Effect of Porous Bleed in a High-Performance Axisymmetric, Mixed-Compression Inlet at Mach 2.50. NASA TM X-1692, 1968.

3. Cubbison, Robert W.; Meleason, Edward T.; and Johnson, David F.: Performance Characteristics From Mach 2.58 to 1.98 of an Axisymmetric Mixed-Compression Inlet System With 60-Percent Internal Contraction. NASA TM X-1739, 1969.

4. Anderson, Warren E.; and Wong, Norman D.: Experimental Investigation of a Large-Scale, Two-Dimensional, Mixed-Compression Inlet System: Performance at Design Conditions, M + 3.0. NASA TM X-2016, 1970.

5. Wasserbauer, Joseph F.; and Choby, David A.: Mach 2.5 Performance of a Bicone Inlet With Internal Focused Compression and 40-Percent Internal Contraction. NASA TM X-2294, 1971.

6. Anderson, Bernhard H.: Design of Supersonic Inlets by a Computer Program Incorporating the Method of Characteristics. NASA TN D-4960, 1969.

7. Coltrin, Robert E.; and Calogeras, James E.: Supersonic Wind Tunnel Investigation of Inlet-Engine Compatability. Paper 69-487, AIAA, June 1969.

8. Obery, Leonard J.; and Stitt, Leonard E.: Performance of External-Internal Compression Inlet With Abrupt Internal Turning at Mach Numbers 3.0 to 2.0. NACA RM E57HO7a, 1957.

9. Calogeras, James E.: Experimental Investigation of Dynamic Distortion in a Mach 2.50 Inlet With 60-Percent Internal Contraction and Its Effect on Turbojet Stall Margin. NASA TM X-1842, 1969.

10. Bowditch, David N.; Coltrin, Robert E.; Sanders, Bobby W.; Sorensen, Norman E.; and Wasserbauer, Joseph F.: Supersonic Cruise Inlets. Aircraft Propulsion. NASA SP-259, 1971, pp. 283-312.

11. Mitchell, Glenn A.; and Cubbison, Robert W.: An Experimental Investigation of the Restart Area Ratio of a Mach 3.0 Axisymmetric Mixed-Compression Inlet. NASA TM X-1547, 1968.

TABLE I. - INLET COORDINATES

Centerbody		Cowl		Centerbody		Cowl	
x/R_c	r/R_c	x/R_c	r/R_c	x/R_c	r/R_c	x/R_c	r/R_c
0	0	2.1167	1.0000	4.900	0.5448	4.600	0.9374
		2.150	1.0028	4.950	.5320	4.650	.9324
10^o conical section		2.200	1.0070	5.000	.5195	4.700	.9276
1.0323	0.1820	2.250	1.0111	5.050	.5075	4.750	.9232
		2.300	1.0154	5.100	.4983	4.800	.9191
18.5^o conical section		2.350	1.0193	5.150	.4895	4.850	.9153
		2.400	1.0228	5.200	.4805	4.900	.9120
2.7620	0.7608	2.450	1.0261	5.250	.4715	4.950	.9087
2.8000	.7696	2.500	1.0290	5.300	.4622	5.000	.9050
2.850	.7794	2.550	1.0317	5.350	.4534	5.050	.9044
2.900	.7874	2.600	1.0340	5.400	.4444	5.100	.9049
2.950	.7937	2.650	1.0360	5.450	.4352	5.150	.9058
3.000	.7986	2.700	1.0373	5.500	.4264	5.200	.9071
3.050	.8025	2.750	1.0382	5.550	.4175	5.250	.9086
3.100	.8045	2.800	1.0386	5.600	.4085	5.300	.9102
3.150	.8043	2.850	1.0386	5.650	.3995	5.350	.9118
3.200	.8030	2.900	1.0381	5.700	.3900	5.400	.9132
3.250	.8015	2.950	1.0370	5.750	.3815	5.450	.9145
3.300	.8000	3.000	1.0356	5.800	.3732	5.500	.9157
3.350	.7982	3.050	1.0337	5.850	.3650	5.550	.9166
3.400	.7964	3.100	1.0320	5.900	.3566	5.600	.9173
3.450	.7944	3.150	1.0304	5.950	.3488	5.650	.9177
3.500	.7925	3.200	1.0290	6.000	.3412	5.700	.9179
3.550	.7906	3.250	1.0275	6.050	.3339		
3.600	.7886	3.300	1.0262	6.100	.3266	Cylinder	
3.650	.7862	3.350	1.0251	6.150	.3196	6.1747	0.9179
3.700	.7834	3.400	1.0239	6.200	.3130		
3.750	.7798	3.450	1.0227	6.250	.3068	Bypass gap	
3.800	.7757	3.500	1.0215	6.300	.2985		
3.850	.7711	3.550	1.0204	6.350	.2910	6.7847	0.8868
3.900	.7655	3.600	1.0192	6.400	.2845	6.800	.8865
3.950	.7590	3.650	1.0176	6.450	.2780	6.850	.8855
4.000	.7513	3.700	1.0160	6.500	.2716	6.900	.8846
4.050	.7426	3.750	1.0144	6.550	.2655	6.950	.8837
4.100	.7330	3.800	1.0124	6.600	.2597	7.000	.8823
4.150	.7230	3.850	1.0100	6.650	.2545	7.050	.8805
4.200	.7133	3.900	1.0071	6.700	.2501	7.100	.8785
4.250	.7036	3.950	1.0037	6.750	.2464	7.150	.8760
4.300	.6924	4.000	1.0000	6.800	.2430	7.200	.8734
4.350	.6810	4.050	.9955	6.850	.2410	7.250	.8707
4.400	.6692	4.100	.9908	6.900	.2400	7.300	.8677
4.450	.6577	4.150	.9858	6.950	.2396	7.350	.8654
4.500	.6455	4.200	.9808	7.000	.2394	7.400	.8639
4.550	.6330	4.250	.9756			7.450	.8631
4.600	.6205	4.300	.9702	Cylinder		7.500	.8627
4.650	.6085	4.350	.9659			7.550	.8623
4.700	.5960	4.400	.9595	7.8858	0.2394	7.600	.8621
4.750	.5825	4.450	.9538				
4.800	.5700	4.500	.9481			Cylinder	
4.850	.5573	4.550	.9426			7.8858	0.8621

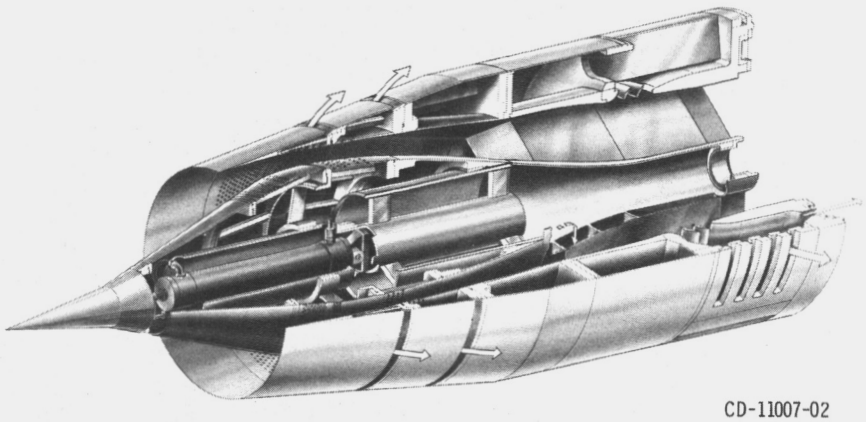

CD-11007-02

(c) Isometric view of model.

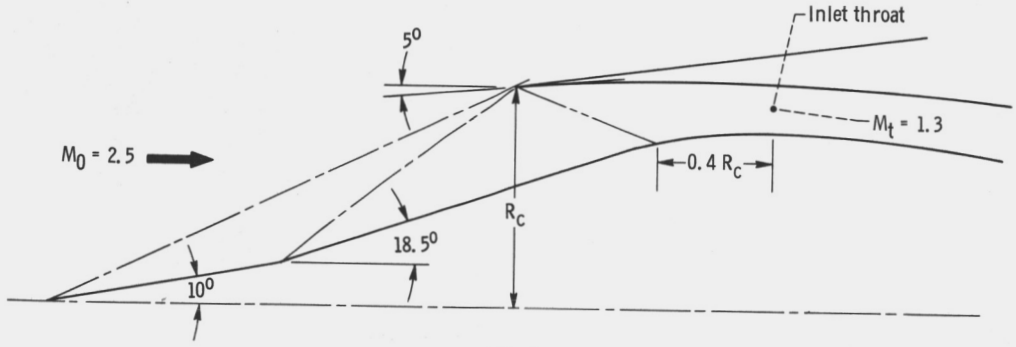

(d) Sketch of model.

Figure 1. - Concluded.

TABLE II. - LOCATIONS OF STATIC-PRESSURE TAPS

Top centerline cowl statics		Top centerline centerbody statics	
x/R_c	x/R_c	x/R_c	x/R_c
2.361	3.369	0.859	3.247
2.468	3.410	.966	3.285
2.576	3.440	1.074	3.317
2.683	3.507	1.181	3.352
2.747	3.542	2.308	3.389
2.778	3.585	2.603	3.440
2.809	3.628	2.669	3.488
2.852	3.671	2.716	3.542
2.882	3.714	2.751	3.585
2.926	3.794	2.775	3.628
2.969	3.875	2.802	3.671
3.009	3.950	2.834	3.714
3.045	4.191	2.857	3.794
3.088	4.519	2.893	3.875
3.130	4.846	2.962	3.950
3.166	5.228	3.029	4.192
3.209	5.529	3.102	4.519
3.247	6.119	3.140	4.846
3.281	6.742	3.173	5.227
3.317	7.311	3.209	7.311

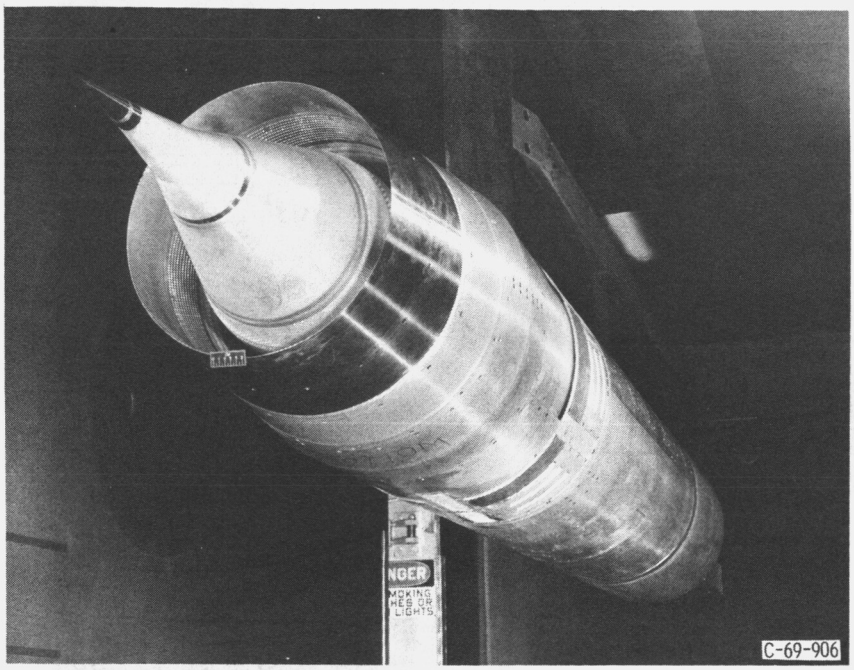

(a) Installation in 10- by 10-Foot Supersonic Wind Tunnel.

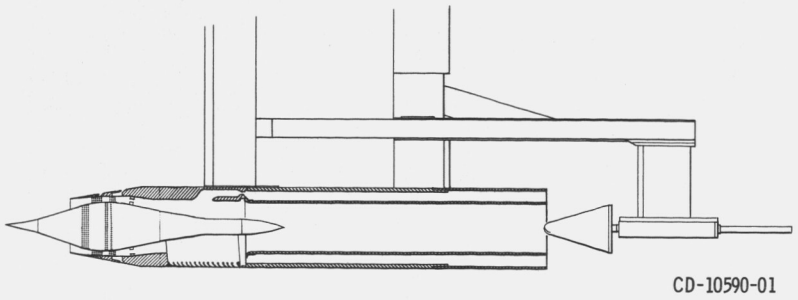

(b) Cold-pipe assembly.

Figure 1. - Distributed-compression inlet model.

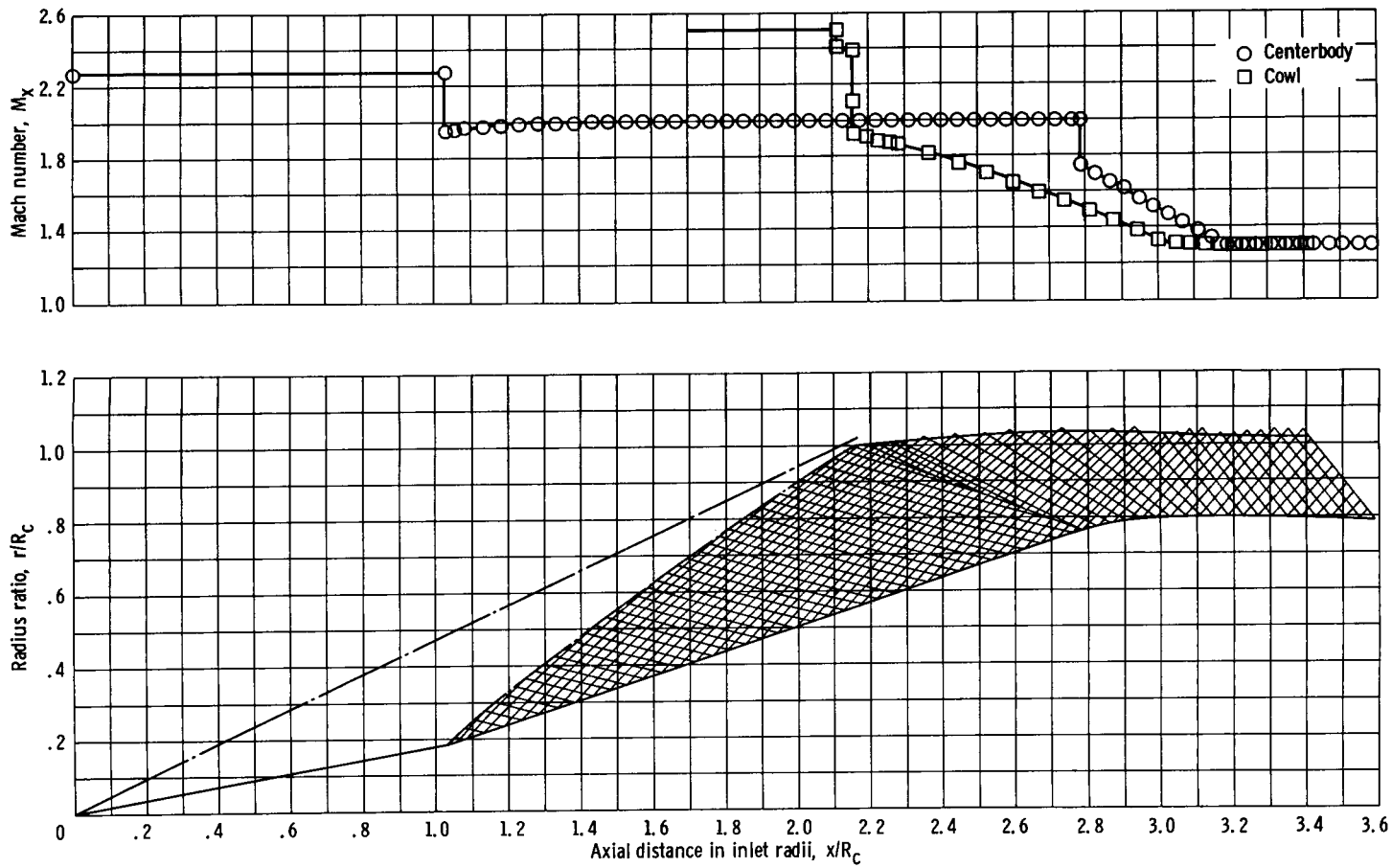

Figure 2. - Characteristic solution.

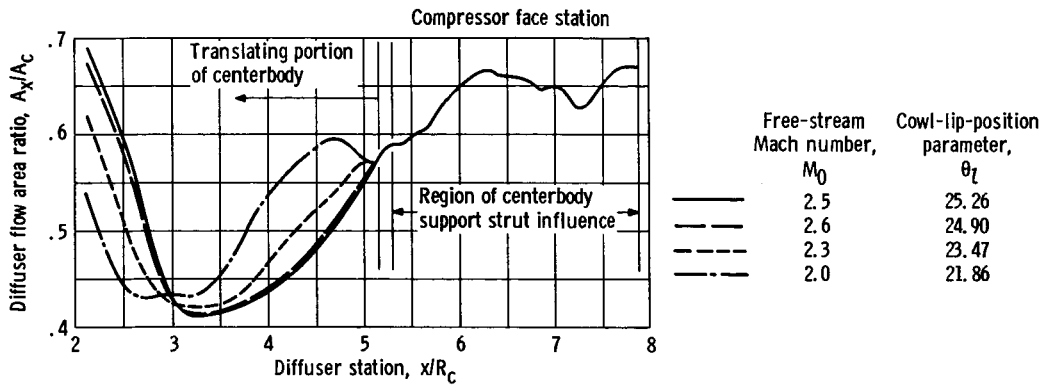

Figure 3. - Diffuser area variation.

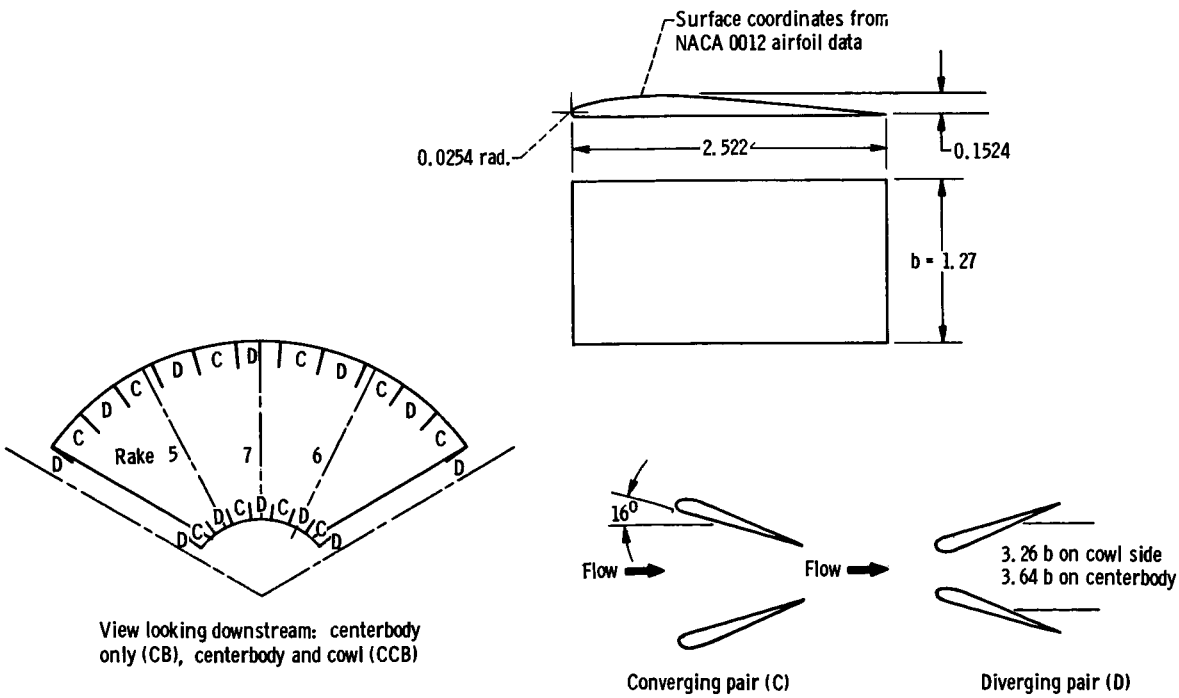

Figure 4. - Vortex generator design. All dimensions in centimeters.

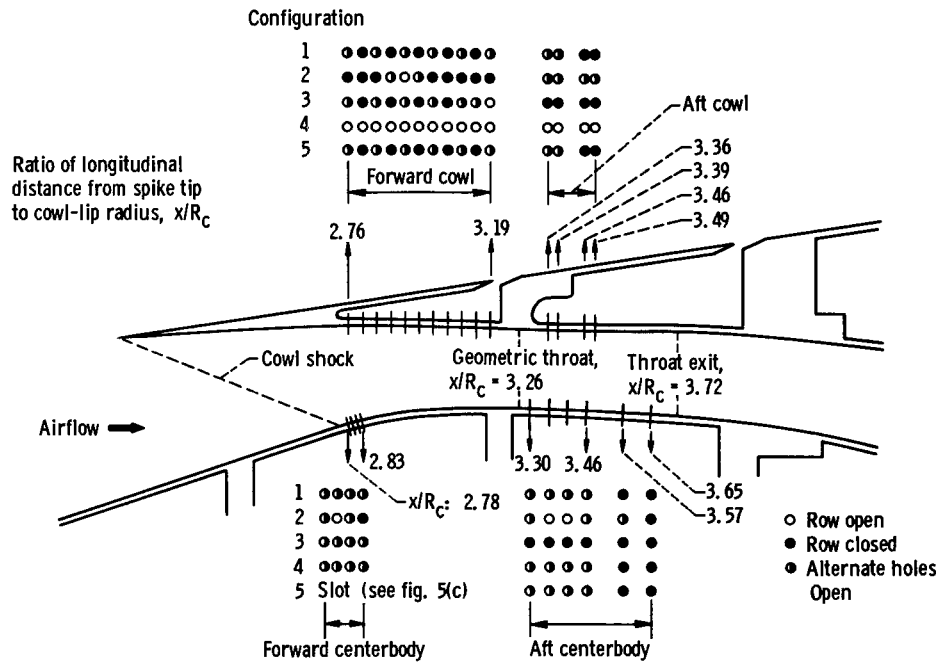

(a) Inlet bleed locations.

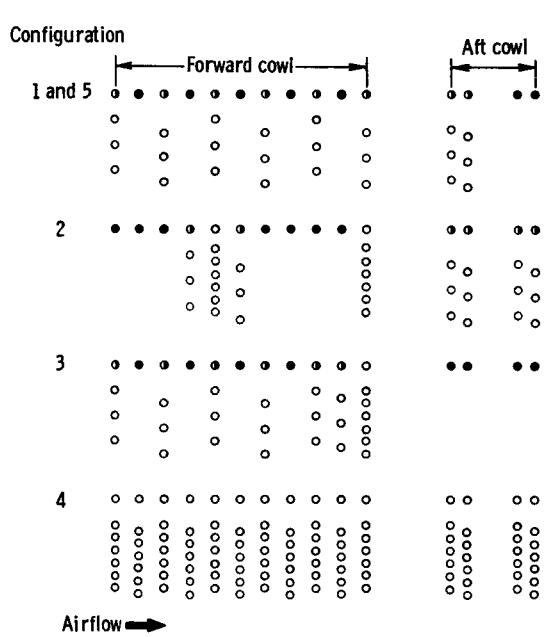

(b) Cowl bleed patterns.

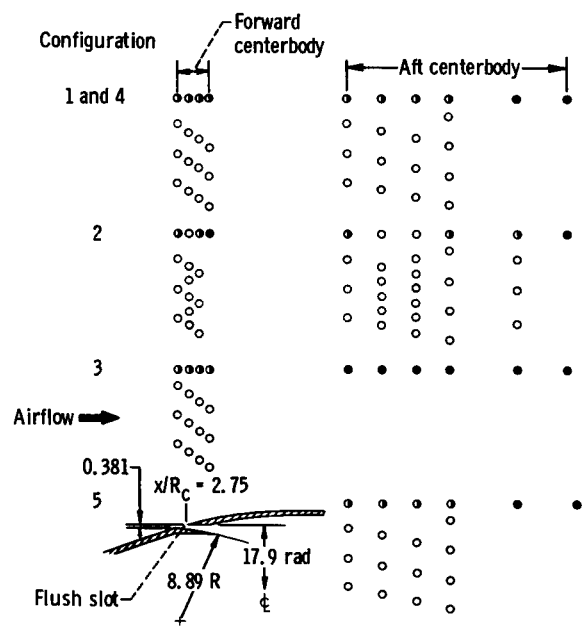

(c) Centerbody bleed pattern.

Figure 5. - Performance bleed configurations.

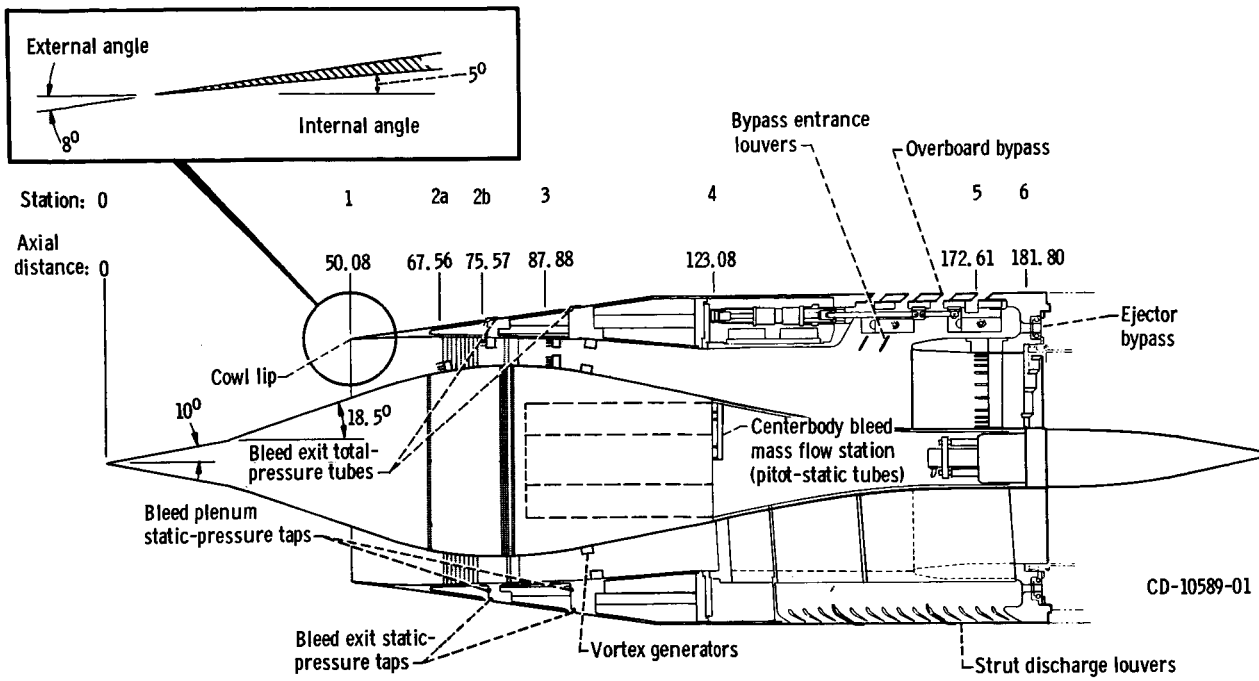

(a) Total-pressure-tube rake locations.

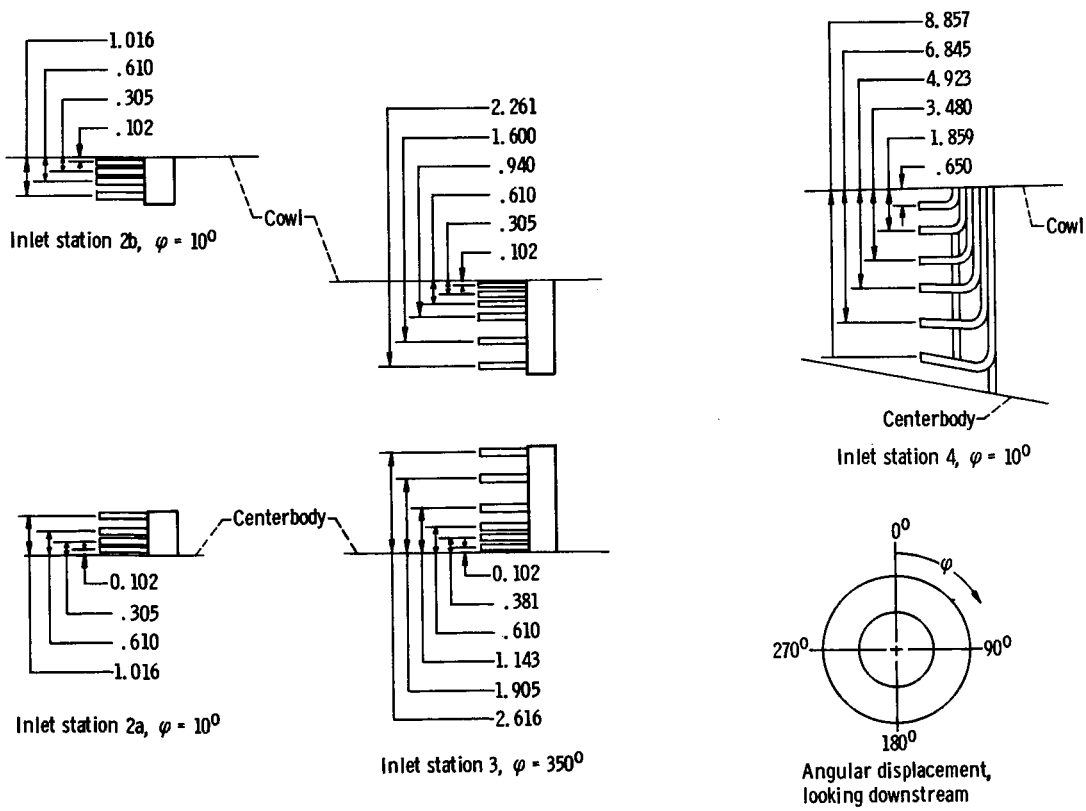

(b) Diffuser total-pressure rakes, at circumferential rake position φ.

Figure 6. - Pressure instrumentation. All dimensions in centimeters.

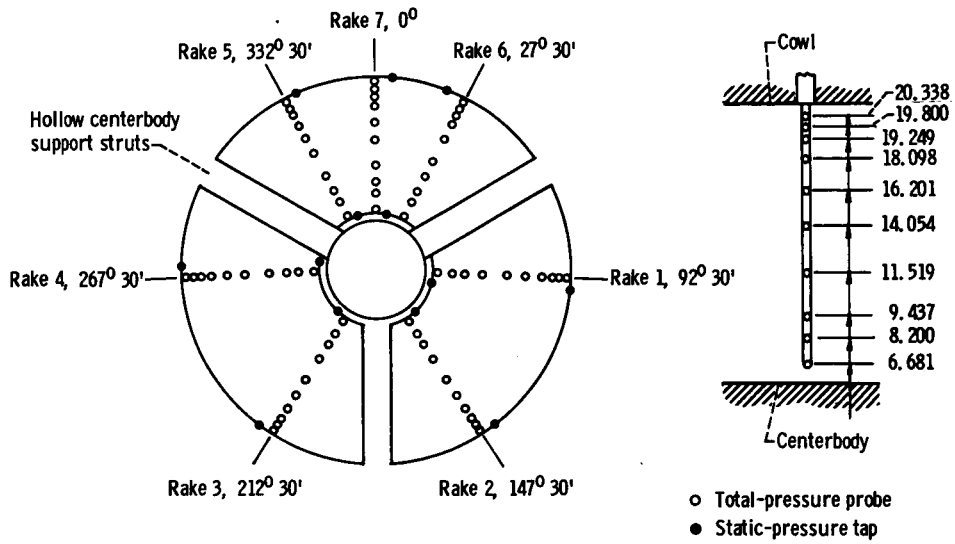

(c) Compressor face steady-state pressure instrumentation, at station 5 (looking downstream).

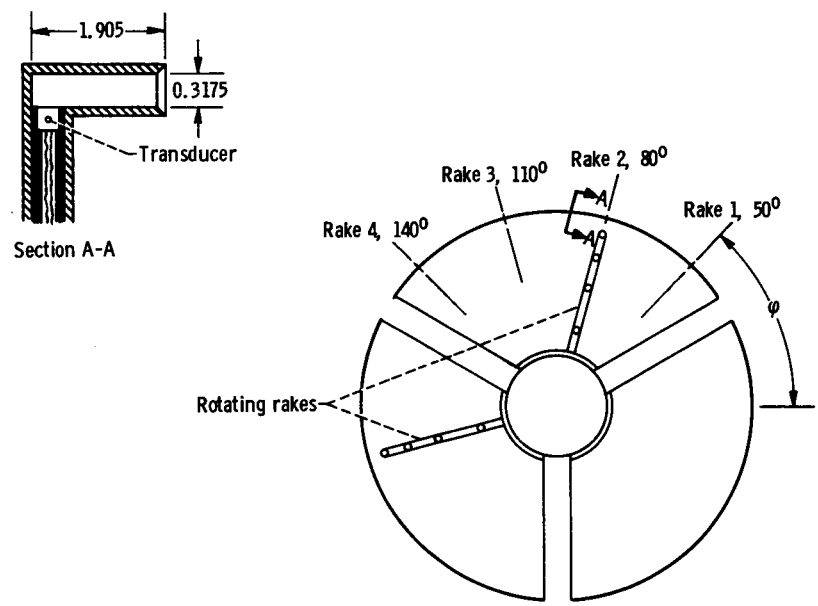

(d) Compressor face dynamic instrumentation, at station 6 (looking downstream).

Figure 6. - Concluded.

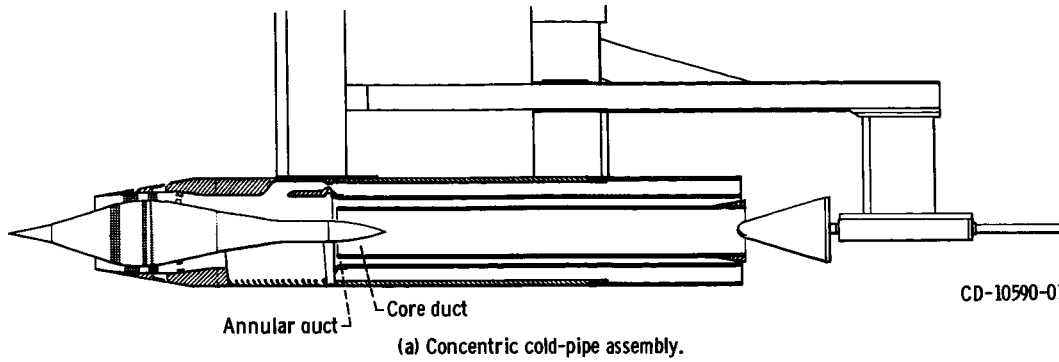

(a) Concentric cold-pipe assembly.

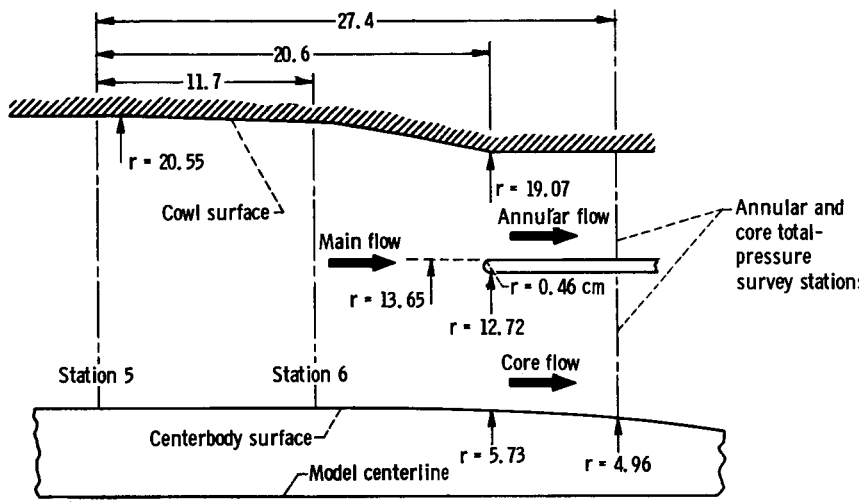

(b) Details of region of flow split. Annulus area, 556.92 square centimeters; core area, 405.59 square centimeters.

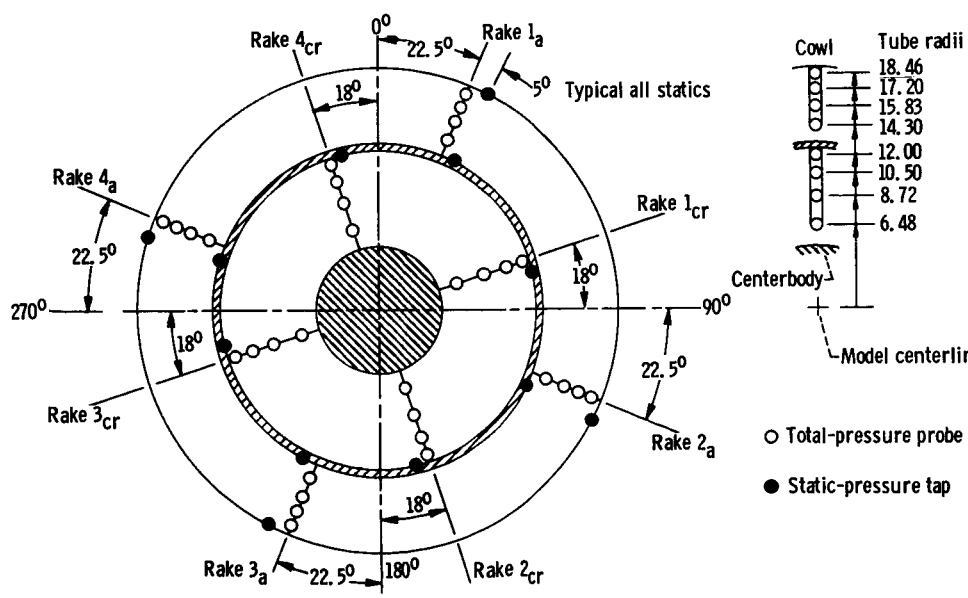

(c) Concentric cold-pipe steady-state instrumentation, looking downstream.

Figure 7. - Details of concentric cold-pipe model. All dimensions in centimeters.

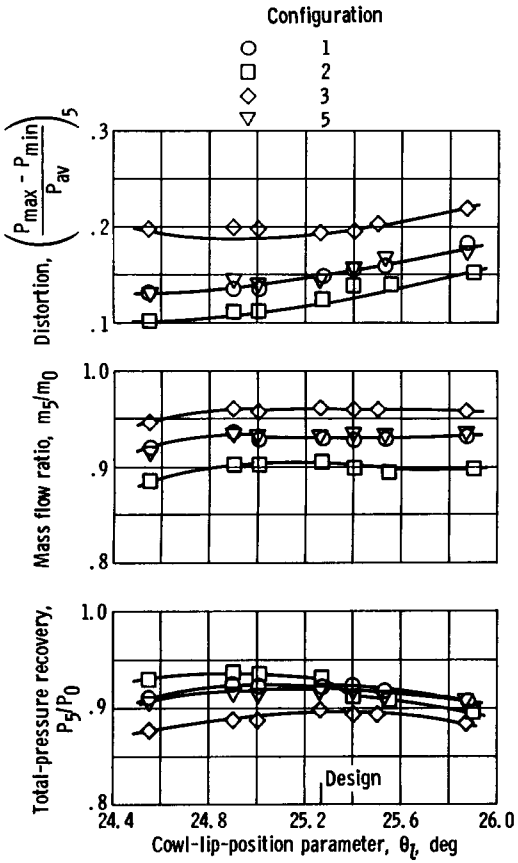

Figure 8. - Effect of spike position on peak inlet performance for various bleed locations. No vortex generators; angle of attack, 0^0; free-stream Mach number, 2.5.

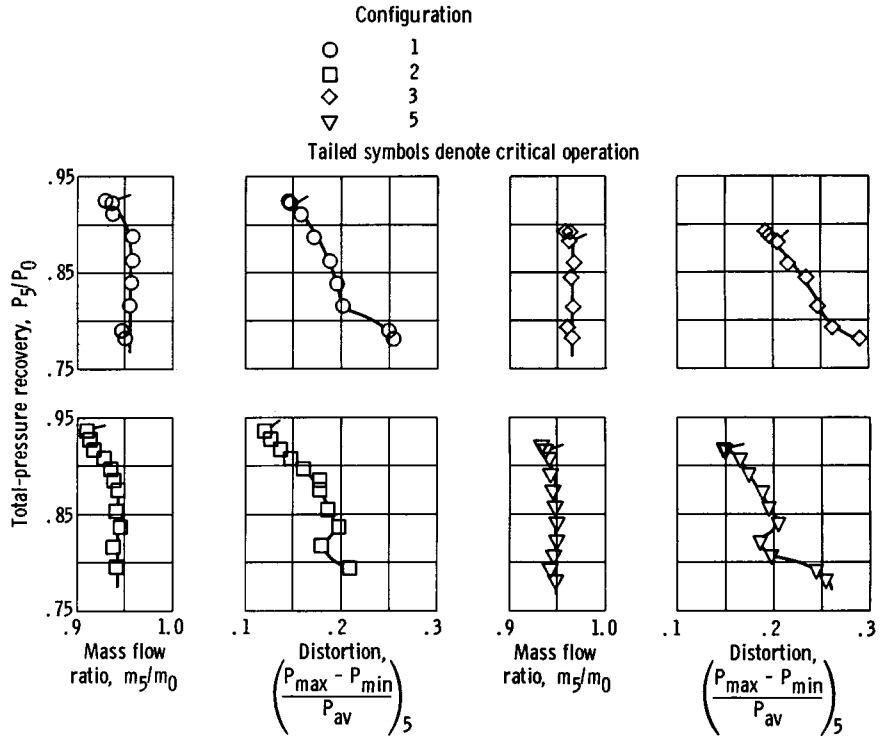

Figure 9. - Effect of bleed on overall inlet performance. No vortex generators; angle of attack, 0; free-stream Mach number, 2.5; cowl-lip-position parameter, 25.26^0.

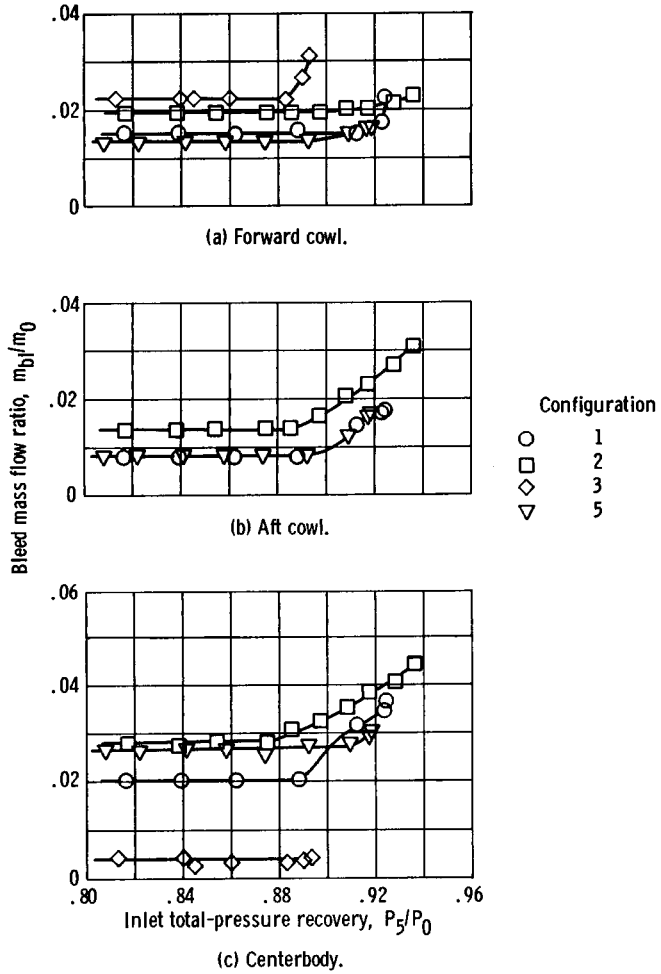

Figure 10. - Variation of bleed flow with overall inlet recovery. No vortex generators; angle of attack, 0^0; cowl-lip-position parameter, 25.26^0; free-stream Mach number, 2.5.

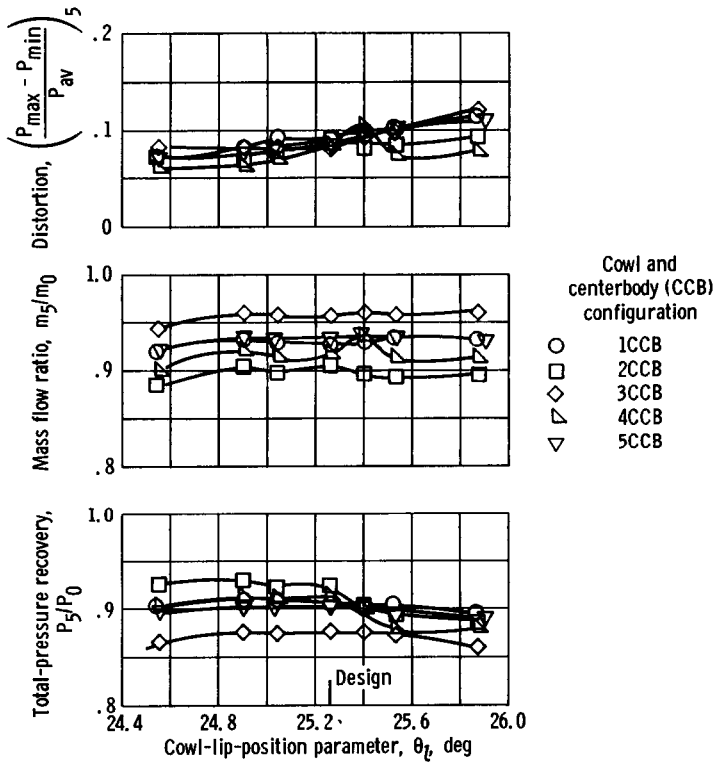

Figure 11. - Effect of spike position on peak inlet performance for various bleed locations. Vortex generators on cowl and centerbody; angle of attack, 0^0; free-stream Mach number, 2.5.

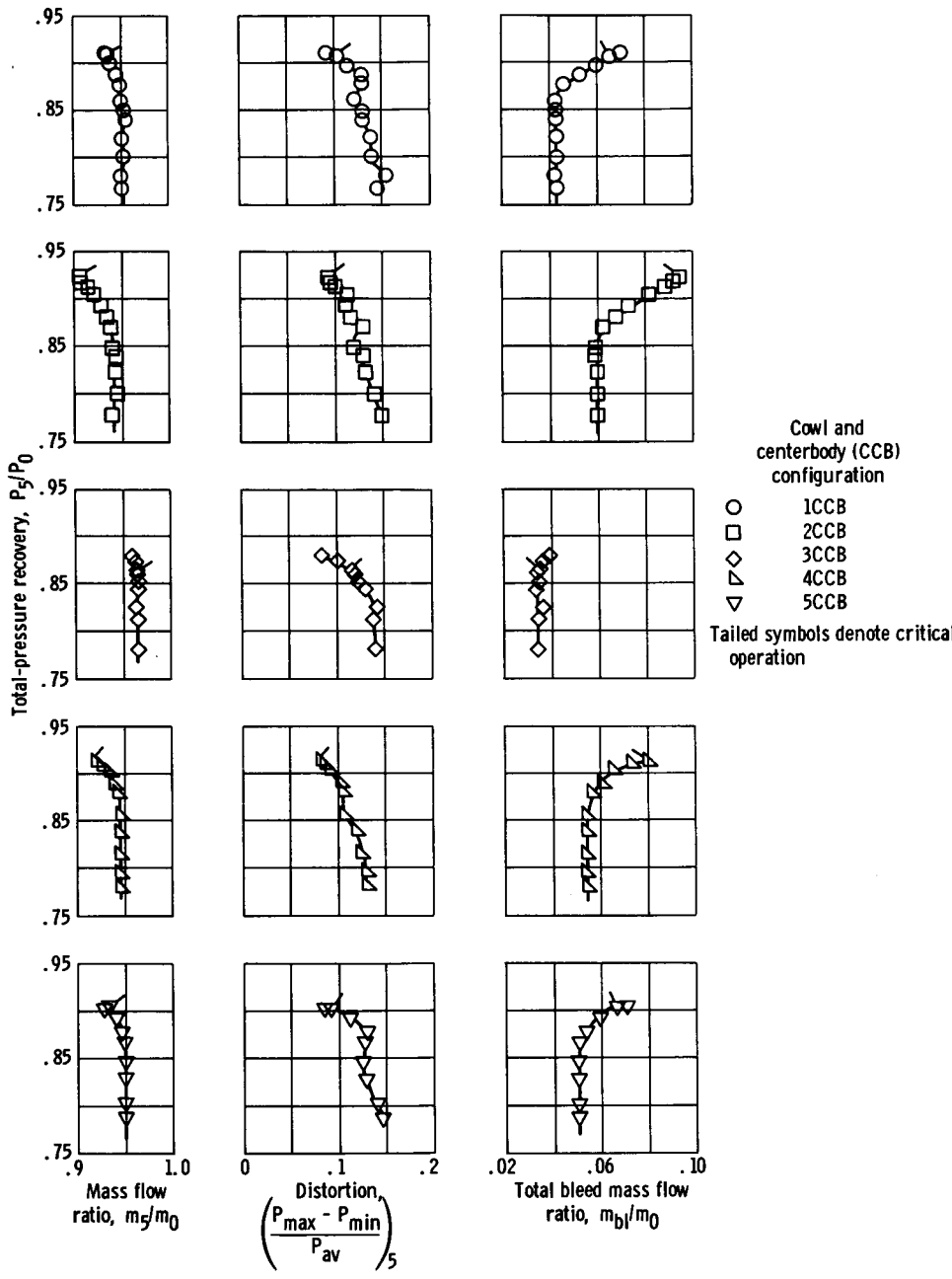

Figure 12. - Overall inlet performance. Vortex generators on cowl and centerbody; angle of attack, 0°; cowl-lip-position parameter, 25.26°; free-stream Mach number, 2.5.

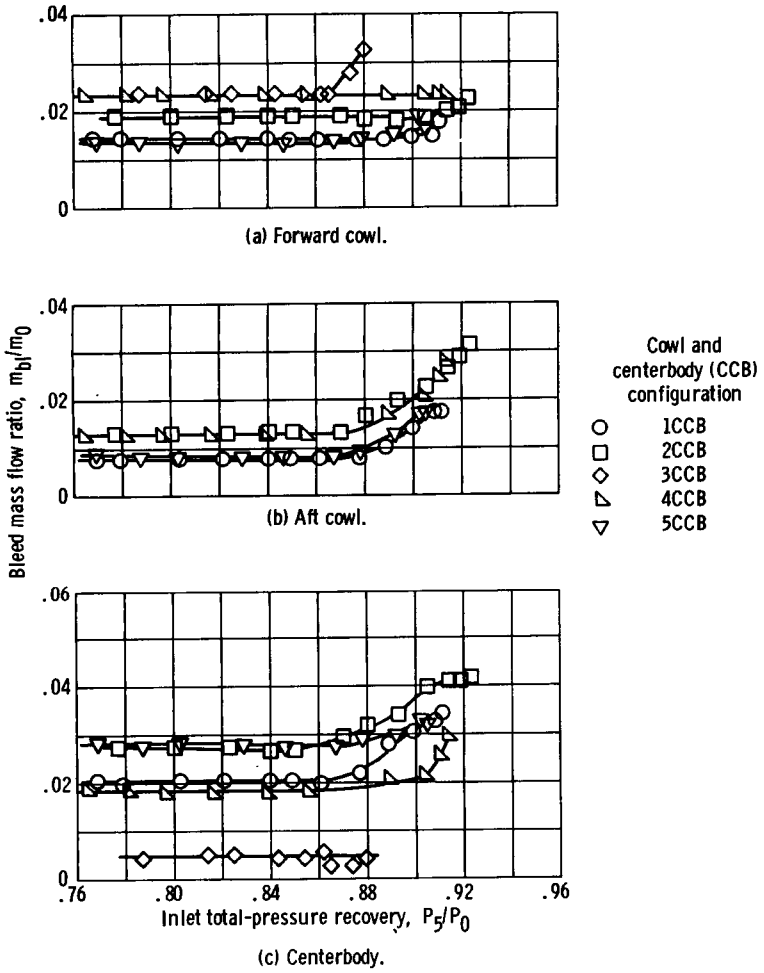

Figure 13. - Variation of bleed flow with overall inlet recovery. Vortex generators on cowl and centerbody; angle of attack, 0^0; cowl-lip-position parameter, 25.26^0; free-stream Mach number, 2.5.

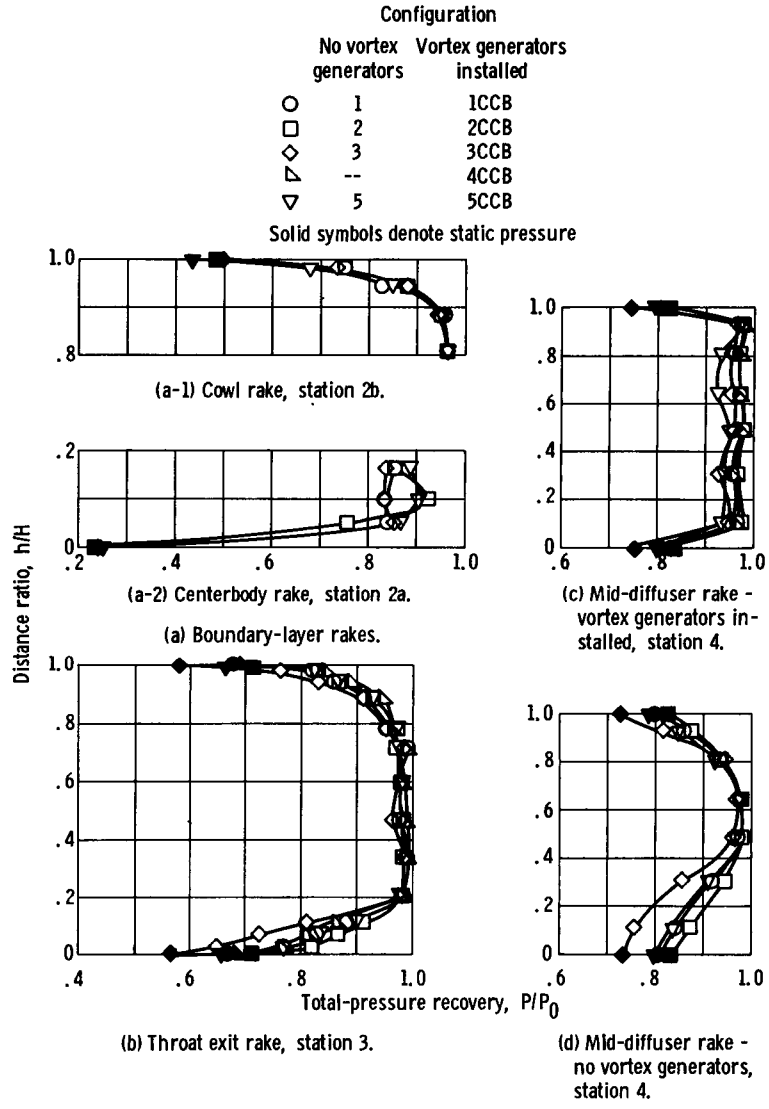

Figure 14. - Diffuser performance for critical inlet operation. Angle of attack, 0^0; cowl-lip-position parameter, 25.26^0; free-stream Mach number, 2.5.

Solid symbols denote static pressure

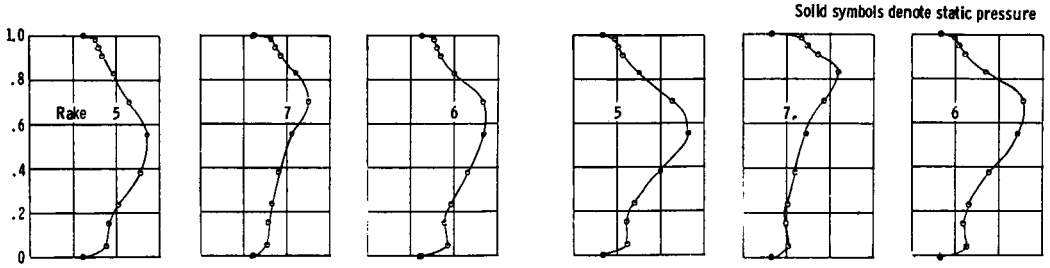

(e-1) Configuration 1; m_5/m_0 = 0.936; P_5/P_0 = 0.924; distortion = 0.148.

(e-5) Configuration 3; m_5/m_0 = 0.961; P_5/P_0 = 0.883; distortion = 0.204.

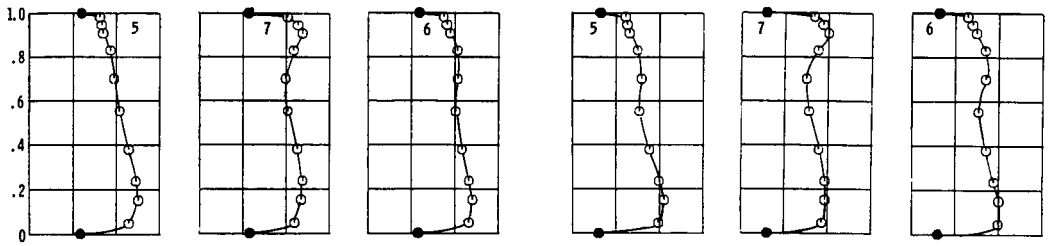

(e-2) Configuration 1CCB; m_5/m_0 = 0.935; P_5/P_0 = 0.908; distortion = 0.102.

(e-6) Configuration 3CCB; m_5/m_0 = 0.964; P_5/P_0 = 0.865; distortion = 0.117.

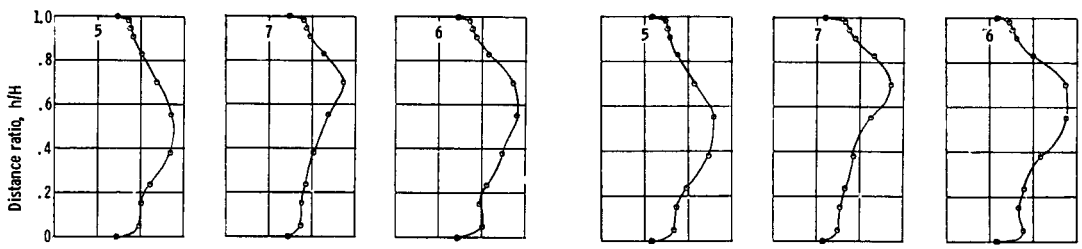

(e-3) Configuration 2; m_5/m_0 = 0.910; P_5/P_0 = 0.937; distortion = 0.121.

(e-7) Configuration 5; m_5/m_0 = 0.937; P_5/P_0 = 0.917; distortion = 0.148.

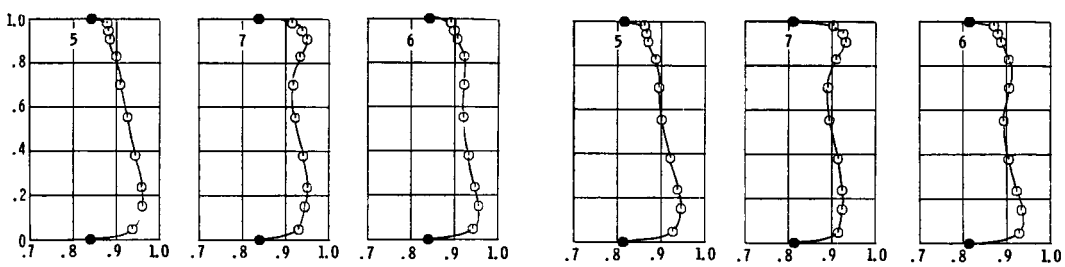

(e-4) Configuration 2CCB; m_5/m_0 = 0.906; P_5/P_0 = 0.924; distortion = 0.092.

(e-8) Configuration 5CCB; m_5/m_0 = 0.938; P_5/P_0 = 0.905; distortion = 0.094.

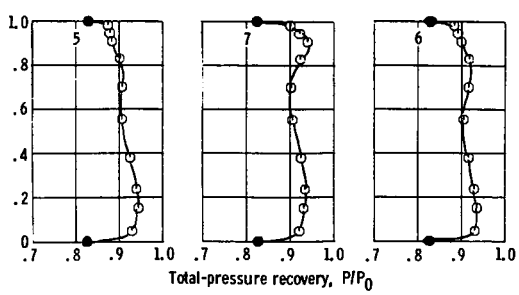

(e-9) Configuration 4CCB; m_5/m_0 = 0.919; P_5/P_0 = 0.913; distortion = 0.084.

(e) Compressor face rake, station 5; diffuser performance for various mass flow ratios m_5/m_0, total pressure recoveries P_5/P_0, and distortions at station 5.

Figure 14. - Concluded.

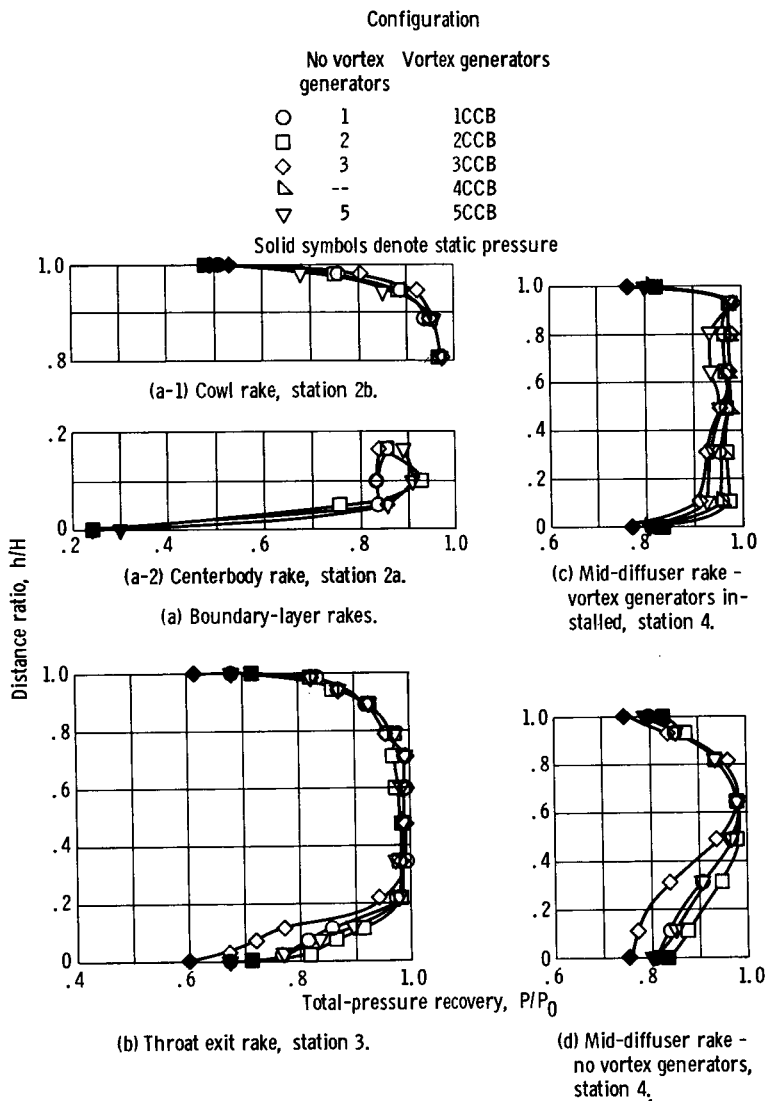

Figure 15. - Diffuser performance for peak inlet operation. Angle of attack, 0^{0}; cowl-lip-position parameter, 25.26^{0}; free-stream Mach number, 2.5.

Solid symbols denote static pressures

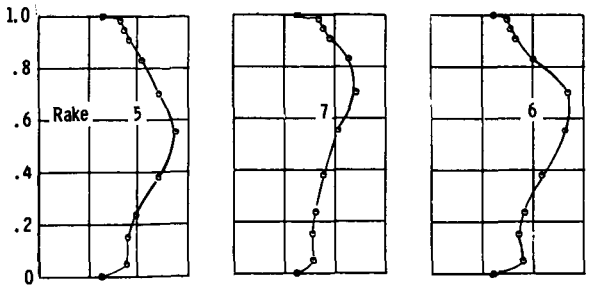

(e-1) Configuration 1; m_5/m_0 = 0.929; P_5/P_0 = 0.924; distortion = 0.147.

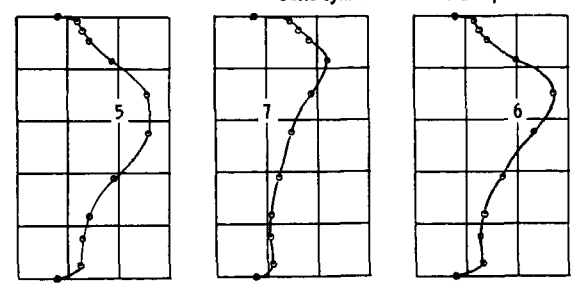

(e-3) Configuration 3; m_5/m_0 = 0.958; P_5/P_0 = 0.894; distortion = 0.193.

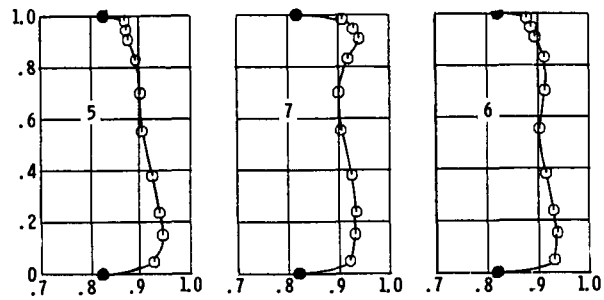

(e-2) Configuration 1CCB; m_5/m_0 = 0.935; P_5/P_0 = 0.911; distortion = 0.092.

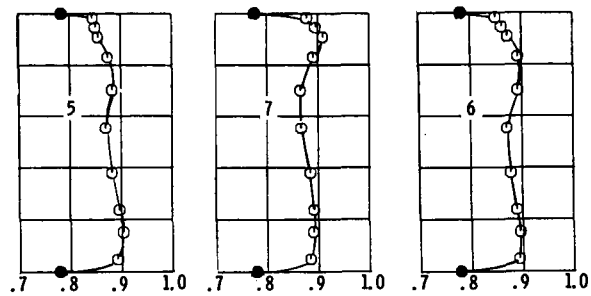

(e-4) Configuration 3CCB; m_5/m_0 = 0.961; P_5/P_0 = 0.880; distortion = 0.085.

Distance ratio, h/H

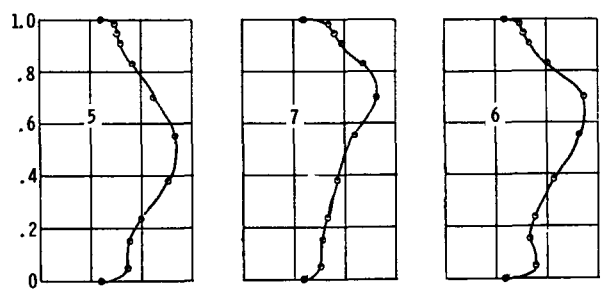

(e-5) Configuration 5; m_5/m_0 = 0.936; P_5/P_0 = 0.919; distortion = 0.147.

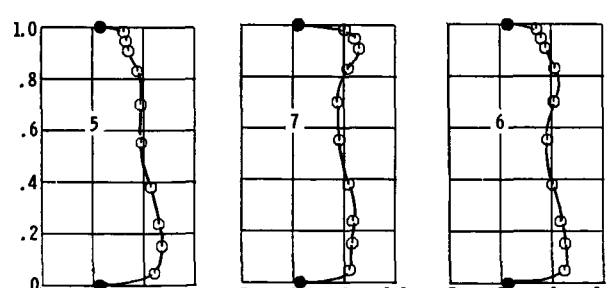

Total-pressure recovery, P/P_0

(e-6) Configuration 5CCB; m_5/m_0 = 0.933; P_5/P_0 = 0.903; distortion = 0.087.

(e) Compressor face rake, station 5: diffuser performance for various mass flow ratios m_5/m_0, total-pressure recoveries P_5/P_0, and distortions at station 5.

Figure 15. - Concluded.

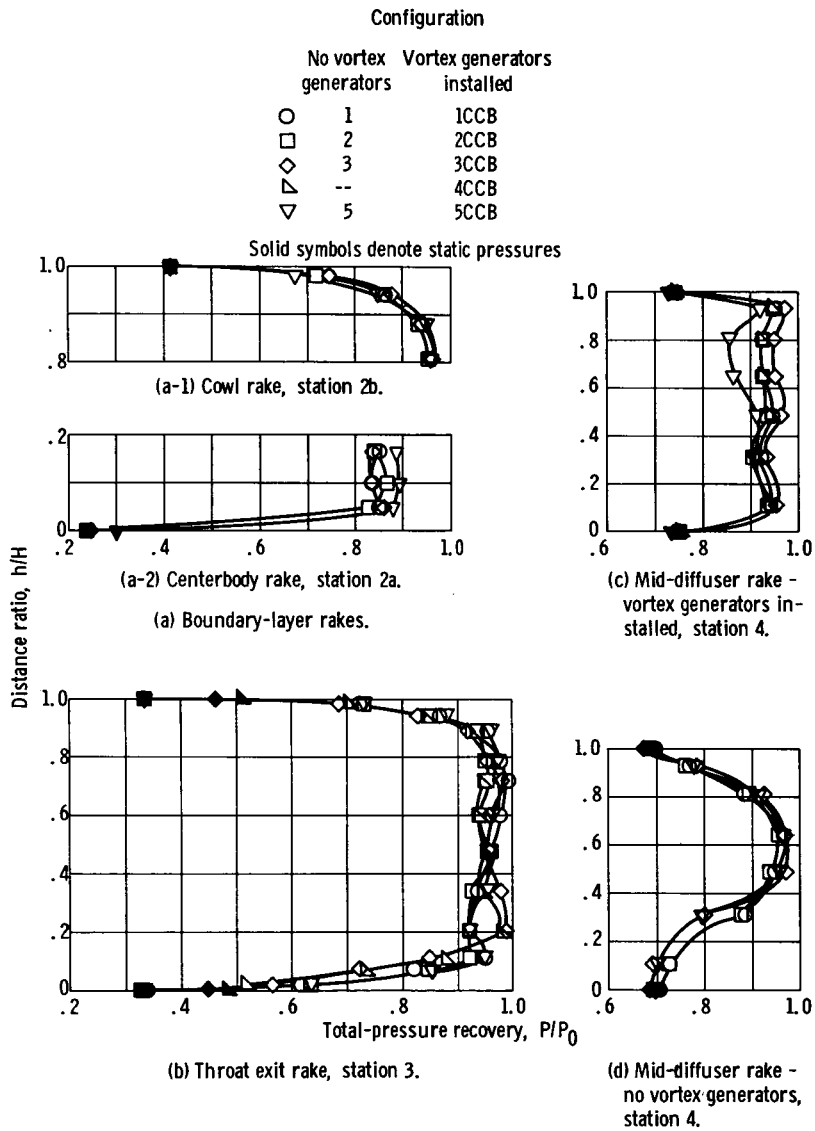

Figure 16. - Diffuser performance for supercritical inlet operation. Angle of attack, 0^{o}; cowl-lip-position parameter, 25.26^{o}; free-stream Mach number, 2.5.

Solid symbols denote static pressure

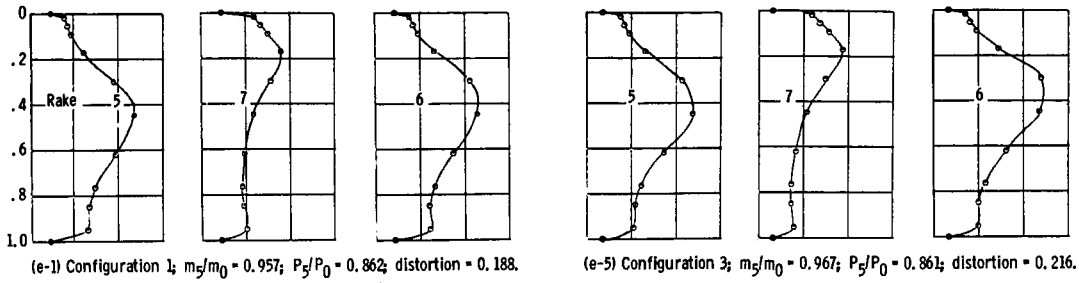

(e-1) Configuration 1; m_5/m_0 = 0.957; P_5/P_0 = 0.862; distortion = 0.188.

(e-5) Configuration 3; m_5/m_0 = 0.967; P_5/P_0 = 0.861; distortion = 0.216.

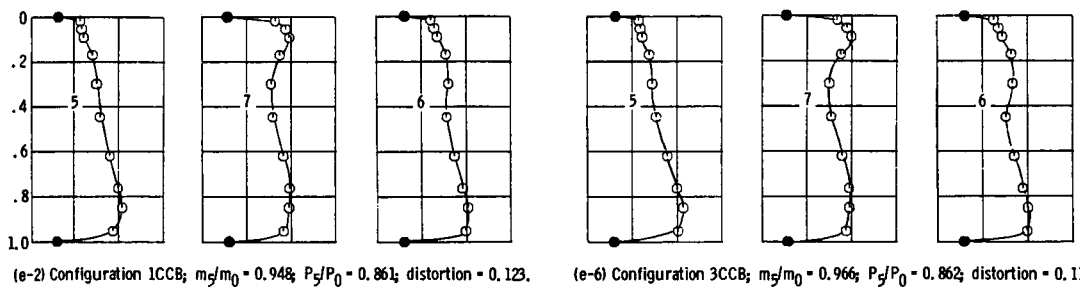

(e-2) Configuration 1CCB; m_5/m_0 = 0.948; P_5/P_0 = 0.861; distortion = 0.123.

(e-6) Configuration 3CCB; m_5/m_0 = 0.966; P_5/P_0 = 0.862; distortion = 0.119.

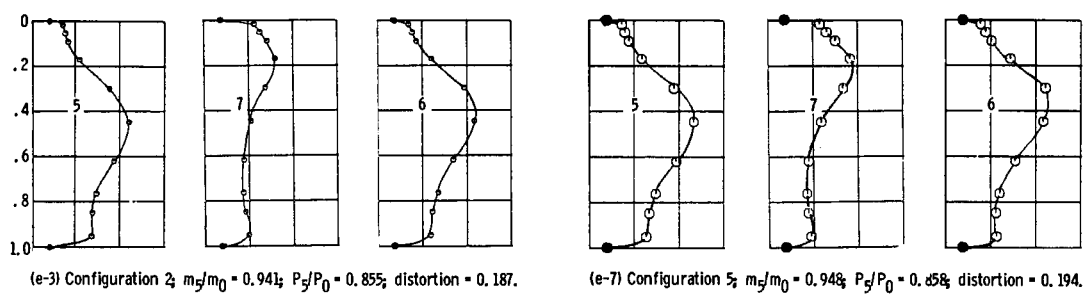

(e-3) Configuration 2; m_5/m_0 = 0.941; P_5/P_0 = 0.855; distortion = 0.187.

(e-7) Configuration 5; m_5/m_0 = 0.948; P_5/P_0 = 0.858; distortion = 0.194.

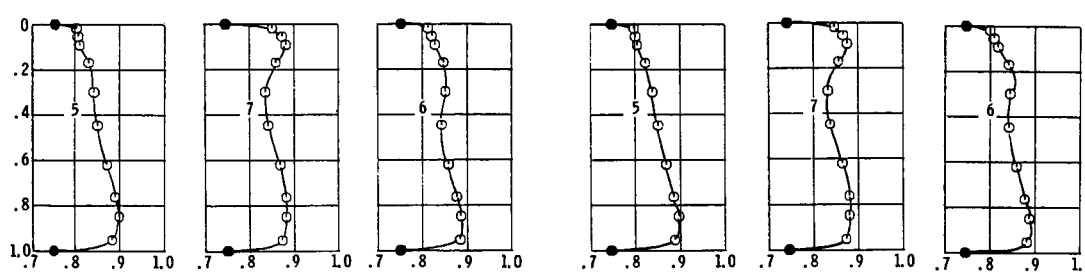

(e-4) Configuration 2CCB; m_5/m_0 = 0.940; P_5/P_0 = 0.850; distortion = 0.119.

(e-8) Configuration 5CCB; m_5/m_0 = 0.948; P_5/P_0 = 0.847; distortion = 0.126.

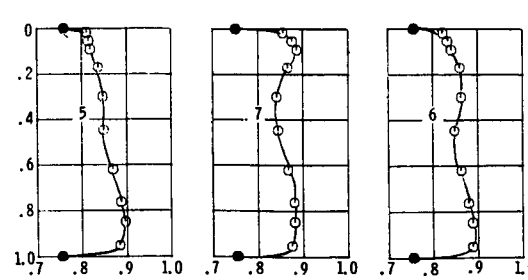

(e-9) Configuration 4CCB; m_5/m_0 = 0.943; P_5/P_0 = 0.856; distortion = 0.108.

(e) Compressor face rake, station 5; diffuser performance for various mass flow ratios m_5/m_0, total-pressure recoveries P_5/P_0, and distortions at station 5.

Figure 16. - Concluded.

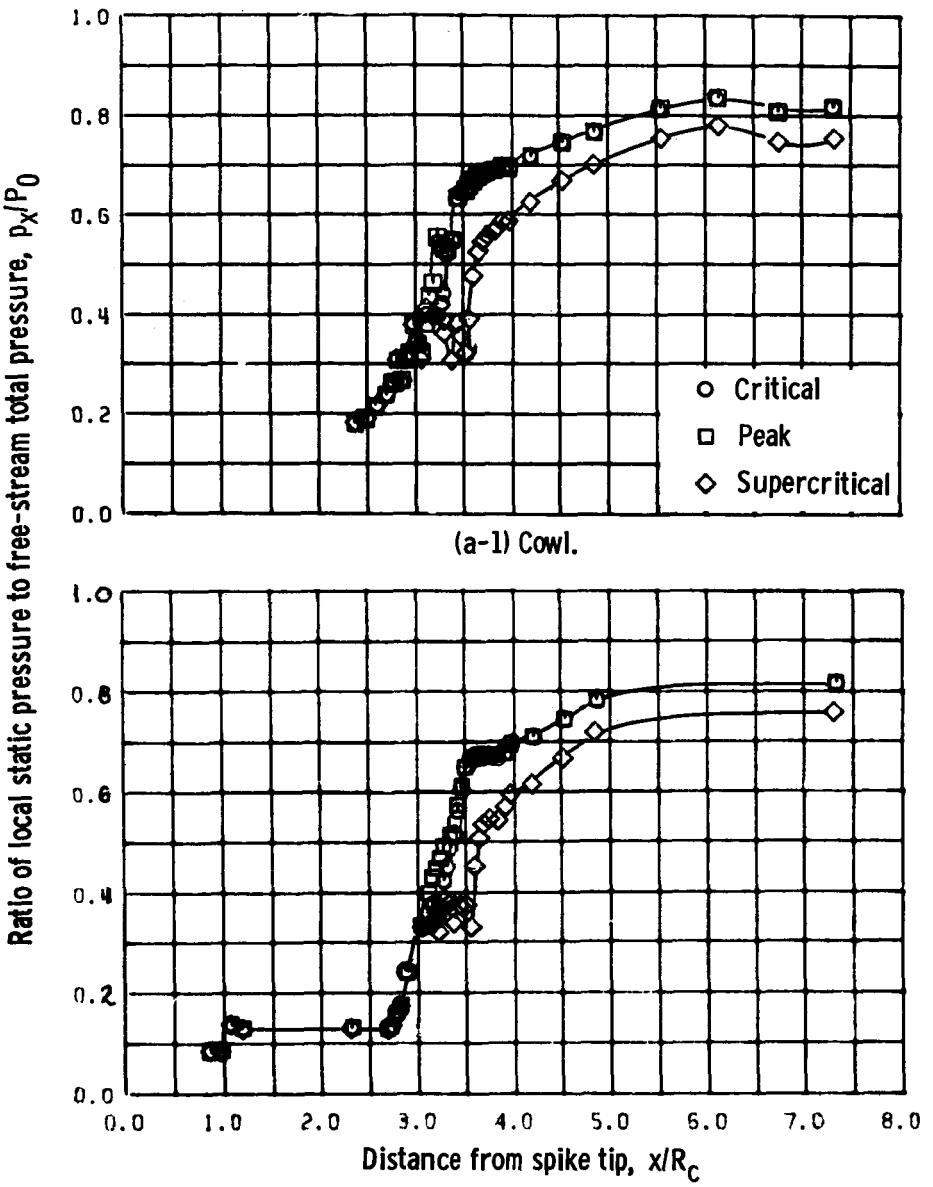

(a-1) Cowl.

(a-2) Centerbody.

(a) Configuration 1CCB.

Figure 17. - Diffuser static-pressure distributions. Free-stream Mach number, 2.5; angle of attack, 0^0; cowl-lip-position parameter, 25.26^0.

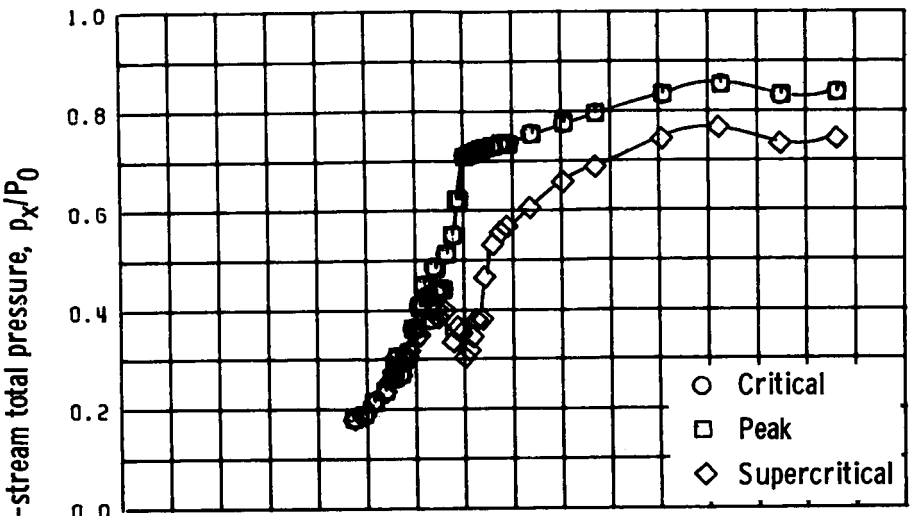

(b-1) Cowl.

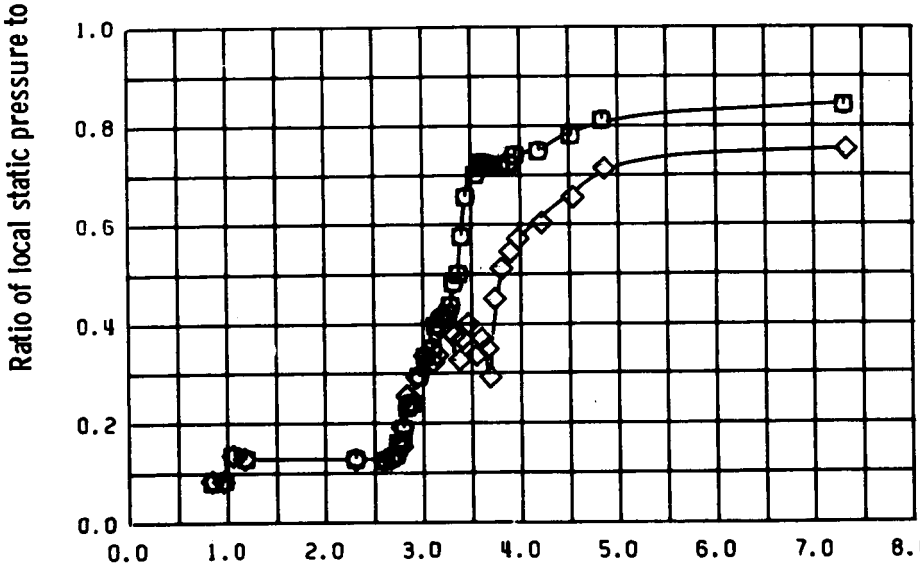

(b-2) Centerbody.

(b) Configuration 2CCB.

Figure 17. - Continued.

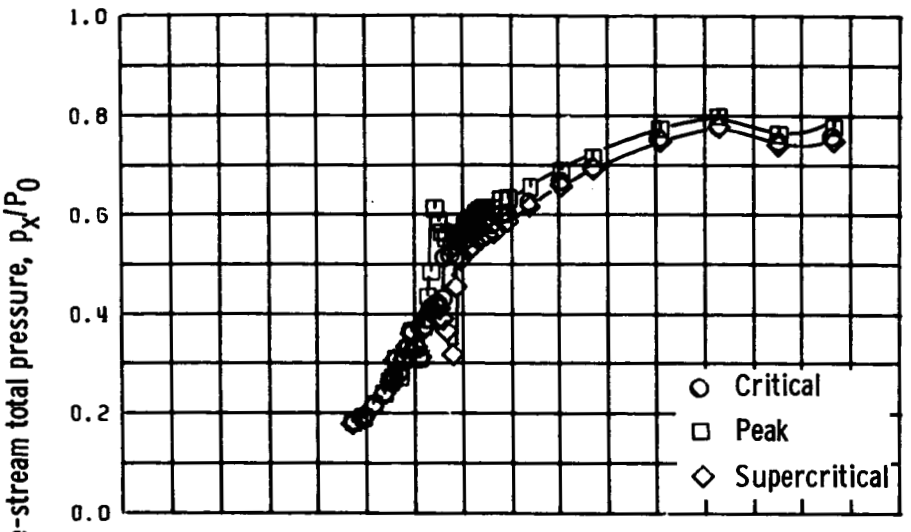

(c-1) Cowl.

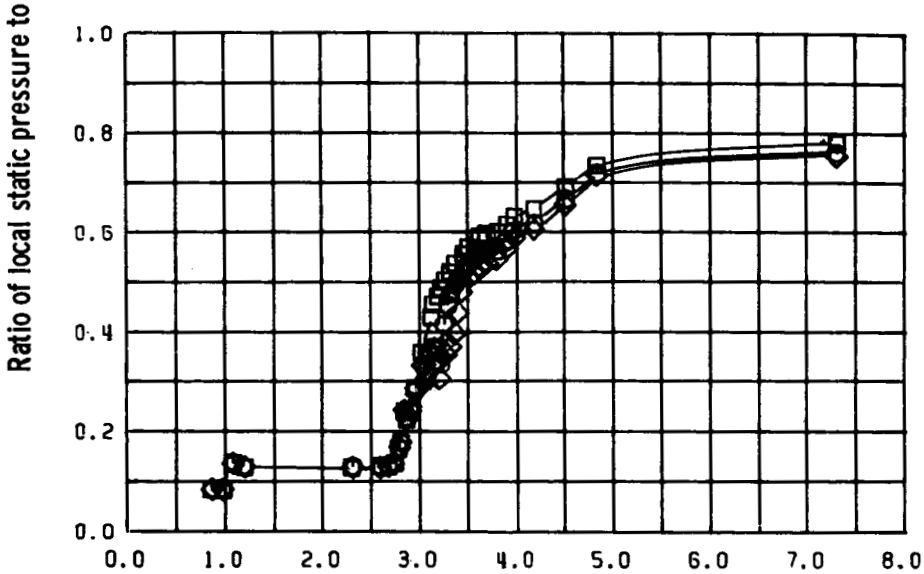

Ratio of local static pressure to free-stream total pressure, p_x/P_0

Distance from spike tip, x/R_c

(c-2) Centerbody.

(c) Configuration 3CCB.

Figure 17. - Continued.

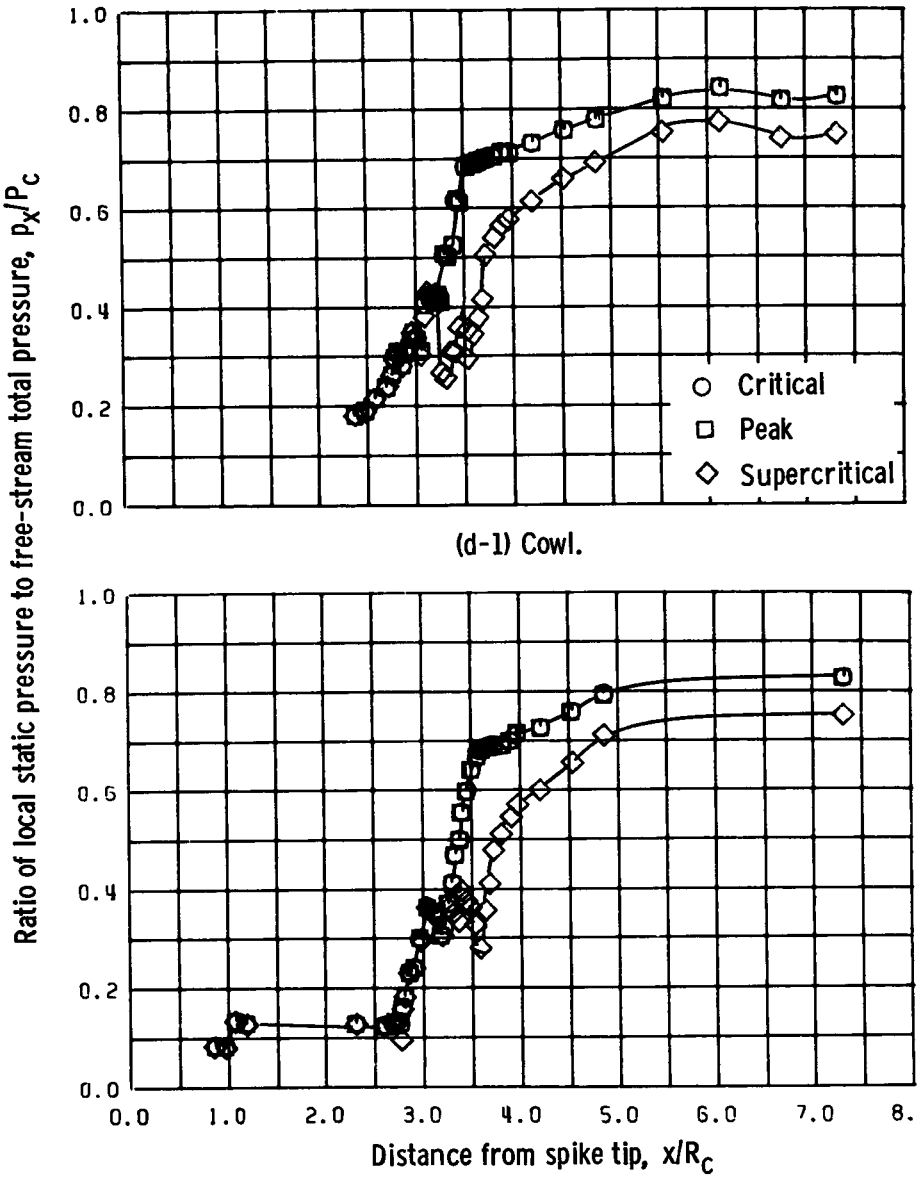

(d-1) Cowl.

(d-2) Centerbody.

(d) Configuration 4CCB.

Figure 17. - Continued.

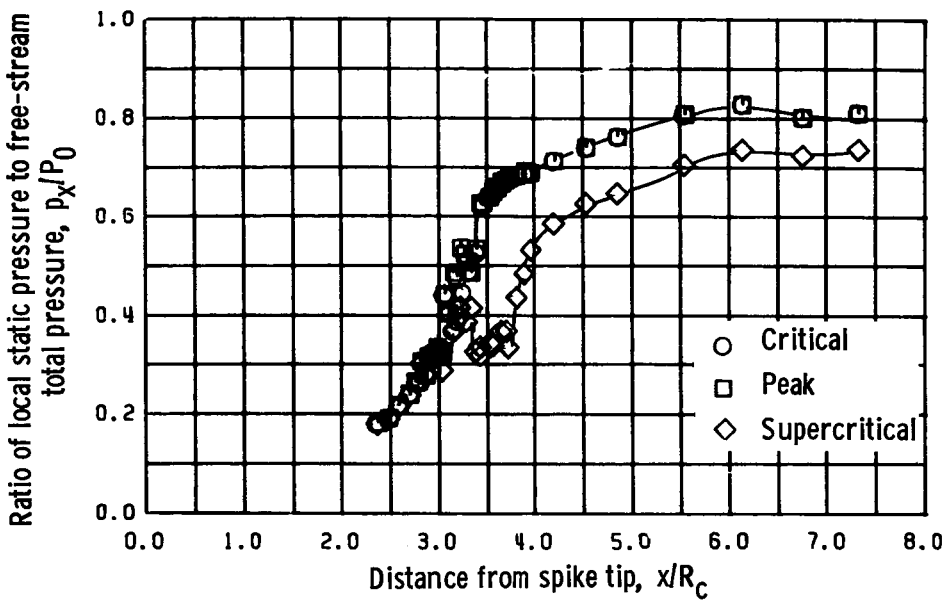

(e) Configuration 5CCB; cowl.

Figure 17. - Concluded.

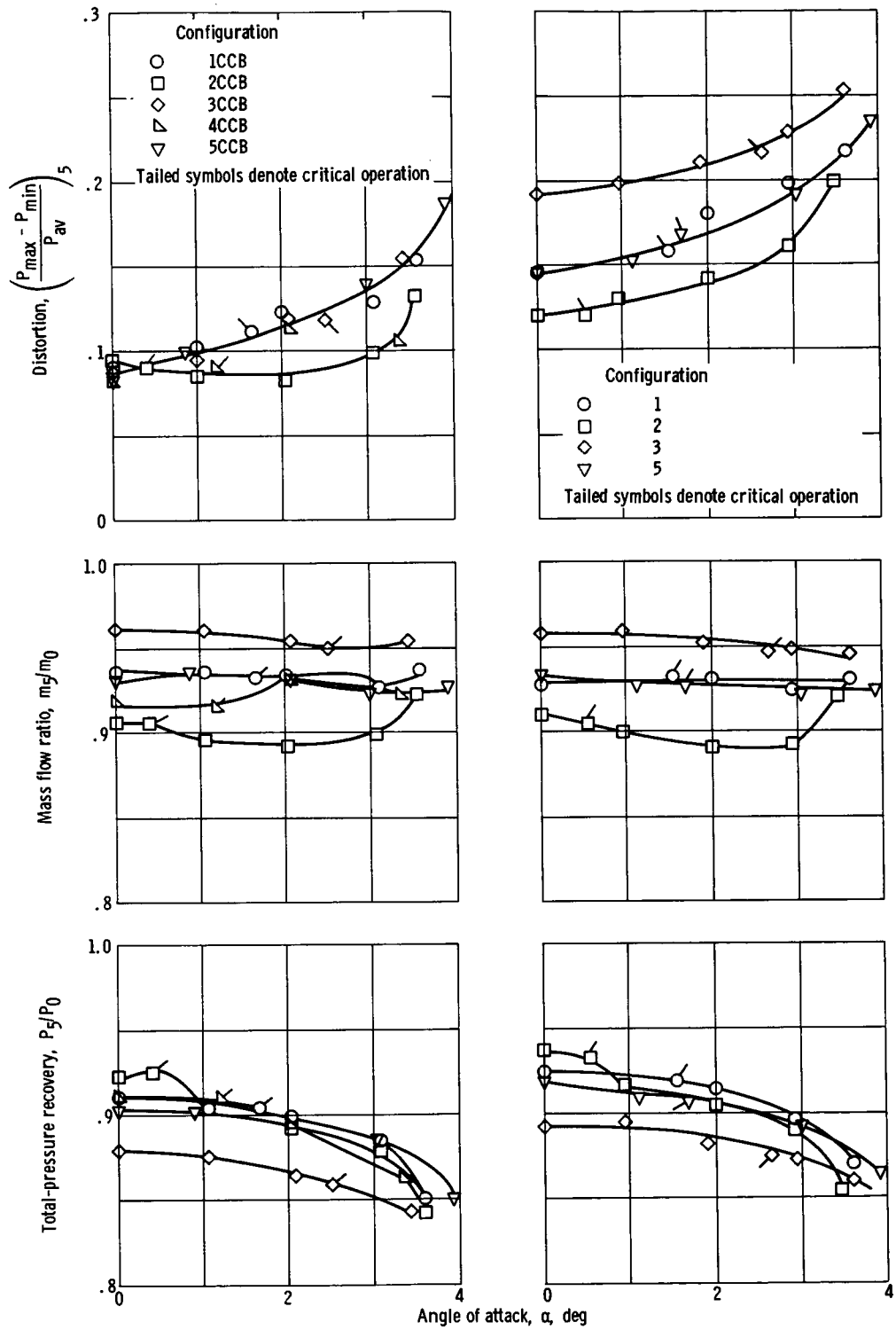

(a) Vortex generators.

(b) No vortex generators.

Figure 18. - Inlet performance at angle of attack. Cowl-lip-position parameter, 25.26°; free-stream Mach number, 2.5.

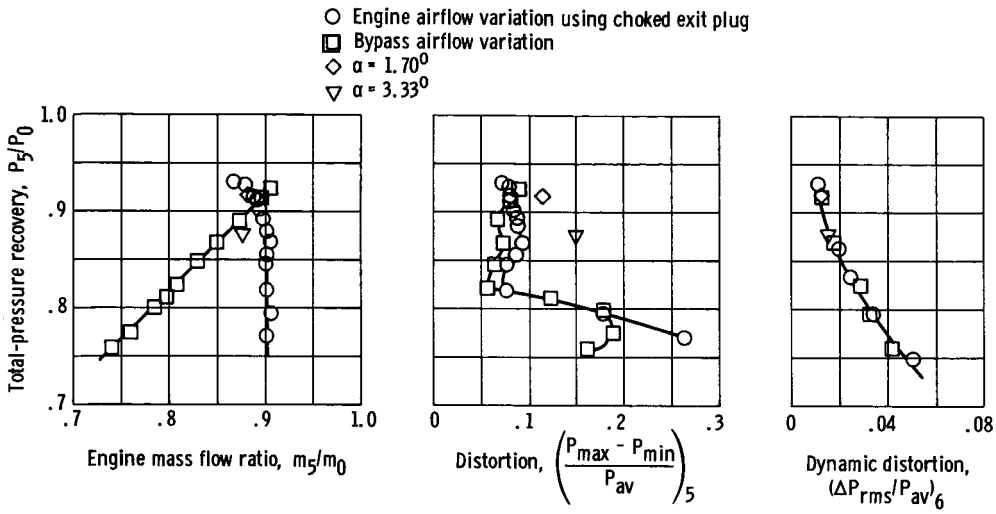

(a) Free-stream Mach number, 2.5; cowl-lip-position parameter, 25.26°; engine-corrected airflow, 15.76 kilograms per second.

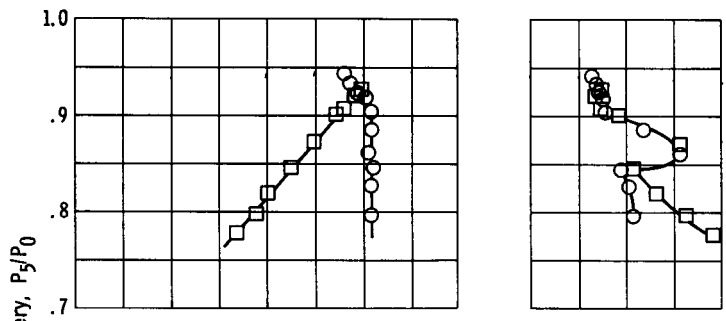

(b) Free-stream Mach number, 2.30; cowl-lip-position parameter, 23.47°; engine-corrected airflow, 16.63 kilograms per second.

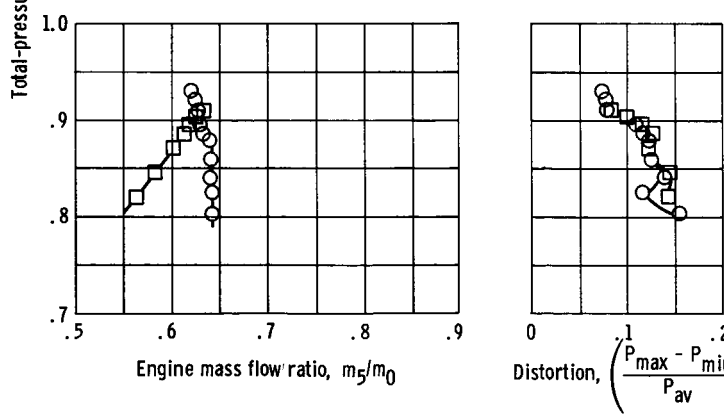

(c) Free-stream Mach number, 2.02; cowl-lip-position parameter, 21.86°; engine-corrected airflow, 17.12 kilograms per second.

Figure 19. - Overall performance of inlet configuration 4CB with bypass flow. Ratio of ejector area to capture area, 0.0117; angle of attack, 0°.

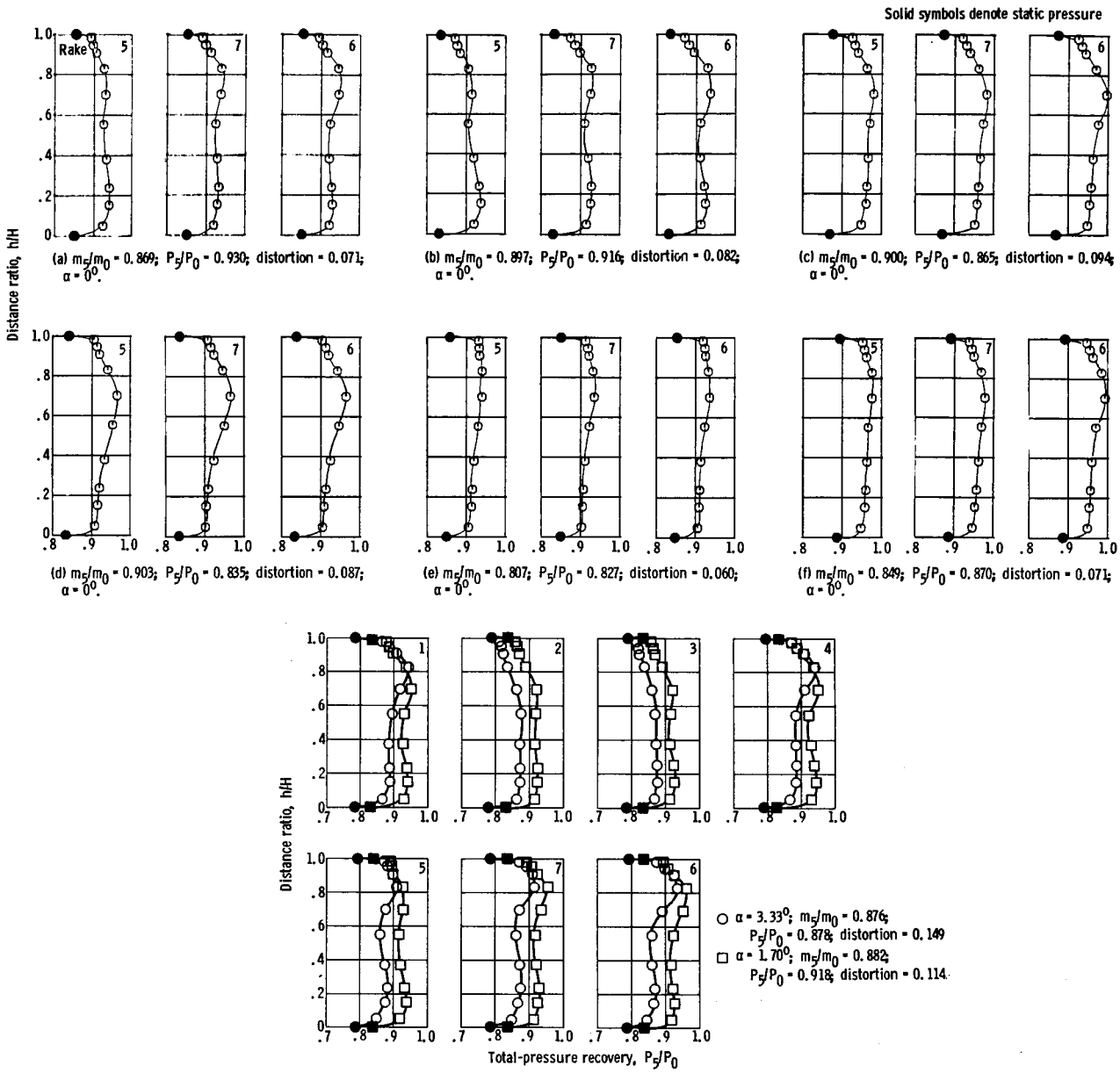

(g) Compressor face total-pressure profiles at angle of attack and peak recovery.

Figure 20. - Configuration 4CB; compressor face total-pressure profiles for various bypass door settings and engine mass flows. Free-stream Mach number, 2.5; cowl-lip-position parameter, 25.26°.

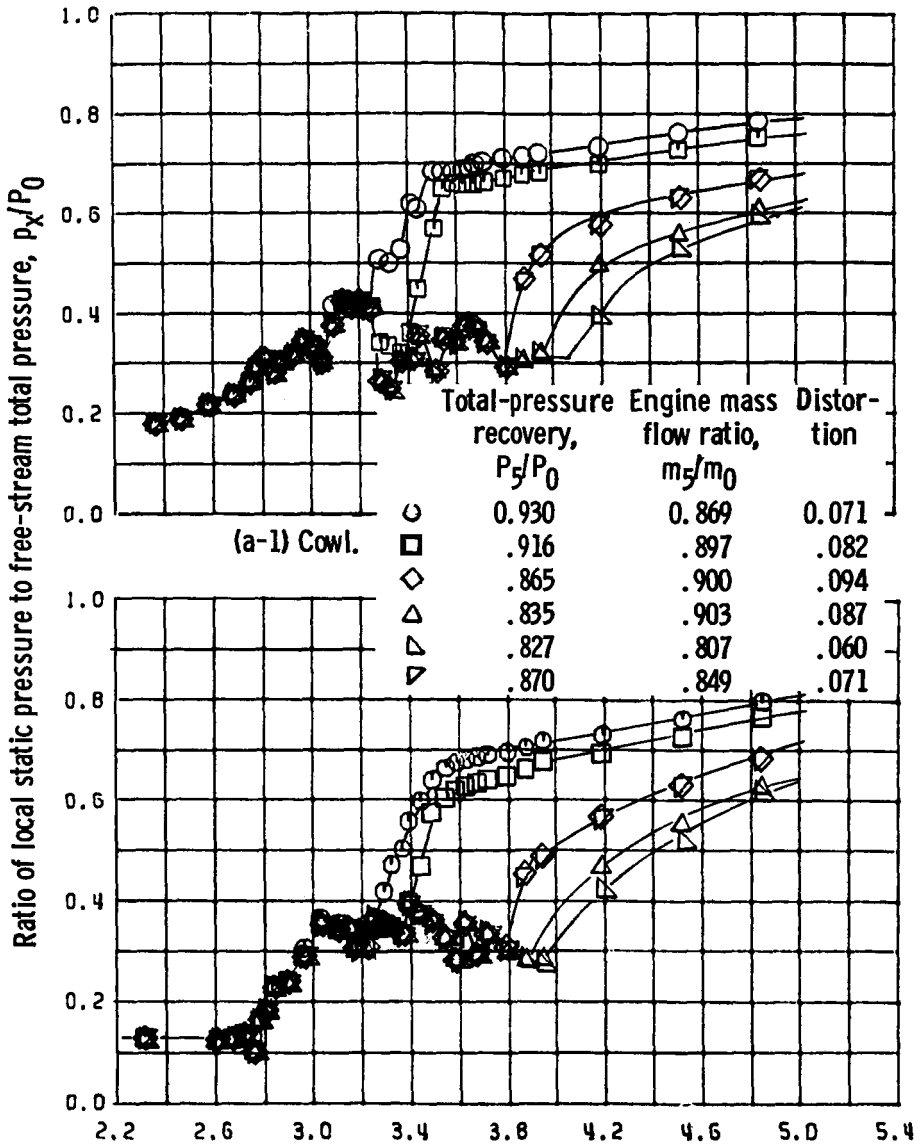

(a) Angle of attack, 0^o.

Figure 21. - Configuration 4CB; cowl and centerbody static-pressure distributions for various bypass door and engine flow settings. Cowl-lip-position parameter, 25.26^o; free-stream Mach number, 2.5.

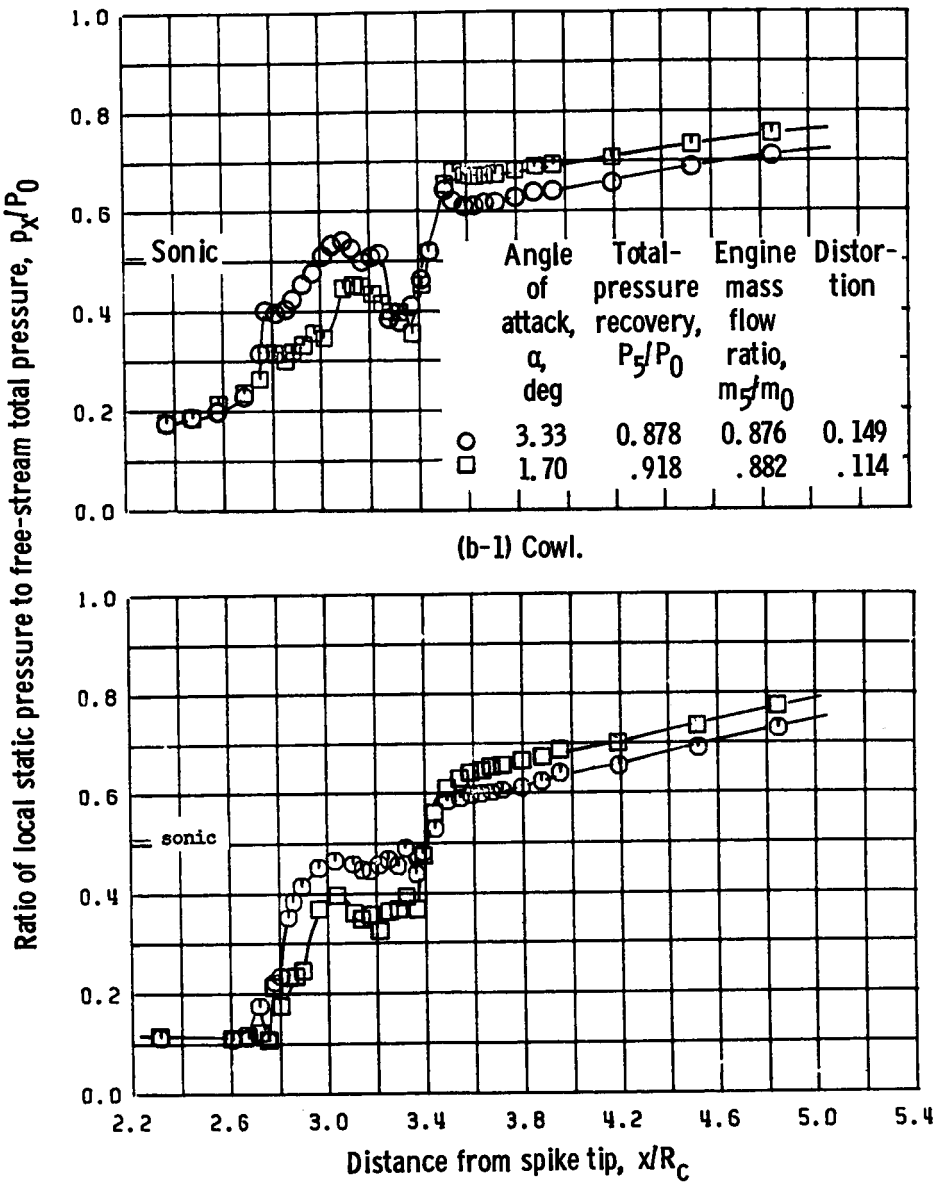

(b-1) Cowl.

(b-2) Centerbody.

(b) Angle-of-attack operation.

Figure 21. - Concluded.

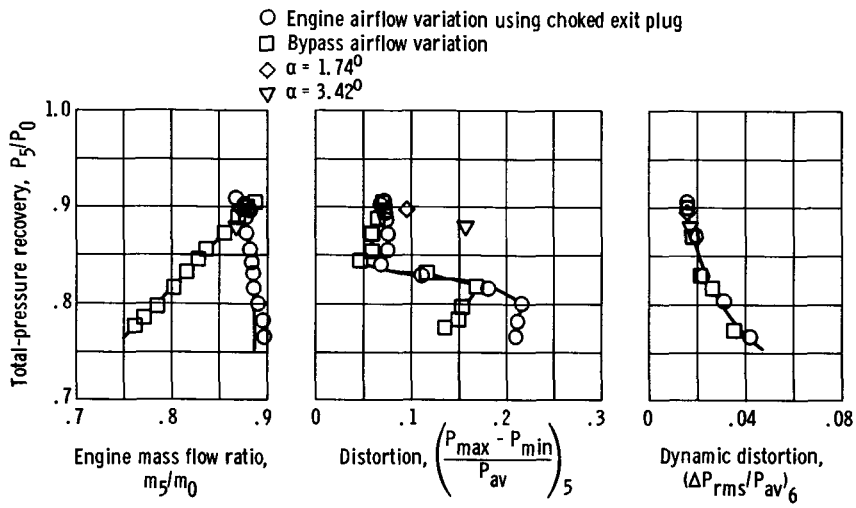

Figure 22. - Overall performance of inlet configuration 3CB with bypass flow. Ratio of ejector area to capture area, 0.0117; angle of attack, 0^0; free-stream Mach number, 2.5; cowl-lip-position parameter, 25.26^0; engine-corrected airflow, 15.76 kilograms per second.

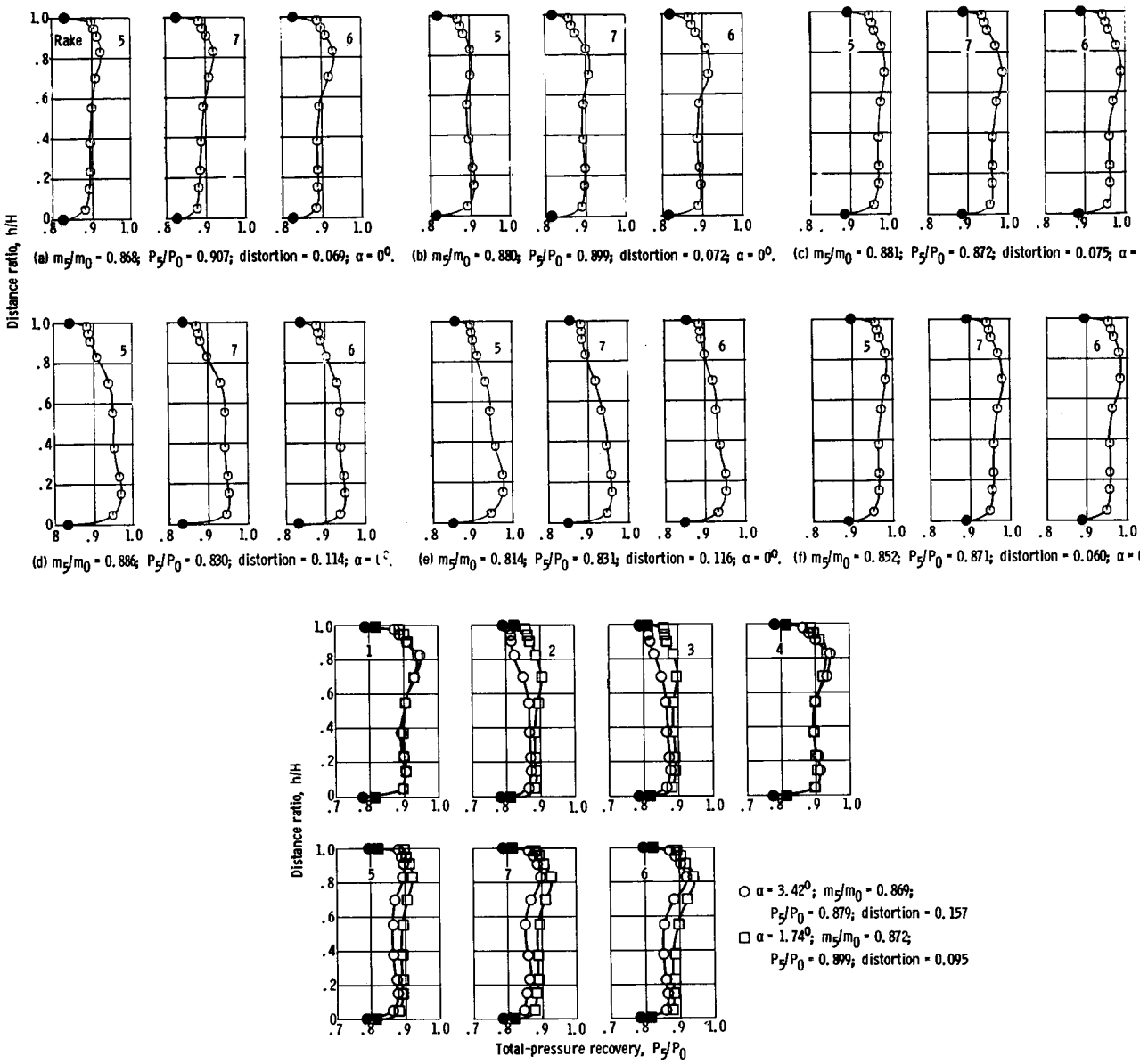

(g) Compressor face total-pressure profiles at angle of attack and peak recovery.

Figure 23. - Configuration 3CB; compressor face total-pressure profiles for various bypass door settings and engine mass flows. Cowl-lip-position parameter, 25.26°; free-stream Mach number, 2.5.

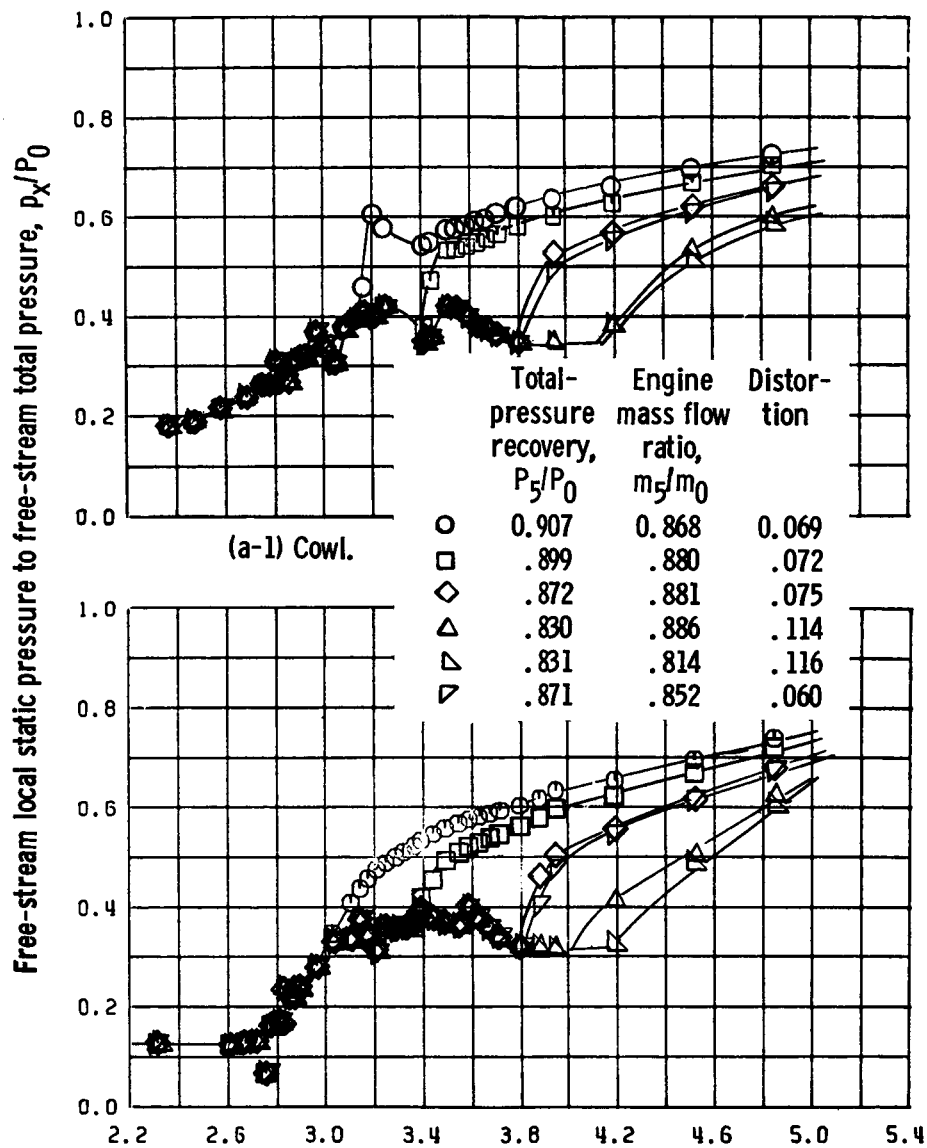

(a) Angle of attack, 0^0.

Figure 24. - Configuration 3CB; cowl and centerbody static-pressure distributions for various bypass door and engine mass flow settings. Cowl-lip-position parameter, 25.26^0; free-stream Mach number, 2.5.

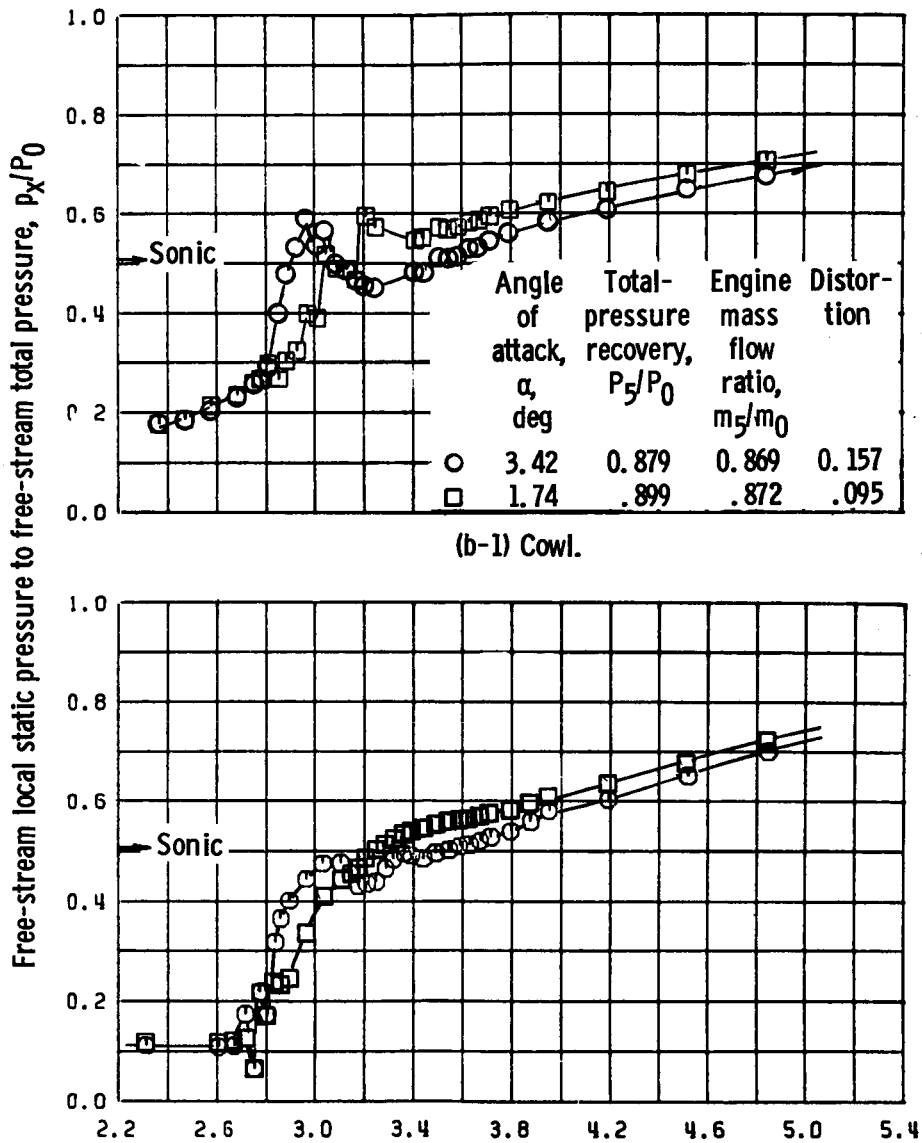

(b-1) Cowl.

(b-2) Centerbody.

(b) Angle-of-attack operation.

Figure 24. - Concluded.

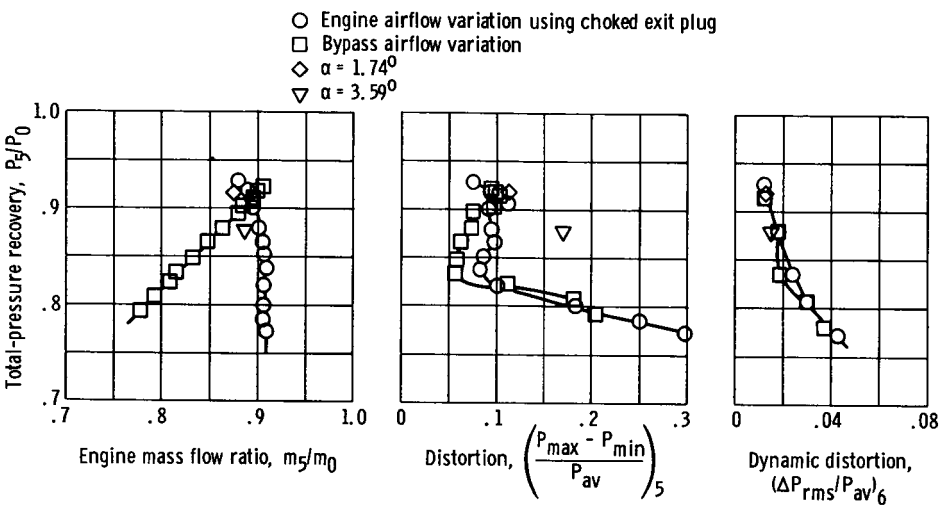

Figure 25. - Overall performance of inlet configuration 1CB with bypass flow. Ratio of ejector area to capture area, 0.0117; angle of attack, 0^0; free-stream Mach number, 2.5; cowl-lip-position parameter, 25.26^0; engine-corrected airflow, 15.76 kilograms per second.

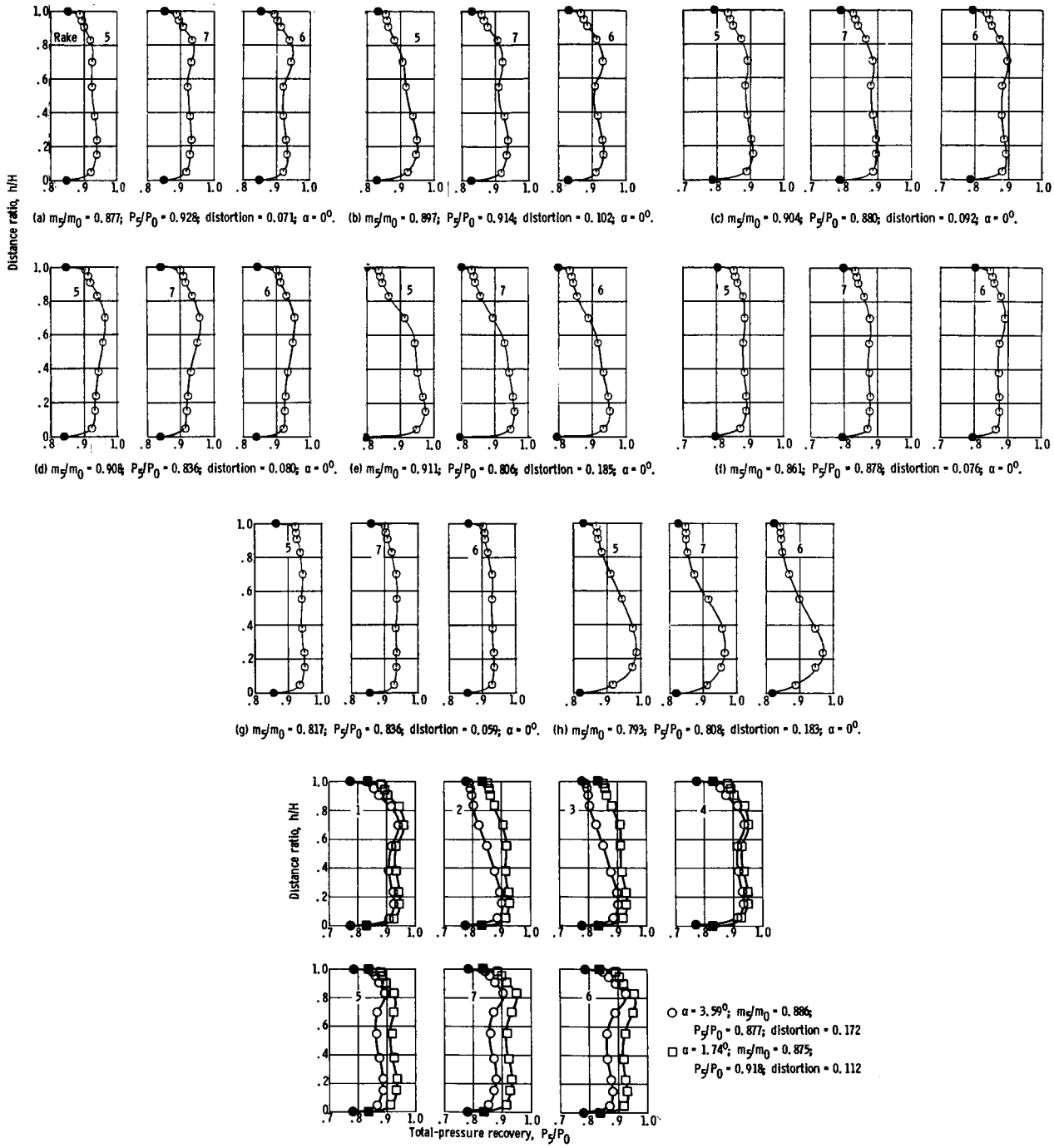

(a) m_5/m_0 = 0.877; P_5/P_0 = 0.928; distortion = 0.071; α = 0°. (b) m_5/m_0 = 0.897; P_5/P_0 = 0.914; distortion = 0.102; α = 0°. (c) m_5/m_0 = 0.904; P_5/P_0 = 0.880; distortion = 0.092; α = 0°.

(d) m_5/m_0 = 0.908; P_5/P_0 = 0.836; distortion = 0.080; α = 0°. (e) m_5/m_0 = 0.911; P_5/P_0 = 0.806; distortion = 0.185; α = 0°. (f) m_5/m_0 = 0.861; P_5/P_0 = 0.878; distortion = 0.076; α = 0°.

(g) m_5/m_0 = 0.817; P_5/P_0 = 0.836; distortion = 0.059; α = 0°. (h) m_5/m_0 = 0.793; P_5/P_0 = 0.808; distortion = 0.183; α = 0°.

(i) Compressor face total-pressure profiles at angle of attack and peak recovery.

Figure 26. - Configuration 1CB; compressor face total-pressure profiles for various bypass door settings and engine mass flows. Cowl-lip-position parameter, 25.26°; free-stream Mach number, 2.5.

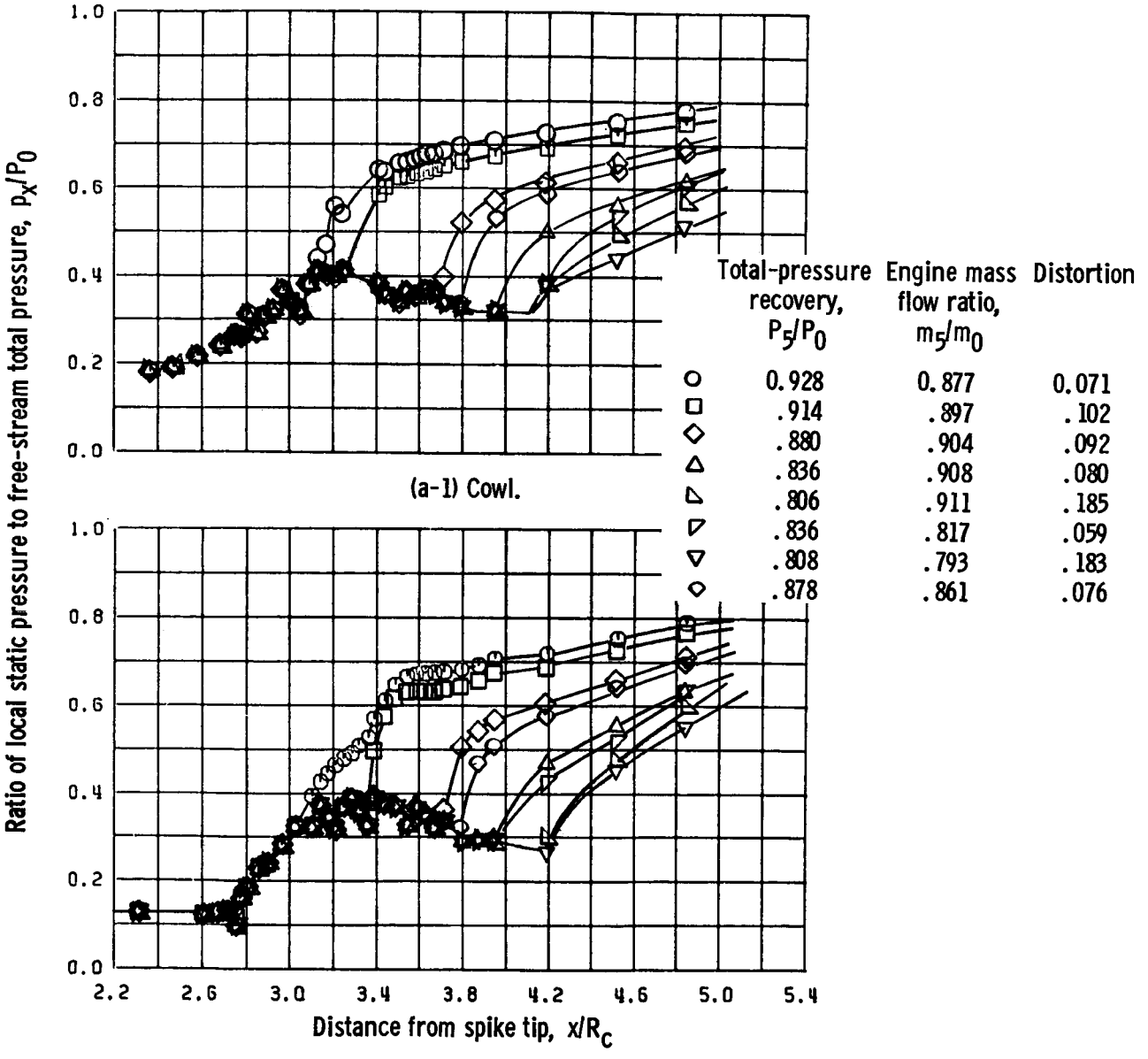

(a) Angle of attack, 0^0.

Figure 27. - Configuration 1CB; cowl and centerbody static-pressure distributions for various bypass door and engine mass flow settings. Cowl-lip-position parameter, 25.26^0; free-stream Mach number, 2.5.

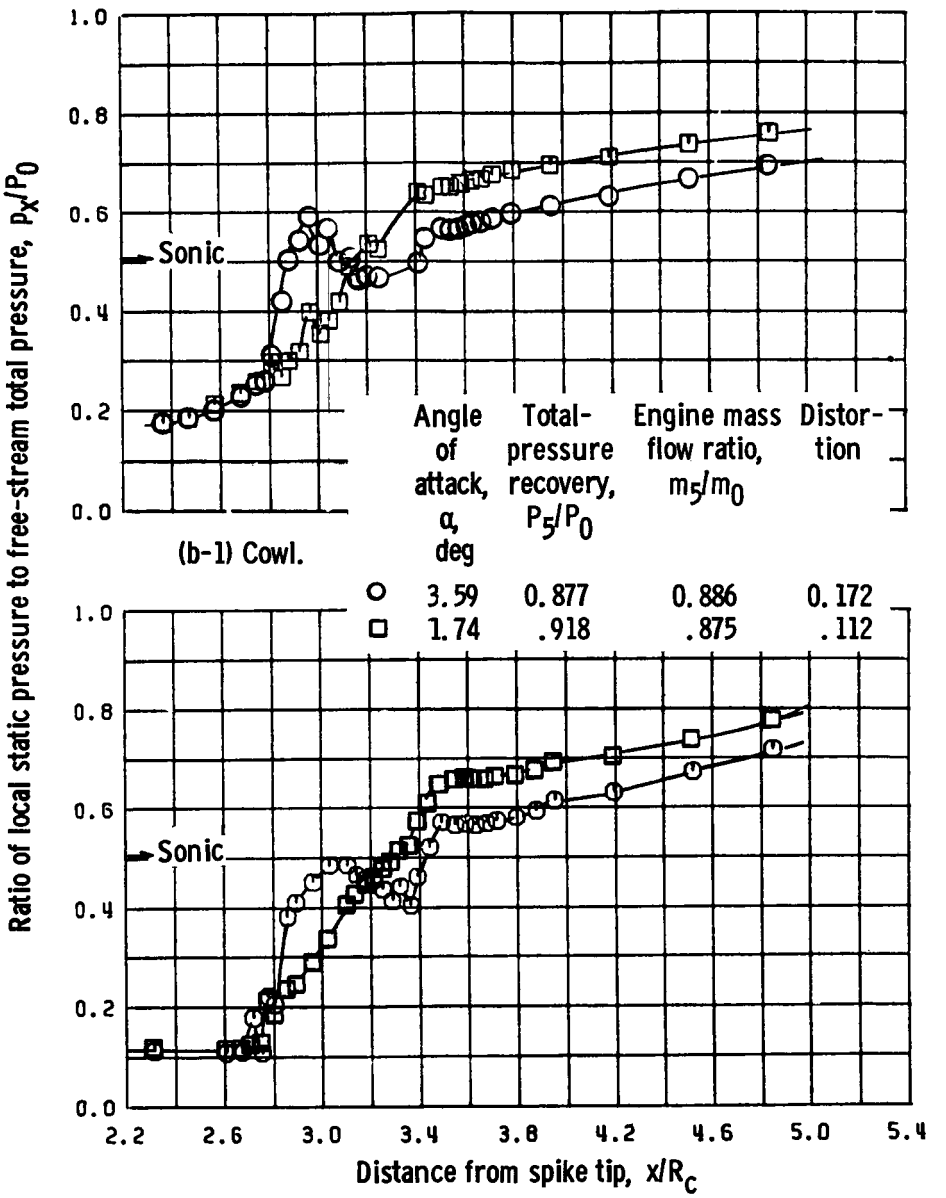

(b) Angle-of-attack operation.

Figure 27. - Concluded.

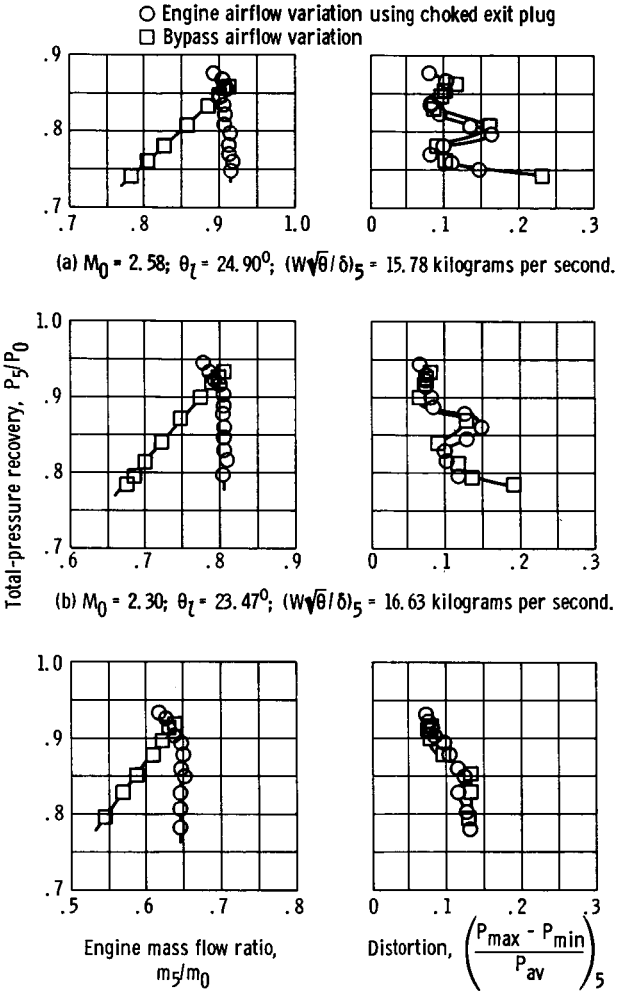

(a) $M_0 = 2.58$; $\theta_t = 24.90^0$; $(W\sqrt{\theta}/\delta)_5 = 15.78$ kilograms per second.

(b) $M_0 = 2.30$; $\theta_t = 23.47^0$; $(W\sqrt{\theta}/\delta)_5 = 16.63$ kilograms per second.

(c) $M_0 = 2.02$; $\theta_t = 21.86^0$; $(W\sqrt{\theta}/\delta)_5 = 17.12$ kilograms per second.

Figure 28. - Overall performance of inlet configuration ICB at off-design Mach numbers M_0, for varying cowl-lip-position parameters θ_t and engine-corrected airflows $W\sqrt{\theta}/\delta$ at station 5.

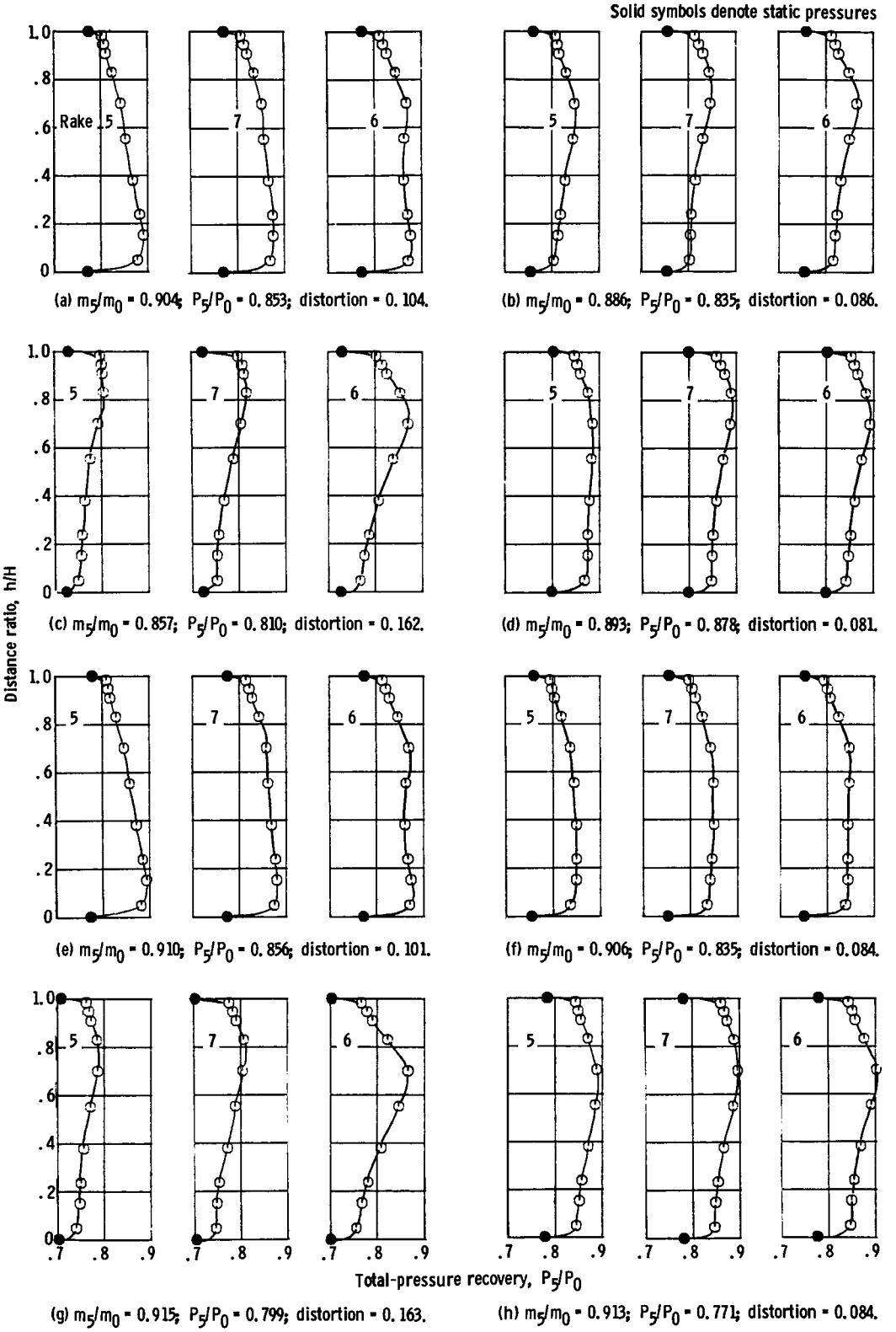

Figure 29. - Configuration 1CB; compressor face total-pressure profiles for various bypass door settings and engine mass flows. Angle of attack, 0^0; cowl-lip-position parameter, 24.90^0; free-stream Mach number, 2.58.

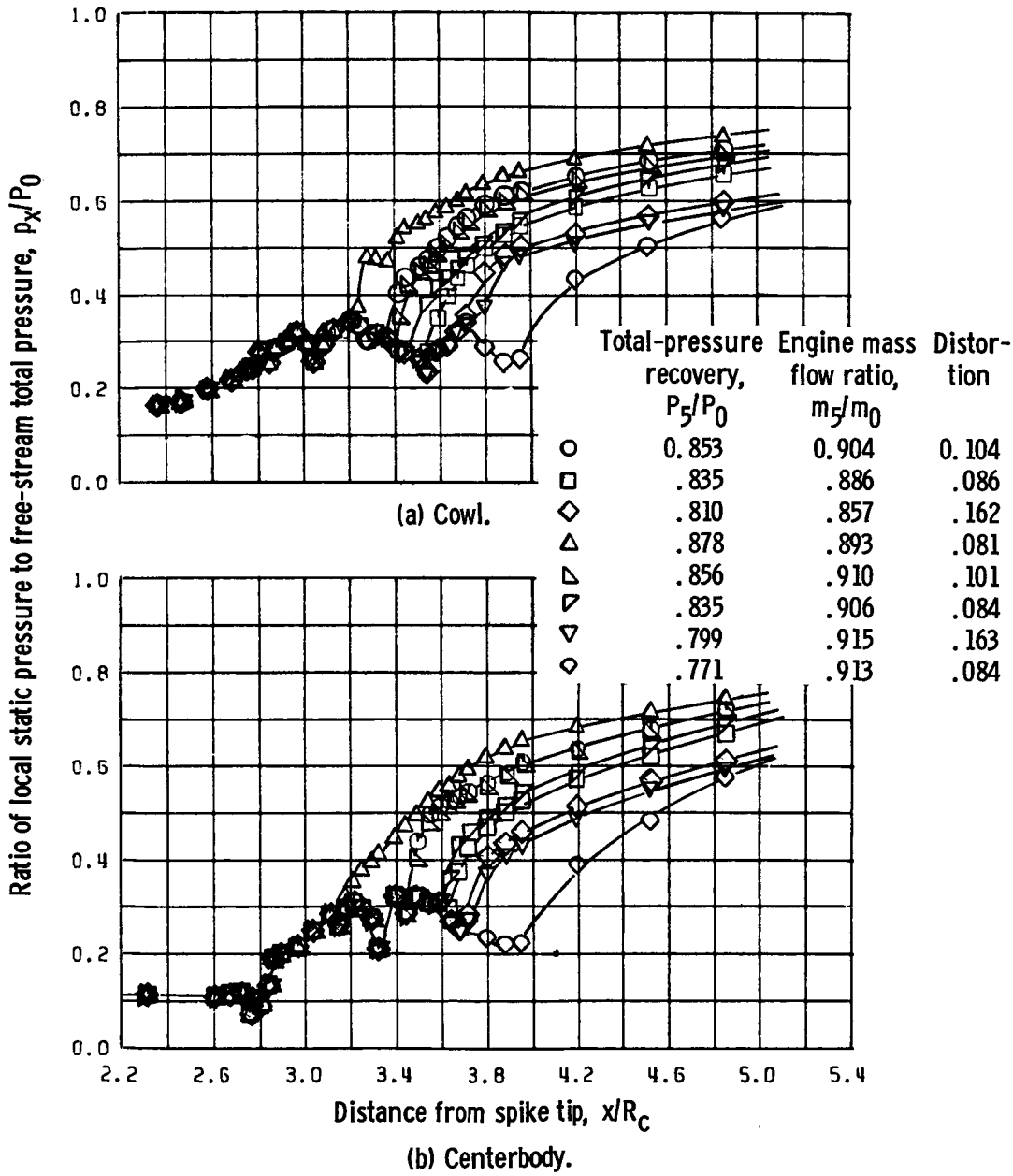

Figure 30. - Configuration 1CB; cowl and centerbody static-pressure distributions for various bypass door and engine mass flow settings. Angle of attack, 0^0; cowl-lip-position parameter, 24.90^0; free-stream Mach number, 2.58.

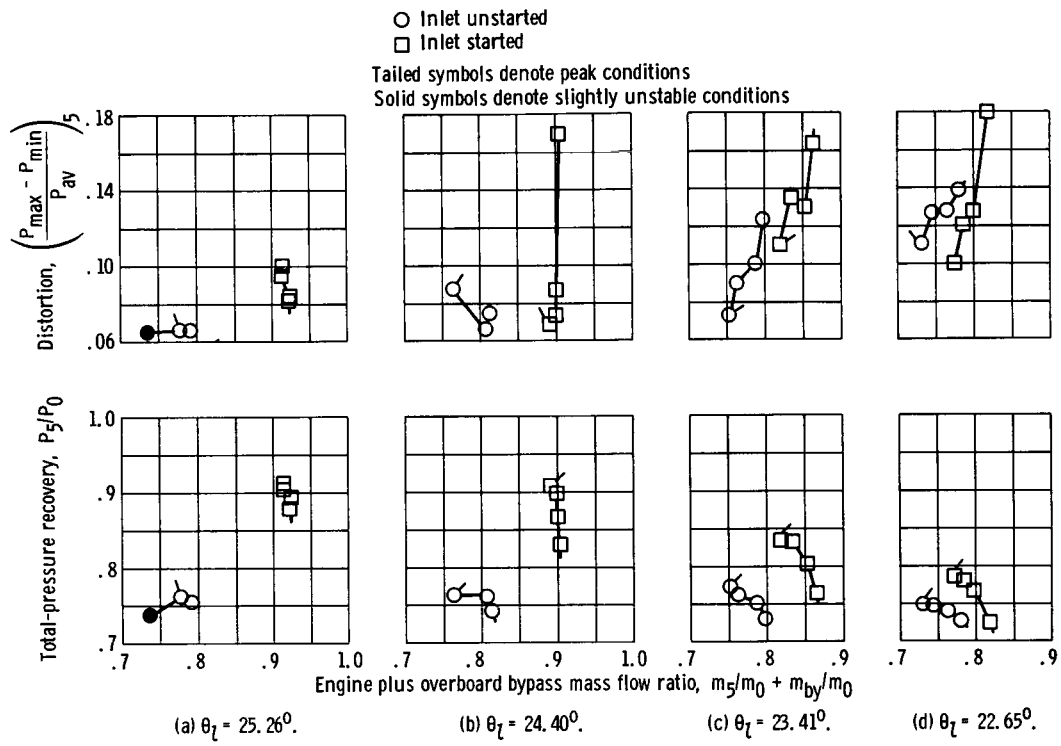

Figure 31. - Inlet performance during restart cycle at Mach 2.5, for various cowl-lip-position parameters θ_l. Configuration 1CB; angle of attack, 0°.

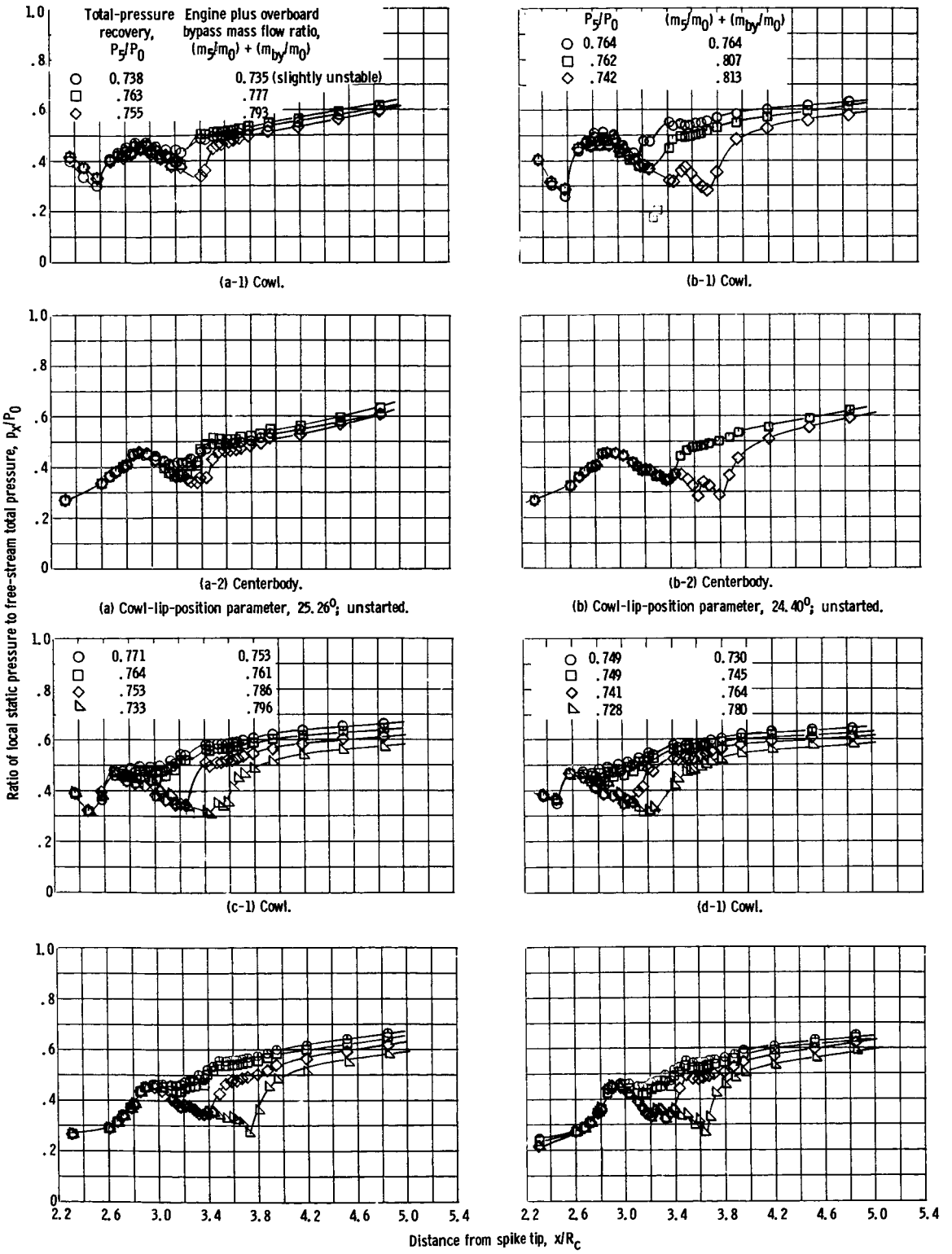

(a-1) Cowl.

(b-1) Cowl.

(a-2) Centerbody.

(a) Cowl-lip-position parameter, 25.26°; unstarted.

(b-2) Centerbody.

(b) Cowl-lip-position parameter, 24.40°; unstarted.

(c-1) Cowl.

(d-1) Cowl.

(c-2) Centerbody.

(c) Cowl-lip-position parameter, 23.41°; unstarted.

(d-2) Centerbody.

(d) Cowl-lip-position parameter, 22.65°; unstarted.

Figure 32. - Internal cowl and centerbody static-pressure distributions during inlet restart sequence. Configuration 1CB.

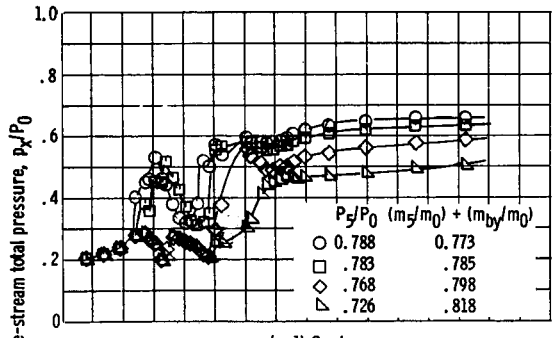

(e-1) Cowl.

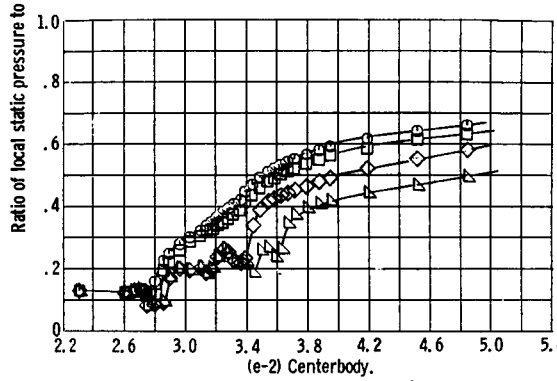

(e-2) Centerbody.

(e) Cowl-lip-position parameter, 22.62°; started.

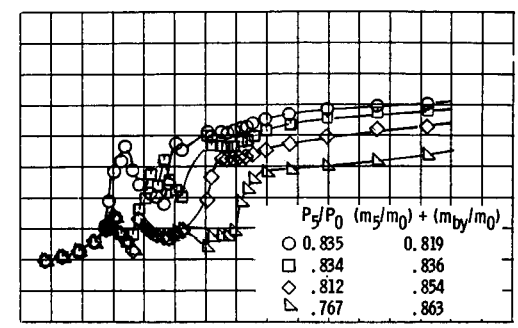

(f-1) Cowl.

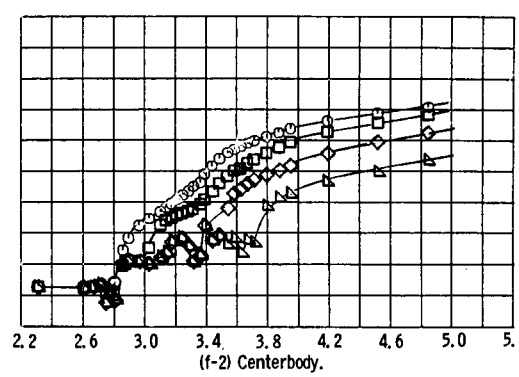

(f-2) Centerbody.

(f) Cowl-lip-position parameter, 23.41°; started.

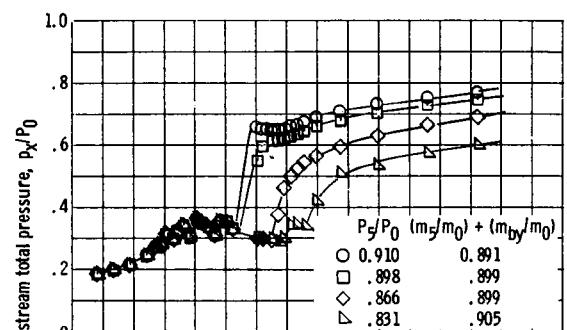

(g-1) Cowl.

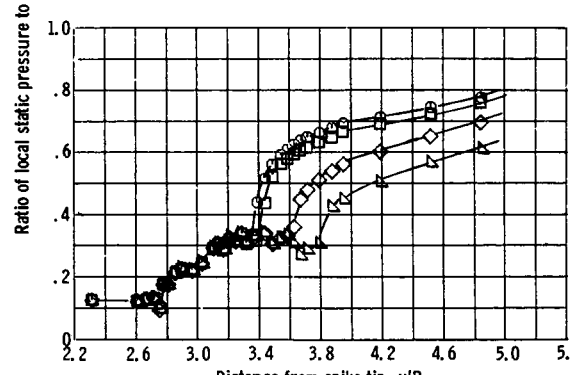

(g-2) Centerbody.

(g) Cowl-lip-position parameter, 24.40°; started.

Figure 32. - Concluded.

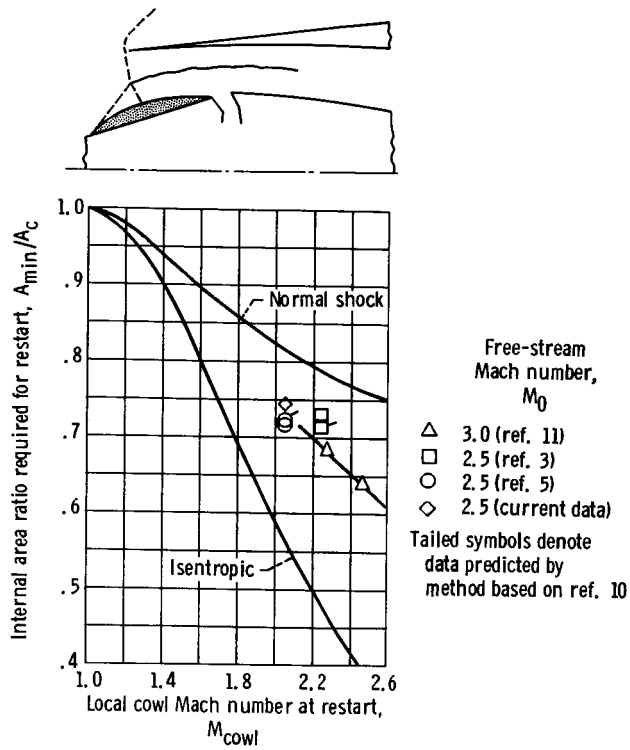

Figure 33. - Comparison of actual to predicted restart area ratio.

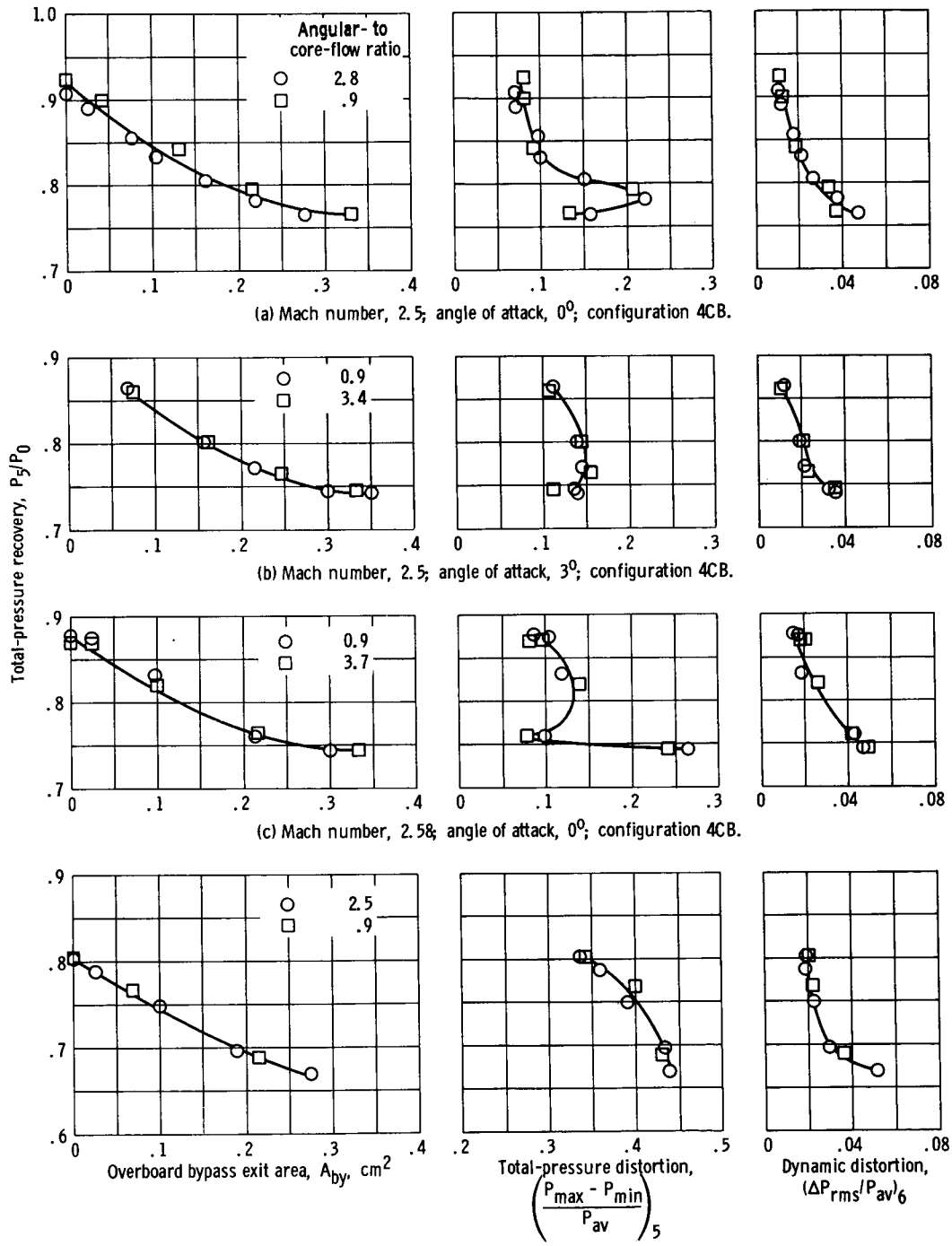

(a) Mach number, 2.5; angle of attack, 0^0; configuration 4CB.

(b) Mach number, 2.5; angle of attack, 3^0; configuration 4CB.

(c) Mach number, 2.58; angle of attack, 0^0; configuration 4CB.

(d) Mach number, 2.58; angle of attack, 8^0; configuration 4CB.

Figure 34. - Effect of annular- to core-flow ratio on inlet performance.

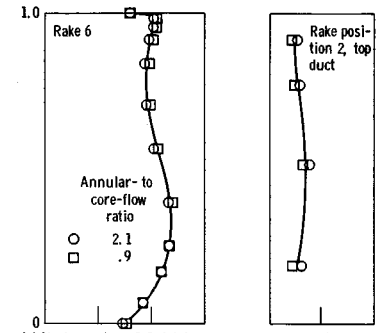

(a) Mach number, 2.5; total-pressure recovery, P_5/P_0 = 0.904; overboard bypass exit area, A_{by} = 316 square centimeters; configuration 4CB.

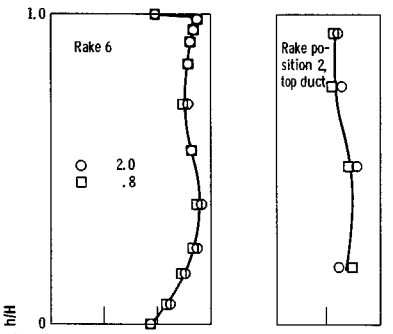

(b) Mach number, 2.5; total-pressure recovery, P_5/P_0 = 0.828; overboard bypass exit area, A_{by} = 480 square centimeters; configuration 4CB.

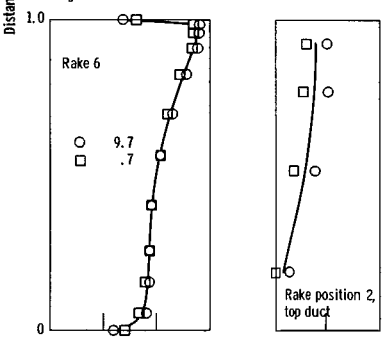

(c) Mach number, 2.58; total-pressure recovery, P_5/P_0 = 0.869; overboard bypass exit area, A_{by} = 122 square centimeters; configuration 4CB.

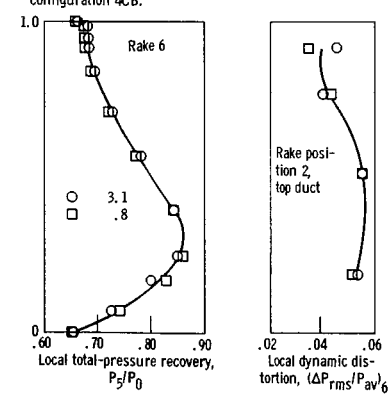

(d) Mach number, 2.58; total-pressure recovery, P_5/P_0 = 0.744; overboard bypass exit area, A_{by} = 294 square centimeters; configuration 4CB.

Distance ratio, h/H

Figure 35. - Effect of annular- to core-flow ratio on flow at compressor face at angle of attack of 0^0.

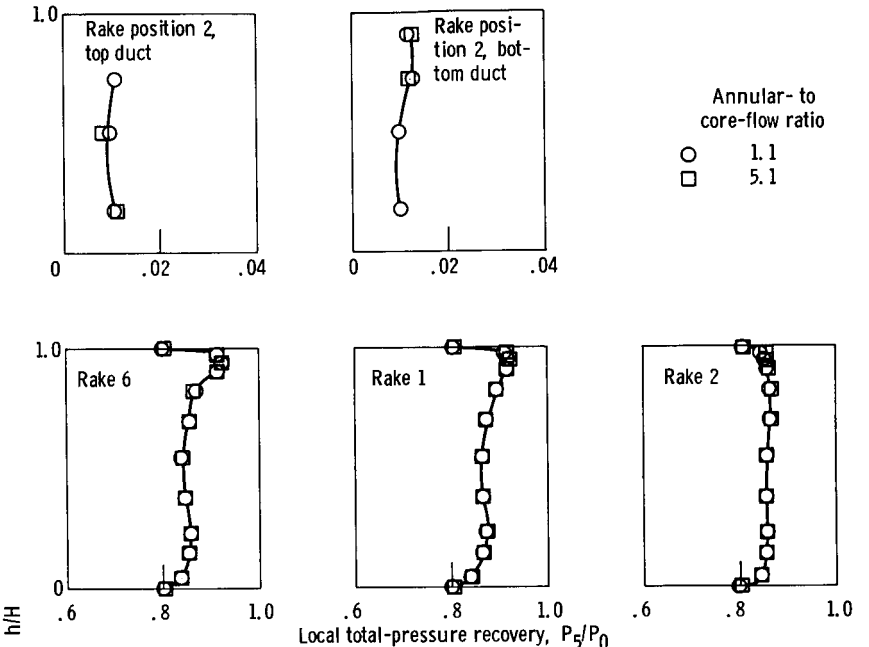

(a) Mach number, 2.5; angle of attack, 3^0; total-pressure recovery, $P_5/P_0 = 0.864$; overboard bypass area, A_{by} = 142 square centimeters; configuration 4CB.

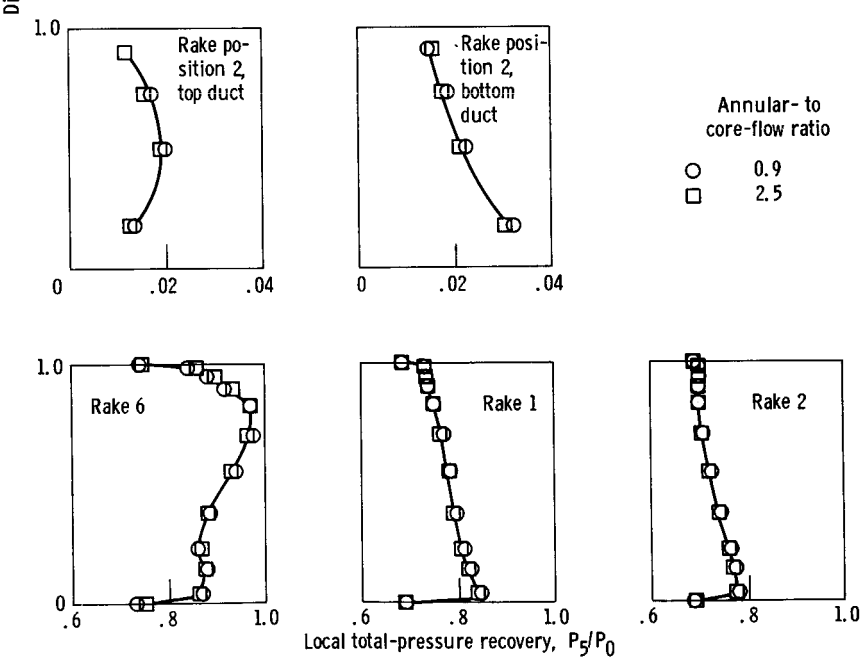

(b) Mach number, 2.58; angle of attack, 8^0; total-pressure recovery, $P_5/P_0 = 0.804$; overboard bypass exit area, $A_{by} = 0$; configuration 4CB.

Figure 36. - Effect of annular- to core-flow ratio on flow at compressor face at various angles of attack.

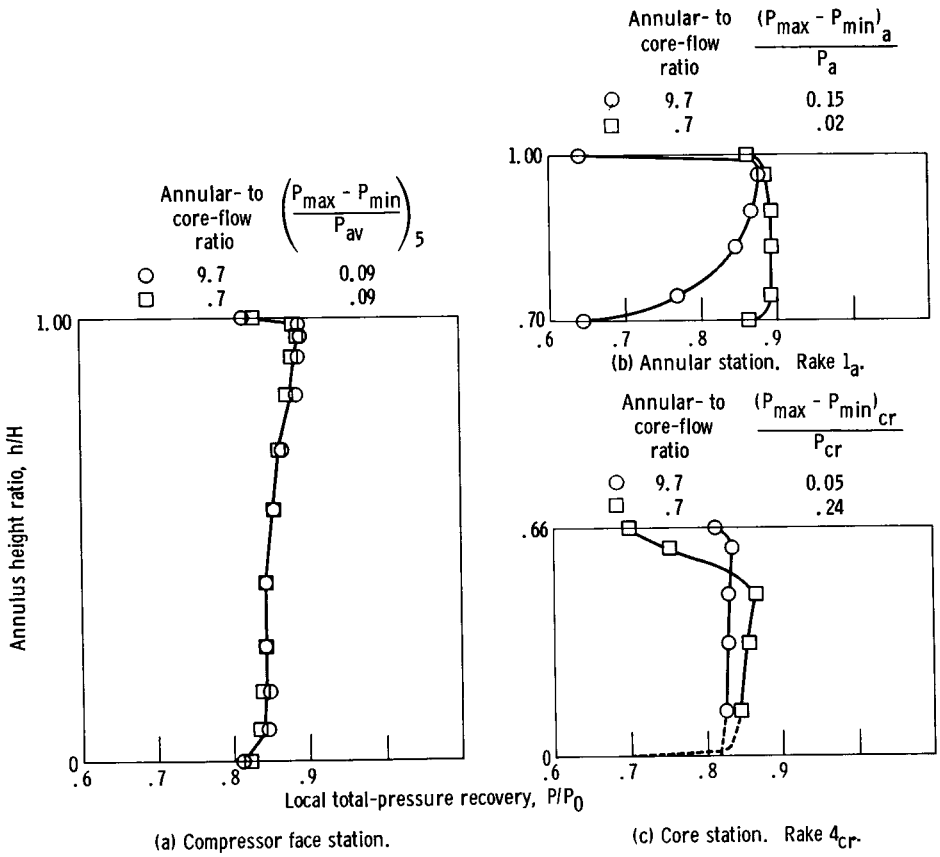

(a) Compressor face station.

(b) Annular station. Rake 1_a.

(c) Core station. Rake 4_{cr}.

Figure 37. - Effect of annular- to core-flow ratio on flow in concentric cold-pipe for constant compressor face conditions - bleed configuration 4CB.